THE EFFECT OF SOLUTES FROM THE SIXTH PERIOD OF THE PERIODIC TABLE ON THE MELTING POINT AND THE ALLOTROPIC TRANSFORMATION TEMPERATURE OF PRASEODYMIUM

by

Richard Bruce Griffin

A Dissertation Submitted to the
Graduate Faculty in Partial Fulfillment of
The Requirements for the Degree of
DOCTOR OF PHILOSOPHY

Major Subject: Metallurgy

Approved:

Signature was redacted for privacy.
In Charge of Major Work

Signature was redacted for privacy.
Head of Major Department

Signature was redacted for privacy.
Dean of Graduate College

Iowa State University
Ames, Iowa

1969

TABLE OF CONTENTS

INTRODUCTION

Given two metal components, one would like to calculate from first principles the effects that these two materials would have on each other when alloyed. In return, given the system already determined, one would like to calculate the thermodynamic properties associated with the two components for the different phases involved. At the present time, the calculation of equilibrium diagrams from first principles is not possible. It is possible to construct equilibrium diagrams from known thermodynamic data, if the free energies are known as functions of composition and temperature for each component (1). According to Wagner (2), theoretical calculations of equilibrium diagrams can only be made by the introduction of approximations. If these approximations are made, such as assuming ideal solution, then there must be accurate equilibrium diagrams available to compare to the calculated diagrams.

Since equilibrium diagrams and heats of fusion can be determined relatively easily, one can try the reverse procedure of calculating the thermodynamic functions from the phase diagrams. This type of study is being carried out by several investigators with reasonable success for simple systems (3, 4, 5, 6). In order to do this, accurate experimental data must be available.

For many binary metal systems, in particular the rare earths (R.E.'s), good equilibrium diagram data is lacking. Gschneidner and Waber (7) concluded that, from a theoretical point of view, the most important area for future work with the R.E.'s would be in obtaining accurate liquidus, solidus, solvus, solubility limits, lattice spacings, heats of transformations, and allotropic transformation data.

The primary purpose of this work is to supply part of the above information for one of the R.E.'s, specifically praseodymium (Pr), alloyed with the elements of the sixth period (Cs through Bi except the lanthanides) of the periodic table. A secondary objective is to look at some of the theories that have been derived for equilibrium between phases and see if they can be applied to the above systems (8, 9, 10, 11).

For predicting what happens when two metals are alloyed, the usual starting point is the work of Hume-Rothery, Channel-Evans, and Mabbott (12). From their work, they concluded that there were three important factors affecting the solid solubility of metals. These were:

1. Size Factor - For extensive solid solubility to occur, the atomic radii of the two components should be within 15% of each other, provided the other factors are favorable.

2. Relative Valence Factor - The greater the valency difference between two elements, the less likelihood of extensive solubility.
3. Chemical Factor - This is concerned with the chemical similarity of two metals, and it is related to the tendency of atoms from opposite ends of the periodic table to form ionic compounds. A measure of this tendency is an element's electronegativity. Maximum solubility is most likely to occur for those elements which are chemically similar, assuming the other two factors are favorable.

Most elementary metallurgy textbooks use the above rules as a starting point for a discussion of alloy behavior. The qualitative nature of the rules often makes them easier to apply after a diagram has been determined experimentally.

Darken and Gurry (13) refined the rules by pointing out only two of the first three are independent, and the limit on primary solid solubility is composed of two factors, one geometrical and the other chemical. They plotted the electronegativity versus radius and found that all elements with a solubility greater than 5 at.% in Mg and Al and a solubility greater than 10 at.% in Ag were included within an ellipse whose minor axis was $\pm$ 15% of the radius of the solvent and whose major axis was $\pm$ 0.4 electronegativity

units. Waber and co-workers (14) extended this analysis to 59 other elements from the periodic table. They found experimental data available for 1455 binary combinations, and correctly predicted whether the solute would be soluble or insoluble for 1115 cases. This broke down to a 61.7% reliability for predicting solubility greater than 5 at.% and an 84.8% reliability for predicting solubility of less than 5 at.%. Rider and co-workers (15) showed for some R.E.-Au alloys that by applying correction terms to the atomic radii, the extent of solubility could be correctly predicted for those alloys. This was done for solutes from period six dissolved in Pr, and no solubility was predicted for any solute.[1]

From this brief discussion, one notes the prediction of alloying behavior is a difficult task, and one of the hinderances is the lack of good experimental data. This study provided the data necessary for a critical evaluation of the effects governing the alloying behavior of Pr with elements from the sixth period of the periodic table. The equilibrium diagrams were determined from 100% Pr to the composition of the first liquid to solid reaction at the Pr-rich end of the diagrams.

---

[1] O. D. McMasters, Ames, Iowa. The data from Teatum and co-workers compilation (16) and Rider's (15) study was extended to include additional binary systems. Private communication, 1965.

EXPERIMENTAL

Materials

Solvent

Pr was chosen as the solvent because of the lack of good experimental data available on it. It is one of the R.E. metals which appear in the sixth period of the periodic table between La and Hf. For La, the first lanthanide, the valence electron configuration (17) is $5\underline{d}^1 6\underline{s}^2$ and for Ce, which has one more electron, it becomes energetically more favorable for the electron to go into the 4f subshell rather than the 5d shell. This is true for the remaining lanthanides, Pr through Lu, and at Lu the 4f subshell has its full compliment of 14 electrons. The elements La through Lu are remarkably similar in physical, chemical, and electronic properties, so much so they make a useful research tool (18).

The secondary reasons were that Pr is representative of the light lanthanides, which roughly include La through Sm, although this may change with the particular property being looked at. Pr is characterized by a double c/a hexagonal structure at room temperature (α-Pr), and a transformation to a b.c.c. structure at 800 C, β-Pr. Pr does not show the anomalous valence states of metallic Ce, and Pr's low melting point of 934 C makes it much simpler to study experimentally than some of the other R.E.'s. Lastly,

Pr is somewhat more corrosion resistant than either La or Ce.

The Pr used was the highest purity available (19). It was made by converting the oxide to the fluoride, and adding Ca to reduce the fluoride, and finally vacuum casting the Pr in Ta crucibles. The chemical analysis of the Pr is given in Table 1.

Solute

There were several reasons for selecting the elements from period six--Cs, Ba, Hf, Ta, W, Re, Os, Ir, Pt, Au, Hg, Tl, Pb, and Bi. The solutes are in the same period as the solvent and this eliminates any parameter related to using solutes and solvents from different periods of the periodic table. Period four has Fe, Ni, and Co which introduces the complication of ferromagnetism, and the atomic radii are smaller than period five or six. The atomic radii of period five elements is just slightly smaller than those of the sixth period, but several of the elements from period six were readily available in high purity form. The chemical analyses for the solutes used in this study are given in Table 1.

Table 2 lists some of the pertinent data about each of the solutes and the solvent.

Crucible Material

All of the alloys were contained in Ta crucibles because Ta does not react with Pr (20) and Ta crucibles are easily fabricated (21). Dennison and co-workers (20) showed the solubility of Ta in Pr, at the melting point of Pr was 0.0055 at.% Ta.

Figure 1 (A) is a drawing showing the size and shape of the crucibles used in this study. All tubing was outgassed by heating the crucibles and lids in a dynamic vacuum of 10^{-6} torr at a temperature greater than 1600 C for a minimum of twenty minutes. Approximately 15 grams of Pr were used to make up each pure Pr sample. The crucibles containing the Pr were heated in an induction coil to melt the Pr, and then each sample was run in the differential thermal analysis (D.T.A.) system to check the melting and transformation temperatures, and to look for leaky crucibles.

Alloys were prepared by cutting off the lid of the above crucibles, weighing the amount of solute added to within $\pm$ 0.1 mg, using an Ainsworth electronic balance. A new Ta lid was welded on the crucible in an arc-welder under a partial atmosphere of helium (21). Fortunately, the density of the elements from period six is greater than that of Pr, except for Cs and Ba, and so it was assumed alloying

occurred as the solute settled down through the molten Pr. The homogenizing heat treatment normally consisted of heating the sealed crucibles, in a vacuum, by induction at approximately 200 to 250 C above the liquidus for about one hour. This same crucible would be used again for another alloy by removing the lid, adding more solute, and then proceeding as above. The composition of the new alloy would be calculated by assuming that the amounts of material lost in any preceding operation were negligible. This procedure has been successfully used by McMasters and Gschneidner (22, 23, 24, 25, 26, 27) in their determination of the R.E.-Pb systems.

Periodically D.T.A. samples were inverted twice to assure good mixing of the alloys, and agreement with transformation temperatures previously determined was good. After being used for a number of runs, each D.T.A. crucible was sectioned, polished, and examined metallographically. Sections were taken from the top and bottom portions of the crucible. There were no indications of segregated alloys, or undissolved solute.

Cs, Ba, Hg, Tl, Pb and Bi have relatively low melting points (Table 2), and a concern was that portions of the solute would volatilize while sealing the Ta crucibles, used for D.T.A. Two methods of checking for this were used. In the arc-welding of Ta (21), a volatilizing component can be

seen as a different color in the Ta tip to Ta crucible arc. The second method involved weighing the amount of Ta lost during the welding process in full versus empty crucibles. If there was no difference in the weight lost, then it was assumed that no solute was lost. Negligible amounts of solute were lost because four inch long crucibles were used, and brass chill blocks were placed around the crucibles in order to absorb the heat.

The alloys were prepared for D.T.A. by the following methods. Re, Os, Ir, and Pt were in sponge form and the powder was placed on top of the premelted Pr. Hg was placed on top of the premelted Pr, in the Ta crucibles with an eye dropper. Tl corrodes very rapidly in air, so it was stored in distilled water and removed only when Tl was needed for alloying. Since Tl can be poisonous (28), all handling was done with either washable rubber or disposable plastic gloves. Pb was easier to handle because it could be left in air, and it was soft enough to cut with a razor blade. The easiest of the eight elements to work with was Bi because it did not corrode in air, and it was brittle enough to fracture into small pieces on shearing.

Since each crucible was used for several alloys, the attack of liquid Pr alloys on the Ta crucibles might be a concern. To see if this was a problem a 20.9 at.% Hg alloy, which had been used for eight D.T.A. runs was sectioned,

polished, and submitted for electron microprobe analysis, which had a lower detection limit of better than 0.1 wt.% Ta (29). Scans across the crucible showed no high Ta contents within the alloy, and a sharp delineation was obtained between the Ta crucible and the alloy. Metallographic examination of each of the D.T.A. crucibles further substantiated the above findings.

Techniques

The standard metallurgical techniques (30, 31) used for determining equilibrium diagrams were used in this study. For most of the systems, D.T.A. was used to determine the phase boundaries. Metallography and x-rays were used to confirm the D.T.A. results. Two systems (Pr-Hf and Pr-Re) were studied by quenching in the phase of interest and then analyzing chemically to establish the liquidus phase boundary.

Differential thermal analysis (D.T.A.)

The D.T.A. system used for this study was based on a design that had been used for a number of years by members of Dr. K. A. Gschneidner's group (22, 23, 24, 25, 26, 27). Several changes in the design were made because the maximum temperature was not as high as previously used; 1/2 inch diameter crucibles were used instead of 3/4 inch because of

a size limit in the D.T.A. apparatus and to conserve Pr; and a six-inch long constant heat zone was required to obtain the precision needed in this study. Figure 2 is a photograph of the system, which was designed to operate up to a maximum temperature of 1100 C. The vacuum chamber and sample holder arrangement are represented schematically in Figure 3.

The vacuum chamber was constructed of three inch, o.d. inconel tubing, which was selected because of its high temperature properties (32) and availability. A Veeco oil diffusion pump, model no. EP2W5, with a liquid nitrogen cold trap was used in conjunction with a Welch Dou-Seal Vacuum pump to evacuate the system. A bellows vacuum valve was located between the diffusion pump and the sample chamber, so that any time during an experiment, the sample chamber could be pressurized. A cold cathode gauge measured the vacuum from 10^{-3} to 10^{-6} torr, and when a partial atmosphere was in the system a compound gauge indicated the pressure in inches of Hg.

As shown in Figures 2 and 3 the top of the vacuum chamber had a brass cover plate containing the conax seal, through which the thermocouples entered the system. A stainless steel rod hung from the brass plate and, as Figure 3 shows, held the Ta sample holder. The two thermocouples were sheathed in alumina and held in place in the sample

holder by small circular alumina discs. One thermocouple went to the sample, while the other went to the Mo-standard. The weight of the samples rested on the thermocouple bead to insure good thermal contact. To minimize extraneous e.m.f.'s, all samples and the standard were covered with alumina crucibles which electrically isolated the thermocouples from the rest of the system.

The differential aspect of this apparatus comes from the fact that two identical thermocouple wires, one from the sample and one from the standard, are connected in series and this e.m.f. is fed to the Y-axis of an X-Y recorder. When the temperature difference between sample and standard is zero, then the Y-axis records zero. If a temperature difference develops, then a Δ e.m.f. is recorded. For example, at a melting point, on heating, the sample remains at a constant temperature while the Mo-standard continues to heat up. The X-axis records the temperature of the sample. Figure 4 represents a typical D.T.A. curve.

The furnace used to heat the samples is a Lindberg Hevi-Duty split tube furnace operating on 220 volt single phase current controlled by a variable transformer. One of the advantages of this furnace was its sluggish response time which made rapid cooling impossible, but allowed relatively easy control of the 2 to 5 C per minute heating and cooling rates. A second benefit was the split tube feature

which allowed more rapid cooling rates when samples needed to be changed.

Chromel-alumel thermocouples were used throughout this study. The thermocouples were calibrated against Pb, Zn, Cu-Ag eutectic, and Ag melting point standards. There was less than one degree difference between the temperatures recorded and those listed in Kehl (30) or certified by the National Bureau of Standards. The installed thermocouples were checked periodically by means of a Ag standard and when the measured temperature differed by more than $\pm$ 1 C the thermocouples were replaced. Temperatures reported in this study are believed to be known within $\pm$ 1 C for reaction horizontals and $\pm$ 2 C for liquidus curves. All the temperatures have been corrected to conform to the IPTS-68 scale (33). A distilled water-ice bath was used as the reference junction and the temperatures were measured by means of a Leeds and Northrup K-3 potentiometer using a d.c. null detector. The output was recorded on a Moseley X-Y recorder, model 7001AM. The sensitivities used were 0.5 mv per cm for the X-axis and 0.05 mv per cm for the Y-axis.

For some of the solutes, the liquid to solid or the α to β transformation boundaries could not be determined because of low solubility limits. The lowering or raising of the transformation temperatures was detected by replacing the Mo-

standard normally in the D.T.A. system with a crucible of pure Pr. If the solute lowers the transformation temperature, then, on heating, the D.T.A. curve will appear the same as if the Mo-standard is there; see Figure 4. However, on cooling, the pure Pr standard will transform first, and the D.T.A. curve will break in the opposite direction of the cooling curve shown in Figure 4. The converse is true if the solute raises the transformation temperature. This technique was used to determine the effect of Cs, Ba, Hf, Re, and Bi on the liquid to solid or α to β transformation.

Most of the phase boundaries, reaction temperatures, and compositions were determined by D.T.A. In the book, Phase Diagrams in Metallurgy, Rhines (34) points out that non-equilibrium cooling leads to coring and solidus temperatures that are too low. To avoid this, randomly selected samples from the systems studied were homogenized at temperatures slightly below the solidus. No difference could be detected in the solidi temperatures, so it was concluded that the alloys were solidifying under equilibrium conditions.

All eight of the systems for which extensive D.T.A. data were taken used several different samples of pure Pr for making the alloys. Each new crucible was made up with a composition that overlapped previous data. No difference was detected in the phase boundary temperatures measured when using different crucibles for a given solute in any of the

systems studied.

Metallography

Metallography was used mostly to confirm D.T.A. data. The majority of alloys were reactive in air, and precautions were necessary to protect the polished surfaces. All the alloys, except Pb, were mechanically polished under kerosene or alcohol and etched with either Roman's solution[1], nital (30), or air. Pr-Pb alloys were too soft to mechanically polish. However electropolishing (35) worked very well, and the surfaces remained protected in air for longer periods of time than mechanically polished alloys. Pr-Hg,-Tl, and -Bi alloys corroded very rapidly and all observations or photographs had to be taken quickly. For example, Hg alloys had to be observed through kerosene.

Eutectic compositions, solidus boundaries, and solubility limits were confirmed by metallography. Os, Ir, and Pt eutectic structures were lamellar in appearance.

---

[1]Koch, C. C., and Pickelesimer, M. L.: Trans. Met. Soc. AIME, May 1967, vol. 239, p. 759.

Roman's Solution

Lactic Acid	20 ml
Phosphoric Acid	5 ml
Acetic Acid	10 ml
Nitric Acid	15 ml
Sulfuric Acid	1 ml
Dimethylformamide	25 ml

X-Rays

X-ray techniques were used in confirming which phases were present and in attempts to determine solvus lines for several systems. All of the work was done with either a Debye-Scherrer powder camera or a Norelco diffractometer. All x-ray samples were sealed in 1/8 or 3/8 inch Ta tubing under a partial atmosphere of helium, and then sealed in vycor tubes to protect the Ta. The intermetallic compound in equilibrium with α- or β-Pr was studied for Os through Bi. The determination of the solvus, in either the α- or β-Pr region, by the x-ray parametric method, did not work for several reasons. Because of diffusion, powders bonded together at the solution treating temperatures. For the solvus in the α-Pr region, the solubilities were sufficiently low that the Pr lattice parameters had to be known to $\pm$ 0.0001Å and in general it is difficult to determine them to $\pm$ 0.001Å. The β-Pr phase in Hg, Tl, Pb, or Bi alloys could not be retained by quenching samples in ice water, liquid nitrogen, or brine. The method of protecting the Ta crucibles in vycor tubing makes rapid quenching difficult. Therefore a series of Hg alloys were sealed in Ta and heat treated in a vacuum and quenched into oil, but this did not retain β-Pr.

Glove box

Some of the more reactive samples had to be prepared in a glove box, which had a purified argon atmosphere. The atmosphere was monitored for oxygen and water by Meeco electrolytic oxygen and water analyzers. The oxygen and water levels were maintained at two to five ppm. The argon recirculation system also had a nitrogen removing furnace, but the nitrogen concentration was not monitored.

All Cs and Ba alloys, x-ray powder samples, and the majority of metallographic specimens were prepared in the glove box.

THE EQUILIBRIUM DIAGRAMS

Immiscible Liquid Systems

Cs and Ba

Cs and Ba both form immiscible liquids with Pr, as predicted by Mott's (8) analysis. The equilibrium diagram for Ba is shown in Figure 5, and one for Cs would be almost identical. The liquid to solid reaction is a monotectic reaction. The reaction horizontal in the Ba system is about 930 C or 4 C below the melting point of Pr. Adding Cs lowers the melting point of Pr about 1 C. The α to β transformation is an inverted peritectic, and D.T.A. data indicated the transformation temperatures for Cs and Ba were lowered by less than 1 C. Four alloys were used to determine the Ba system and one alloy was used for Cs. A 10.2 at.% Ba alloy was heated to 1580 C in a D.T.A. apparatus, and no indication was found for the liquidus which separates the single phase liquid solution from the two phase immiscible region. This indicates the liquidus rises steeply from the Pr-rich end of the diagram.

Figure 6 is a photograph of a sectioned D.T.A. crucible showing very clearly the immiscibility of the Ba system. All of the alloys were inverted several times during the homogenizing heat treatment to insure good mixing. Probably no compounds are formed in the Ba system because the 730 C

Table 1. Chemical analysis of Pr and the period six elements

	All compositions in ppm												Wet Chem. ppm (b)		
	O	N	H	Si	Mg	Ca	Cr	Fe	Ta	La	Ce	Nd	C	Ni	Fe
Pr[a]	154	243	8	<250	≤100	<200	<60	100	900	≤50	≤1000	≤600	79	54	4
Pr[a]	427	136	27	<250	50	200	≤600	30	500	≤50	≤1000	≤2000			
Cs[c]	80	N.D.	Alkali Metals 100				Other metals - 120								
Ba[a]	Al, Cu, Ca, Sr, Mg, and Si < 50						Wet Chemistry[b] N-70, C-40, Fe-<10, Mn-80								
Hf[d]	99.9%														
Re[a]	-			<100	<1000										
	Nothing else detected														
Os[d]	99.9+%														
Ir[e]	99.93%														
Pt[e]	99.99+%														
Au[f]	99.99														
Hg	Triply distilled. No analysis available.														
Tl[a]	99.999% Pb-5 Fe,Cu,Zn, and Cd-1; Bi, Si, and Mg-<1														
Pb[a]	99.999% Bi-1; Sb-4; Cu-.2; Ca,Fe,Mg,Si, and Ag-.1; As<.1														
Bi[a]	99.999% Zn-3.2; Fe-1.6; Pb-1; Sb,As, and Ag-<1; Cd-<.2; Cl_2<10 Cu-4														

[a]Ames Laboratory Spectographic Analysis.

[b]Wet chemical analysis performed by Anal. Chem. sect. of the Ames Laboratory.

[c]Analysis provided by Dow Chemical Co.

[d]Typical analysis supplied by United Mineral and Chemical Co. 1964.

[e]Typical analysis, Engelhard Industries.

[f]West Gold Refining Co.

arrest is slightly higher than the melting point of pure Ba, indicating the horizontal extends across the diagram.

Not enough data was taken for Cs to tell if compounds exist in the Pr-Cs system.

Limited Liquid Solubility Systems

Hf, Ta, W, and Re

The solubilities of Ta and W in liquid R.E. metals were determined by Dennison and co-workers (20), and the following equations describe their results for Pr:

$$\ln X_{Ta}^{liq.} = \frac{-8038}{T} - 3.138 \qquad (1)$$

$$\ln X_{W}^{liq.} = \frac{-16,684}{T} + 0.287 \qquad (2)$$

where $X_{Ta \text{ or } W}^{liq.}$ = atom fraction of Ta or W in liquid Pr.

T = temperature, K.

This form of representing the data was shown to be valid by Kleppa and Weil (36) in their study of the solubility of Cu in liquid Pb. Substituting the melting point of Pr into the above equations provides an estimate of the solubility of Ta or W in Pr, at that temperature. These values (20) are 0.0055 at.% Ta and 0.00013 at.% W. Neither Ta or W would be expected to affect the transformation temperatures because of their extremely low solubilities.

D.T.A. indicated that Hf and Re have a low solubility in liquid Pr, and the Pr rich liquidus, solidus, and α to β transformation boundaries could not be determined by D.T.A. The lowering of the melting point and allotropic transformation temperature was determined by the technique described earlier, page 13. Hf lowers the melting point and the allotropic transformation by about 1 C.

Re lowers the melting point approximately 5 C to 929 C, and lowers the α to β transformation temperature by less than 1 C.

To determine the liquidus, Ta crucibles, shown in Figure 1 (B), containing premelted Pr had arc-melted spheres of Hf and Re added to them. The crucibles were heat-treated in a high vacuum system capable of maintaining 2000 C. W/W-Re thermocouples, protected by BeO insulators were used to measure the temperatures. Samples were equilibrated at the temperature of interest for approximately one hour and then cooled at the fastest rate the system allows, about 100 C per minute. After the heat treatment, the crucibles were sectioned and the undissolved Hf or Re was removed. This is shown schematically in Figure 1 (B). The remaining alloy was then analyzed chemically for its Hf (37) or Re (38) content, and results are shown in the following table:

Table 2. Tabulation of some useful physical properties for the elements used in this study

Element	Crystal Structure (32)	Melting point C(85)	Atomic Volume Å/atom (85)	Radii C.N.=12 (16)	$\left(\frac{r_{solute}-r_{Pr}}{r_{Pr}}\right)$ r_{Pr} (16)	Electro negativity Difference (16)	Valence (16)	Debye Temp. Θ_D (85)	Density g/cm^3 (32)
Pr	HCP to 800	934[a]	34.56	1.828	-	-	3	137	6.77
	BCC to M.Pt.	α to β transformation temperature is 800 C[a]							
Cs	BCC	28.6	114.84	2.731	+49.4	0.34	1	40	1.903
Ba	BCC	725	63.20	2.236	+22.7	0.20	2	110	3.5
Hf	HCP to 1750C	2226	22.32	1.580	-13.6	-0.23	4	256	13.09
	BCC to M.Pt.	±30							
Ta	BCC	3004±30	17.92	1.467	-19.8	-0.42	5	247	16.6
W	BCC	3387	15.85	1.408	-33	-0.94	6	388	19.3
Re	HCP	3166±20	14.71	1.375	-25	-0.95	7	429	21.04
Os	HCP	3033±18	14.01	1.353	-26	-0.97	8	500	22.57
Ir	FCC	2447	14.15	1.357	-26	-1.02	9	425	22.5
Pt	FCC	1772	15.09	1.387	-24	-1.05	10	234	21.45
Au	FCC	1064.4	16.96	1.442	-21	-0.77	1	165	19.32
Hg	Rhombohedral	-38.87	23.38	1.594	-14	-0.65	2	75	13.55
Tl	HCP to 262	303±1	28.58	1.716	-6.2	-0.73	3	88	11.85
	BCC to M.Pt.								
Pb	FCC	327.4	30.32	1.750	-4.3	-0.80	4	102	11.36
Bi	Rhombohedral	271.4	35.40	1.689	- 7	-0.73	5	119	9.80

[a]Melting point obtained in this study.

Table 3. Composition versus temperature for Hf and Re

Temp. (C)	Composition (at.% HF)	Temp. (C)	Composition (at.% Re)
1805	3.24[a]	1763	4.50
1612	3.17[a]	1489	2.57
1412	1.77	1362	2.38
1205	0.26	1140	0.63
933	0.026[b]	929	0.24[b]

[a]The closeness of these compositions can quite possibly be attributed to the allotropic transformation in Hf, at 1750 C (32).

[b]Compositions obtained by substituting the eutectic temperatures into Equations 3 and 4.

A least squares analysis of the data yields the following two equations:

$$\ln X_{Hf}^{liq.} = \frac{-16,607}{T} + 5.507 \qquad (3)$$

$$\ln X_{Re}^{liq.} = \frac{-9,167}{T} + 1.560 , \qquad (4)$$

which describe the liquidus at the Pr-rich end of the diagrams. The liquidus lines for the Pr-Hf, -Ta, -W, and -Re alloys are shown plotted in Figure 7. These data clearly show why Ta and W make good crucibles for Pr-alloys. Figure 7 also shows the eutectic composition and temperature for Hf and Re alloys and the increased solubility of Hf and Re in liquid Pr as compared to Ta and W.

Group VIII Element Systems

Os, Ir, and Pt are lumped together because their equilibrium diagrams are similar. The diagrams have a eutectic reaction for the liquid to solid transformation and an inverted peritectic for the allotropic transformation.

Os

Figure 8 shows the equilibrium diagram for the Pr-rich end of the Pr-Os system. The eutectic reaction occurs at 670 ± 1 C and at 13.6 ± 0.1 at.% Os. The α to β transformation temperature is lowered from 800 C to 795 ± 1 C. As predicted (16), there is very little solid solubility in either phase--0.43 ± 0.05 at.% Os in β-Pr at 795 C and less than 0.2 at.% Os in α-Pr at 660 C. Figure 9 shows the eutectic structure of Os, which is also representative of Pr-Ir and Pr-Pt, Pr-rich eutectics.

A $PrOs_2$ compound was reported (18) for the system and x-ray results from this study showed that $PrOs_2$ was the compound in equilibrium with α-Pr.

Ir

The Pr-Ir system is shown in Figure 10. It can be seen that the eutectic temperature has been lowered 205 C to 729 ± 1 C from the melting point of Pr and the eutectic composition is 12.1 ± 0.1 at.% Ir. The α to β transformation

is lowered from 800 C to 793 ± 1 C. But as predicted (16) the solubilities are small, 0.35 ± 0.05 at.% Ir in β-Pr at 793 C and less than 0.2 at.% Ir in α-Pr at 782 C.

A $PrIr_2$ compound has been reported (18), but a 28.3 at.% Ir alloy examined metallographically appeared to be mostly single phase material with some eutectic at the grain boundaries. There were no lines from the $PrIr_2$ structure in the x-ray powder pattern. A La_7Ir_3 compound with a hexagonal $D10_2$ structure and a = 10.235 Å and c = 6.473 Å has been reported (39), but no intensity data was given. The powder pattern from the 28.3 at.% Ir alloy could not be indexed as being isostructural with the La_7Ir_3 structure.

Pt

For the Pr-Pt system, shown in Figure 11, the melting point of Pr is lowered to 718 ± 1 C by a eutectic reaction which has a composition of 13.4 ± 0.1 at.% Pt. The α to β transformation temperature has decreased from 800 C to 789 ± 1 C. As expected (16) the solubilities are low: at the inverted peritectic temperature 0.45 ± 0.05 at.% Pt, and at 690 C the solubility of Pt in α-Pr is less than 0.12 at.% Pt.

The compound that was reported to be richest in Pr was PrPt (40); with the FeB structure. This was confirmed to be the compound in equilibrium with α-Pr by taking an x-ray

powder pattern of filings from a 41.6 at.% Pt alloy.

The Pivotal System

Au

Au is considered to be a pivotal element in this study because it is the first element to show a solid solubility greater than 1 at.% in Pr. The form of the equilibrium diagram is the same as previously described for Os, Ir, or Pt and is shown in Figure 12. It can be seen that the eutectic temperature has decreased to 619 $\pm$ 1 C, and correspondingly, the eutectic composition has increased to 17.7 $\pm$ 0.1 at.% Au. The α to β transformation temperature is lowered from 800 C to 757 $\pm$ 1 C and the solubility at the inverted peritectic temperature is 1.56 $\pm$ 0.05 at.% Au. Metallography was used to confirm the solidus. A photograph of an alloy quenched from 790 C is shown in Figure 13 (B). This 1.2 at.% Au alloy was quenched from the liquid plus β-Pr region. The liquid phase shows up as the dark region surrounding the large white grains.

The solubility of Au in α-Pr is low, as predicted (16). From D.T.A. data, the solubility was estimated to be less than 0.12 at.% Au at 619 C and metallography indicated less than 0.10 at.% Au in Pr at 598 C.

Three different pure Pr samples were used in the study of the Pr-Au system, and for each new alloy, the compositions

overlapped previous data. In no instances were any discrepancies found in the phase boundary temperatures recorded.

X-ray powder samples taken from an 18.8 and a 33 at.% Au alloy showed the intermetallic compound in equilibrium with α-Pr was Pr_2Au, with the $PbCl_2$ type structure. The powder patterns were very poor in the back reflection region, and therefore lattice parameters have been calculated from front reflection lines. Pr_2Au has an orthorhombic structure with $\underline{a} = 7.13 \pm .01$, $\underline{b} = 5.01 \pm .02$, and $\underline{c} = 9.28 \pm .04$ Å. A listing of calculated $\sin^2\theta_c$'s and intensities compared with measured $\sin^2\theta_m$'s and intensities is shown in the Appendix.

The Pr-Au system had been studied by Rossi in 1934, as reported by Gschneidner (18). Rossi's diagram indicates no α to β transformation. The eutectic temperature is 19 C below that found in this study, and the eutectic composition is 1 at.% Au less. His diagram was determined with only six alloys compared to the 19 used in this investigation. Furthermore the purity of his Pr was considerably less than that used in this study.

The Eutectoid Systems

The last four elements examined in this study were Hg, Tl, Pb, and Bi, which are grouped together because all exhibit a eutectoid reaction for the α to β transformation. The

liquid to solid reaction is a eutectic transformation.

The Pr-Tl and -Pb equilibrium diagrams were determined by Vogel and Heumann in 1943, as reported by Gschneidner (18). The Tl diagram was determined with three alloys, the Pb diagram with five, and their expected similarity with La and Ce. This study used 16 alloys for the Pr-Tl and 36 alloys for the Pr-Pb systems. No chemical analyses were given for any of the components.

Hg

The most interesting feature in the Pr-Hg system, Figure 14, is the unexpectedly (16) large solubility shown in β-Pr, which at the eutectic temperature is 14.6 ± 0.2 at.% Hg. At the eutectoid temperature, 519 ± 1 C, the solubility is 12.0 ± 0.2 at.% Hg in Pr. Figure 15 shows photographs of some metallographic samples used to confirm the β-Pr solvus at 600 C. The 9.06 at.% Hg alloy shown in Figure 15 (B) was quenched from the (α+β)-Pr region and is typical of the microstructures obtained when alloys are quenched from the (α+β)-Pr regions (Pr-Tl systems). The light colored material in the center is some type of inclusion and is not associated with the Pr-Hg system. Figure 15 (C) was quenched from the β-Pr plus PrHg region, and the compound can be seen in the background.

The eutectic temperature, 624 ± 1 C, is about the same

as Au's. The α to β transformation temperature is lowered by 281 C, from 800 C to 519 ± 1 C. The eutectic composition is 20.3 ± 0.2 at.% Hg.

A PrHg compound, with the CsCl type structure has been reported (18). X-ray powder patterns taken from filings of Pr-rich, Pr-Hg alloys proved Pr-Hg to be the compound in equilibrium with α or β-Pr.

Tl

The Pr-Tl system, shown in Figure 16, exhibits extensive solid solubility: 9.0 ± 0.2 at.% Tl at the eutectic temperature, 767 ± 1 C, and 8.0 ± 0.2 at.% Tl at the eutectoid temperature, 687 ± 1 C. The maximum solubility of Tl in α-Pr is 2.5 ± 0.2 at.% Tl at 687 C. The eutectic composition is 13.9 ± 0.1 at.% Tl. Figure 17 shows photomicrographs of a hypoeutectic and a hypereutectic alloy.

Pr_3Tl, which has the Cu_3Au type structure and which undergoes an order-disorder transformation, was reported by Haschke and coworkers (41). A 24.95 at.% Tl alloy was prepared. Metallographic examination showed the alloy to be essentially single phase. X-ray powder samples confirmed the existence of the ordered and the disordered phases and showed that Pr_3Tl was the compound in equilibrium with Pr. Samples water quenched from 400, 500, 600 and 750 C indicated that the amount of ordered Pr_3Tl goes to zero at about

750 C. The lattice parameter for the ordered Pr_3Tl was determined from the sample water quenched from 400 C and a_o = 4.9353 ± .0001A. For the disordered phase, the lattice parameter was determined from the sample water quenched from 600 C and a_o = 5.0309 ± .0005A.

The sample quenched from 400 C showed only a slight amount of disordered phase, the 500 C sample had about 70% ordered and 30% disordered, the 600 C sample had 40% ordered and 60% disordered, and the 750 C sample had only disordered Pr_3Tl and α-Pr. Both phases could be distinguished in the x-ray powder patterns, except for the 750 C sample which had only disordered Pr_3Tl and α-Pr present. Estimates of the relative amounts of the phases present were performed visually.

Pb

Figure 18 shows the Pr-Pb system, which has a eutectic temperature of 824 ± 1 C and eutectoid temperature of 778 ± 1 C. The amount of Pb soluble in β-Pr is 3.5 ± 0.2 at.% Pb at 824 C and 3.1 ± 0.2 at.% Pb at 778 C. Pb's solubility in α-Pr is 2.2 ± 0.2 at.% Pb at 778 C, as determined by D.T.A. data, and about 1.3 at.% Pb at 760 C as determined by metallographic examination of quenched samples. The eutectic composition is 9.3 ± 0.1 at.% Pb. A photomicrograph of the eutectic structure is shown in Figure 9.

Powders filed from a 30.3 at.% Pb alloy were studied with x-rays, and the compound observed to be in equilibrium with Pr was Pr_5Pb_3 which crystallizes in the hexagonal $Mn_5Si_3(D8_8)$ type structure as reported by Jeitschko and Parthe (42).

Bi

The Pr-Bi system is shown in Figure 19. The maximum solubility of Bi in β-Pr is 0.8 at.% Bi at 894 C and is negligible in α-Pr. The melting point of Pr is lowered to 894 ± 1 C, and the eutectic composition is 3.2 ± 0.1 at.% Bi. Figure 13 (A) shows the Pr-Bi eutectic structure. The α to β transformation temperature is lowered by approximately 1 C.

A Pr_4Bi_3, anti-Th_3P_4, structure has been reported (43) for the Pr-Bi system. X-ray powder patterns and metallography for a 30.9 at.% Bi alloy have confirmed the structure.

General Summary of the Diagrams

The experimental data obtained can best be summarized by looking at Figures 20, 21, 22, and 23 and Table 4. All four figures show a periodic variation for the parameter being plotted versus the atomic number.

Figure 20 plots the liquid to solid reaction temperature against the atomic number of the solute. It is apparent from the Figure that the solutes Cs through Re lower the melting

point of Pr very little. The solubilities of Ta or W in liquid Pr are so low at the melting point that it is assumed they have no effect on the melting or α to β transformation temperature. Os lowers the melting point of Pr 264 C to 670 C. Ir's eutectic temperature is 59 C higher than Os at 729 C, and for Pt the eutectic temperature decreases 11 C to 718 C. A minimum occurs in the curve at Au and Hg, whose eutectic temperatures are 619 and 624 respectively. From Hg, the eutectic temperatures increase almost linearly through Tl at 767 C, to Pb at 824 C, and finally to Bi at 894 C. As Figure 20 indicates, the same type of periodic behavior occurs for the elements from the fourth and fifth periods of the periodic table dissolved in Pr (18, 44, 45, 46). Similar behavior occurs for the solutes from the fourth, fifth, and sixth periods dissolved in La (18, 22, 45, 47, 48, 49), Ce, (18, 44, 50, 51, 52, 53, 54, 55, 56), Sm (44, 57, 58, 59, 60), Gd (18, 27, 57, 61, 62, 63, 64, 65, 66), and Y (18, 59, 67, 68, 69, 70, 71, 72, 73, 74, 75).

Figure 21 represents the eutectic composition plotted against the atomic number of the solute. A very small composition is shown for Cs through Re and then the eutectic composition increases to a maximum at Hg of 20.3 at.% Hg. Next it decreases linearly through Tl at 13.9 at.%, Pb at 9.3 at.%, to Bi with a composition of 3.2

at.% Bi in Pr.

The data for the α to β transformation temperatures versus atomic number of the solute is shown in Figure 22. The most striking feature is the large minimum at Hg, which lowers the transformation temperature from 800 C for pure Pr to 519 C for Hg alloys. The temperatures for the solutes on either side of Hg increase asymetrically up to almost 800 C at Bi and Re. Adding the solutes Cs through Re to Pr has virtually no effect on the α to β transformation temperature. The effect of Ta or W was assumed to be negligible because of their low solubilities.

The most interesting and unexpected data (16) is shown in Figure 23, which plots the solubilities of the solutes in α and β-Pr. As mentioned in the discussion of the individual diagrams, very little solubility is shown for Os through Pt. At Au, the solubility in β-Pr increases to 1.56 at.% Au, and then it jumps to 14.6 at.% Hg in β-Pr. From Hg, the solubility decreases linearly to 9 at.% Tl, to 3.5 at.% Pb, and finally to 0.8 at.% Bi in β-Pr. The solubility in α-Pr also increases slightly to a peak at 2.5 at.% Tl and decreases to virtually zero at Au and Bi. Some of the possible reasons for the solubility behavior will be analyzed in the discussion section.

Table 4. Tabulated phase diagram data

Solute	Liquid to Solid Reaction			
	Reaction	Temp (C)	Comp. (at.% solute)	Solubility at the eutectic temp. at.% solute
Cs	Monotectic	<1[a]	negligible	undetermined for Cs, Ba, Hf, Ta, W, and Re
Ba	Monotectic	930-31	<0.8	
Hf	Eutectic	933	0.026	
Ta	Undetermined		0.0055	
W	Undetermined		0.00013	
Re	Eutectic	929	0.24	
Os	Eutectic	670	13.6	<0.2
Ir	Eutectic	729	12.1	<0.2
Pt	Eutectic	718	13.4	<0.08
Au	Eutectic	619	17.7	<0.12
Hg	Eutectic	624	20.3	14.6
Tl	Eutectic	767	13.9	9
Pb	Eutectic	824	9.3	3.5
Bi	Eutectic	894	3.2	0.8

[a]Reaction temperature is <1C below the melting point of Pr.

Reaction	α to β Transformation		
	Temp (C)	Max. Solubility of β at reaction temp (at.% solute)	Max. Solubility of α at reaction temp (at.% solute)
Inverted Pertectic (I.P.)	<1[a]	Negligible for Cs thru Re	
I.P.	<1[a]		
Eutectoid (E)	lower		
Undetermined	-		
Undetermined	-		
E.	lower		
I.P.	795	≤0.43	<0.2
I.P.	793	≤0.35	<0.14
I.P.	789	≤0.45	≤0.08
I.P.	757	1.56	≤0.12
E.	519	12.0	0.9
E.	687	8.0	2.5
E.	778	3.1	2.2
E.	<1[a]	<0.07	<0.07

THEORY

From basic thermodynamic principles (76), expressions can be written to describe the phase boundaries of a system. The first step will be to define some terms.

r = number of independent components

ν = number of phases

μ_r^ν = chemical potential of component r in phase ν

X_r^ν = atom fraction of component r in phase ν

$\bar{V}^\alpha$ = partial molal volume, phase α

$\bar{S}^\alpha$ = partial molal entropy, phase α

T = temperature, K

P = pressure

i,k = summation indexes

The thermodynamic state of a heterogeneous system can be described by an (r+1)-dimensional phase diagram space. $T,P,X_1^\beta, \ldots X_{r-1}^\beta$ are usually chosen as the variables which span this phase diagram space. To describe the thermodynamic state of the heterogeneous system in terms of the r+1 variables, Equation 5 is transformed from the

$$\sum_{i=1}^{r} X_i^\alpha (d\mu_i^\alpha - \bar{v}_i^\alpha \, dp + \bar{S}_i^\alpha \, dT) = 0 \qquad (5)$$

set of ν equations relating r+2 variables $(T,P,X_1^\beta \ldots X_r^\beta)$ to ν-1 equations relating r+1 variables $(T,P,X_1^\beta \ldots X_{r-1}^\beta)$.

At constant T and P the above equation is the familiar Gibbs-Duhem equation (13).

The total differential of the chemical potential of component i in phase β is expressed in terms of dT, dP, dX_k^β, k=1,...,r-1, where β is now the reference phase.

$$d\mu_i^\beta = \sum_{k=1}^{r-1} \left(\frac{d\mu_i^\beta}{dX_k^\beta}\right)_{T,P,X_{j\neq k}^\beta} dX_k^\beta - \bar{S}_i^\beta \, dT + \bar{v}_i^\beta \, dP \qquad (6)$$

For heterogeneous equilibrium,

$$d\mu_i^\alpha = d\mu_i^\beta \qquad \alpha=1,\ldots\nu, \text{ and therefore}$$

$$d\mu_i^\alpha = d\mu_i^\beta = \sum_{k=1}^{r-1} G_{ik}^\beta \, dX_k^\beta - \bar{S}_i^\beta \, dT + \bar{v}_i^\beta \, dP, \qquad (7a)$$

where

$$G_{ik}^\beta = \left(\frac{d\mu_i^\beta}{dX_k^\beta}\right)_{T,P,X_{j\neq k}^\beta} \qquad (7b)$$

Equation 7 is substituted into Equation 5 and the result is

$$\sum_{k=1}^{r-1} \sum_{i=1}^{r} X_i^\alpha G_{ik}^\beta \, dX_k^\beta + \sum_{i=1}^{r} X_i^\alpha (\bar{S}_i^\alpha - \bar{S}_i^\beta) dT + \sum_{i=1}^{r} X_i^\alpha (\bar{v}^\beta - \bar{v}^\alpha) dP. \qquad (8a)$$

let

$$G_k^{\alpha\beta} = \sum_{i=1}^{r} X_i^\alpha \, G_{ik}^\beta \qquad (8b)$$

Equation 8 is now equivalent to a set of Gibbs-Duhem equations subject to the equilibrium condition of Equation 5. Since $G_k^{\alpha\beta} = 0$, when $\alpha=\beta$, Equation 8 becomes a set of ν-1 differential equations in r+1 variables (dT, dP, dX_1^β, ... dX_{r-1}^β).

The coefficients are usually written to conform to experimentally measurable quantities.

$$\bar{S}_i^\alpha - \bar{S}_i^\beta = \frac{\bar{h}_i^\alpha - \bar{h}_i^\beta}{T} = \frac{\bar{L}_i^{\beta\to\alpha}}{T} \tag{9a}$$

$\bar{h}_i^\alpha$ and $\bar{h}_i^\beta$ are the partial molal enthalpies of component i in phase α or β, and $\bar{L}_i^{\beta\to\alpha}$ is the differential heat of transfer at constant pressure of component i from phase β to α.

$$L^{\alpha\to\beta} = \sum_{i=1}^{r} X_i^\alpha \bar{L}_i^{\alpha\to\beta} \tag{9b}$$

$L^{\alpha\to\beta}$ is the molal differential heat of transfer from phase α to β.

Similarly, the expression for the volume can be expressed as,

$$\Delta v^{\alpha\to\beta} = \sum_{i=1}^{r} X_i^\alpha (\bar{v}_i^\beta - \bar{v}_i^\alpha) = \sum_{i=1}^{r} X_i^\alpha \, \Delta\bar{v}_i^{\alpha\to\beta} \tag{10}$$

where $\Delta v^{\alpha\to\beta}$ is the change in volume of the system when a mole of phase α is transferred to an infinite amount of phase β.

Equation 8 can now be written as,

$$\sum_{k=1}^{r-1} G_k^{\alpha\beta}\, dX_k^{\beta} - \frac{L^{\alpha\to\beta}}{T}\, dT + \Delta v^{\alpha\to\beta}\, dP = 0. \qquad (11)$$

From Equation 11 and the experimental information concerning $G_k^{\alpha\beta}$, $L^{\alpha\to\beta}$, and $\Delta v^{\alpha\to\beta}$ as functions of T, P, and X_k^{β} it is possible to predict states of coexistence.

Consider the system where $\nu=2$ and $r=2$, then choose phase 1 as the reference phase. The variables describing the system are T, P, and X_2^1. Equation 11 can be written as,

$$G_2^{21}\, dX_2^1 - \frac{L^{2\to1}}{T} + \Delta v^{2\to1} dP = 0. \qquad (12a)$$

If phase 2 is chosen as the reference phase, the variables describing the system are T, P, and X_2^2, and Equation 11 becomes,

$$G_2^{12}\, dX_2^2 - \frac{L^{1\to2}}{T}\, dT + \Delta v^{1\to2}\, dP = 0. \qquad (12b)$$

Using Equations 8b, 9b, and 10; the Gibbs-Duhem relationship; and

$$g_{22}^1 = \frac{G_{22}^1}{RT} X_2^1 \text{ and } g_{22}^2 = \frac{G_{22}^2}{RT} X_2^2, \text{ then}$$

substituting g_{22}^1 and g_{22}^2 into Equation 12a and 12b, the following equations are obtained:

$$g_{22}^1 \left(\frac{X_2^2 - X_2^1}{X_1^1\, X_2^1}\right) dX_2^1 + \left(\frac{X_1^2 \bar{L}_1^{12} + X_2^2 \bar{L}_2^{12}}{RT^2}\right) dT - \left(\frac{X_1^2 \Delta\bar{v}_1^{12} + X_2^2 \Delta\bar{v}_2^{12}}{RT}\right) dP = 0, \qquad (13a)$$

and

$$g_{22}^{2}\left(\frac{x_2^2-x_2^1}{x_1^2\ x_2^2}\right)dx_2^2 + \left(\frac{x_1^1\bar{L}_1^{12}+x_2^1\bar{L}_2^{12}}{RT^2}\right)dT - \left(\frac{x_1^1\Delta\bar{v}_1^{12}+x_2^1\Delta\bar{v}_2^{12}}{RT}\right)dP = 0. \tag{13b}$$

Equations 13a and 13b are alternate, equivalent equations that define surfaces of coexistence in three-dimensional phase-diagram space. In the usual representation, one of the variables is held constant, and then the equations involve only two-dimensions and can be written as,

$$\left(\frac{dT}{dx_2^1}\right)_p = g_{22}^{1}\left(\frac{x_2^1-x_2^2}{x_1^1\ x_2^1}\right)\frac{RT^2}{x_1^2\bar{L}_1+x_2^2\bar{L}_2}, \tag{14a}$$

and

$$\left(\frac{dT}{dx_2^2}\right)_p = g_{22}^{2}\left(\frac{x_2^1-x_2^2}{x_1^2\ x_2^2}\right)\frac{RT^2}{x_1^1\bar{L}_1+x_2^1\bar{L}_2}. \tag{14b}$$

Equations 14a and 14b represent the coexistence of pairs of phases in equilibrium at constant pressure and, according to Wagner (2), they could be used to construct the phase boundaries of a binary equilibrium diagram, provided certain starting points were given. Beginning from the melting point of one of the components, these equations describe the initial slope of the liquidus and solidus. The complete curves can be obtained on integration, but this requires a knowledge of the heats of transformation and the activity coefficients as functions of temperature and

composition. For most systems this information is not available. Therefore, if any progress is to be made in the theoretical calculation of equilibrium diagrams, approximations must be introduced.

Consider a two-component, two-phase, liquid-solid system. By rewriting equations 14a and 14b and solving for $\bar{L}_1$ the following equation can be obtained,

$$\bar{L}_1 \frac{dT}{RT^2} = g_{22}^2 \, d \ln X_1^2 - g_{22}^1 \, d \ln X_1^1. \qquad (15a)$$

Now

$$g_{22}^1 = 1 + \frac{d \ln \gamma_2^1}{d \ln X_2^1} \quad \text{and} \quad g_{22}^2 = 1 + \frac{d \ln \gamma_2^2}{d \ln X_2^2}, \qquad (15b)$$

where γ = activity coefficient. The expressions for g_{22}^1 and g_{22}^2 can be derived by substituting,

$$\mu_i^\beta = \mu_i^{0,\beta}(T,P) + RT \ln \gamma_i^\beta X_i^\beta$$

into Equation 7b. Substituting Equation 15b into 15a and using the Gibbs-Duhem Equation allows the following equation to be derived:

$$\bar{L}_1 \frac{dT}{RT^2} = d \ln\left(\frac{X_1^2}{X_1^1}\right) + d \ln \left(\frac{\gamma_1^2}{\gamma_1^1}\right). \qquad (16)$$

Up to this point, Equation 16 is still perfectly general.

If $\bar{L}_1$ is independent of temperature, then Equation 16 can be integrated to yield the following,

$$\frac{\bar{L}_1}{T_1}(T-T_1) + RT \ln\left(\frac{1-X_2^2}{1-X_2^1}\right) = RT \ln \frac{\gamma_1^1}{\gamma_1^2} \qquad (17)$$

where T_1 = the melting point or allotropic transformation temperature of pure component 1.

For the liquid to solid transformation in Pr- alloys.

$$\bar{L}_1 = \Delta H^{Pr}_{Fus.} = (\Delta S^{Pr}_{Fus.})T_1$$

and then Equation 17 becomes

$$\frac{\Delta H^{Pr}_{Fus}}{T_1}(T-T_1) + RT \ln \frac{1-X_2^2}{1-X_2^1} = RT \ln \frac{\gamma_1^1}{\gamma_1^2} . \qquad (18)$$

For an ideal solution, the activity coefficients are assumed to be equal to one, and

$$\gamma_1^1 = \gamma_1^2 = 1,$$

then Equation 18 reduces to,

$$\frac{\Delta H^{Pr}_{Fus}}{T_1}(T-T_1) = -RT \ln\left(\frac{1-X_2^2}{1-X_2^1}\right). \qquad (19)$$

Equation 19 applies equally well to the allotropic transformation by replacing the enthalpy of fusion with the enthalpy of transformation and the melting point with the transformation temperature.

Using Equation 19, the transformation temperatures of Pr and the experimental phase boundaries, the $\Delta H^{Pr}_{Fus.}$ and the

$\Delta H^{Pr}_{Transf.}$ were calculated, and the results are shown in Figures 24, 25, 26, and 27. If ideal solution theory applies, then $\Delta H^{Pr}_{Fus.}$ and $\Delta H^{Pr}_{Transf.}$ should be constants. The Figures clearly show that this is not true for the liquid to solid transformation, although for Os, Ir, Pt, and Au, if it is assumed that $\Delta H^{Pr}_{Fus.}$ is only known within 10%, then the calculated values are reasonable. Hg, Tl, Pb, and Bi do not follow ideal solution theory, for the liquid to solid reaction. For the α to β transformation the calculated $\Delta H^{Pr}_{Transf.}$ follows ideal solution theory reasonably well, except for Os and Pb (Figures 26 and 27). This seems to be the reverse of what would be expected; normally a liquid solution, because of the mobility of its atoms is considered more likely to be ideal than a solid solution.

Most of the curves appear to increase very rapidly within 5 or 10 C of either the melting point or the α to β transformation temperature. This is because the phase boundaries are not known accurately enough in this region.[1] For small X_2^2 and X_2^1 compositions Equation 19 becomes,

$$\frac{\Delta H_{Fus}}{T_1}(T-T_1) = -RT(X_2^1-X_2^2),$$

---

[1] It is estimated that the compositions need to be known within 0.01 at.% and temperatures within 0.1 K in this region in order to get any meaningful results.

which clearly demonstrates how important it is to know the exact difference in the phase boundaries.

Starting from the equivalency of partial molal free energies of one component in two phases, in equilibrium, Jones (9) was able to derive the phase boundaries for the liquid to solid reaction of Ge, Ga, Zn, and Ni in Cu and Sn, In, and Cd in Ag. Gschneidner and Waber (7, 77), using the same analysis showed the equations could be generalized for the equilibrium between any two phases. Using the equilibrium conditions given in Mott and Jones (78),

$$\frac{dG_1}{dX_2^1} = \frac{dG_2}{dX_2^2} = \frac{G_1 - G_2}{X_2^1 - X_2^2} , \tag{20}$$

where G is the free energy, and can be written as

$$G_1(X_2^1,T) = E_1(X_2^1) - TS_1^M - T\int_o^T \frac{C_v^1}{T}\, dT + \int_o^T C_v^1\, dT. \tag{21}$$

E, the internal energy, replaces H, the enthalpy because in solids the difference between them is a PV (pressure x volume) term, and this is negligible. Let,

$$g_1 = E_1(X_2^1) - T\int_o^T \frac{C_v^1}{T}\, dT + \int_o^T C_v^1\, dT \tag{22}$$

and assume random entropy of mixing, then

$$G_1(\bar{X}_2^1) = g_1 + \bar{R}\bar{T}\,[\bar{X}_2^1 \ln \bar{X}_2^1 + (1-\bar{X}_2^1)\ln(1-\bar{X}_2^1)] \tag{23}$$

Using the equilibrium condition, Equation 20, and the expression for the free energy, Equation 23; two relationships can be derived.

$$RT \ln \frac{X_2^2(1-X_2^1)}{X_2^1(1-X_2^2)} = \frac{dg_1}{dX_2^1} - \frac{dg_2}{dX_2^2} \tag{24a}$$

$$RT \ln\left(\frac{1-X_2^2}{1-X_2^1}\right) = g_1-g_2-X_2^1 \frac{dg_1}{dX_2^1} + X_2^2 \frac{dg_2}{dX_2^2} \tag{24b}$$

At the melting point of a pure component, the free energy of the liquid and solid is equal, and at a temperature not too far removed from the melting point, the change in free energy can be written as (79)

$$g_1(O,T)-g_2(O,T) = \frac{\Delta H_{Fus}}{T_1}(T_1-T) + \int_{T_1}^{T}(C_v^1-C_v^2)dT - T\int_{T_1}^{T}\frac{C_v^1-C_v^2}{T}dT. \tag{25}$$

The last two terms were considered negligible (9). If the following approximation is made,

$$[g_1(X_2^1,T)-g_1(O,T)]-[g_2(X_2^2,T)-g_2(O,T)]=[E_1(X_2^1)-E_1(O)]-[E_2(X_2^2)-E_2(O)], \tag{26}$$

which says the free energy difference between two phases,

at any temperature, is equal to the change in internal energy, at O K, then using equations 22, 24, 25, and 26 the following two expressions can be derived.

$$\frac{\Delta H_{Fus}}{T_1}(T-T_1) + RT \ln\left(\frac{1-X_2^2}{1-X_2^1}\right) = [E_1(X_2^1)-E_1(O)] - [E_2(X_2^2)-E_2(O)]$$

$$-X_2^1 \frac{dE_1}{dX_2^1} + X_2^2 \frac{dE_2}{dX_2^2} = J \qquad (27a)$$

$$RT \ln \frac{X_2^2(1-X_2^1)}{X_2^1(1-X_2^2)} = \frac{dE_1}{dX_2^1} - \frac{dE_2}{dX_2^2} = K \qquad (27b)$$

These equations are called the J and K functions after Gschneidner and Waber (7). The left hand side (l.h.s.) of Equation 27a is identical to the l.h.s. of Equation 18, and therefore the ratio of the logarithm of the activity coefficients must equal the right hand side (r.h.s.) of Equation 27a.

Independently of Jones' work (9), Betterton and Frye (10) arrived at similar results for the description of the α to β phase boundaries in the Ti and Zr systems. For their analysis to be applicable, Equation 27b must be a constant, and for the systems they studied, K was almost a constant.

Solving for K requires knowledge of both the liquidus and the solidus compositions, and until this study, the information was not available for Pr. Substituting the experimentally determined phase boundary compositions into Equation 27b established that K was not a constant for the solutes studied, and therefore Betterton and Frye's (10) analysis is not applicable. Figure 28 shows the K-function for the liquid to solid transformation in the Pr-Tl system, and it clearly demonstrates that K is not constant. The other Pr systems show similar behavior for the K-function.

Jones (9) suggested that the internal energies be written as a power series because in the dilute solution region the familiar van't Hoff freezing point depression formula is obtained (79).

$$E_1(X_2^1) = a^1 + b^1X_2^1 + c^1(X_2^1)^2 + d^1(X_2^1)^3 + \ldots \quad (28a)$$

$$E_2(X_2^2) = a^2 + b^2(X_2^2) + c^2(X_2^2)^2 + d^2(X_2^2)^3 + \ldots \quad (28b)$$

Waber and Gschniedner (77) suggested carrying the expansion beyond the second order term, used by Jones (9) because J and K can be calculated from equilibrium diagram data, and, in principle, it should be possible to solve the equations. Substituting Equations 28a and b into Equations 27a and b gives,

$$J = -c^1(x_2^1)^2 - 2d^1(x_2^1)^2 + c^2(x_2^2)^2 + 2d^2(x_2^2)^3 + \ldots, \quad (29a)$$

$$K = B + 2c^1x_2^1 - 2c^2x_2^2 + 3d^1(x_2^1)^2 - 3d^2(x_2^2)^2 + \ldots , \quad (29b)$$

where $B = b^1 - b^2$.

A computer program[1] was prepared that allowed for the solution of J up through six unknown coefficients by solving the equations simultaneously, using a Gauss expansion.

If there are six unknown coefficients, then six temperatures and their corresponding liquidus and solidus values are needed to solve the equations for the coefficients. Selection of the temperatures for the solution of the equations is arbitrary, and many different combinations of temperatures were tried. The smallest temperature interval used was a two degree difference, and the largest was a fifty degree temperature difference. None of these solutions gave very good agreement between calculated J values and experimentally determined J's, except at the temperature selected for solving the equations. The coefficients changed both sign and magnitude as the temperature interval between

---

[1]The computer program was prepared by Margo Johnson, Research Helper in the Computer Operations Group 1 of the Ames Laboratory, Iowa State University. 1969.

temperatures used for solving the equations changed. For the fifty degree temperature interval, the calculated J, using the coefficients virtually exploded between the temperatures selected for solving the equations.

When the internal energy is written out to second degree, then Equation 27a is equal to the regular solution model, and the excess free energy terms are equivalent to those suggested by M. F. Simmons (80). This did not give very good results either, and it was concluded that a regular solution model does not apply to these alloys.

From this analysis, it appears that the expansion of the internal energy as a power series does not provide a very good description of the system. However, Lupis (81) has shown that a polynomial expansion of the thermodynamic parameters can be valid for certain regions, and for the Fe-C-S, Fe-C-Si, and Fe-C-Co systems, he obtained satisfactory results between theory and experiment. In view of this, it may be that our method of solution is inadequate, and by using a different method of solving for the coefficients, the power series expansion of the internal energy would be shown to be valid.

Tiller and Hiskes (3) have used Equation 27a to describe the equilibrium between two components, but instead of using a power series expansion of the internal

energy, they expand the r.h.s. of Equation 27a in terms of a double Taylor series expansion in temperature and composition. Their equation also includes the heat capacity terms, which Jones (9) considered to be negligible. They require accurate phase diagram data, and then, using that, they calculate the thermodynamic properties of the system. For three solid solution systems, Ag-Au, Bi-Sb, and Ge-Si (4), their calculated thermodynamic properties agree extremely well with the experimental data that is available. Recently, they (5) extended their analysis to some simple eutectic systems, Ag-Si, Ag-Cu, Cd-Zn, and Pb-Sn, for which they claimed only good agreement between their calculated thermodynamic values and experimentally determined ones. Chiotti and co-workers (6) are also attempting to obtain thermodynamic properties from the phase diagram and vice versa. Their work has shown encouraging results for some simple systems.

The difficulty in applying the above analyses to the systems in this study is that intermetallic compounds exist, and not enough information is known about them. The minimum data needed would be the liquidus between the eutectic and the melting point of the compound and this study does not include that. It would also be necessary to know the melting points, crystal structures, heats of formation, and heat capacities. Before real progress can be made with the above

techniques (3, 6), more experimental information is necessary.

Another thermodynamic parameter that has been used by various investigators (11, 77, 82, 83, 84) to indicate phase stability can be derived as follows:

$$\frac{d \ln K}{dT} = \frac{\Delta\bar{H}}{RT^2} \text{ , where} \qquad (30)$$

K = equilibrium constant, and

$\Delta\bar{H}$= the change in partial molal enthalpy for a component transforming from one phase to another.

K is equal to $K = \frac{a_2^2}{a_2^1}$, where the a_2^2 and a_2^1 represent the activities. These can be written as

$$a_2^1 = \gamma_2^1 x_2^1$$

and

$$a_2^2 = \gamma_2^2 x_2^2$$

If ideal solution theory holds, $\gamma_2^1=\gamma_2^2=1$, then K can be written in terms of its atom fraction, and Equation 30 becomes,

$$d \ln \frac{x_2^2}{x_2^1} = \frac{\Delta\bar{H}}{RT^2} dT. \qquad (31)$$

$\Delta\bar{H}$ is redefined as Q, to conform to previous investigators (11, 77, 82, 83, 84). If Q is considered to be independent of temperature, Equation 31 can be integrated to yield,

$$\ln \frac{x_2^2}{x_2^1} = \frac{-Q}{RT} \text{ ,} \qquad (32)$$

where the constant of integration, after Worner (84), has been shown to be negligible.

Equation 32 would be identical with Equation 27b if the $1-X_2^1$ and $1-X_2^2$ terms cancel each other, which for dilute solutions is a good approximation. The similarity between Equations 27b and 32 clearly shows that Q represents the change in partial molal enthalpy for one component transferring from phase 1 to phase 2. This analysis can be applied equally well to either the liquid to solid or the α to β transformation, and Figures 29 and 30 show how Q varies with respect to atomic number for the solutes examined in this study. The periodic variation of Q with atomic number and its usefulness will be discussed later.

DISCUSSION

Factors Affecting Solid Solution Behavior

As indicated on p. 29 the four Figures 20, 21, 22, and 23 and Table 4 essentially summarize the experimental data obtained in this study. The actual phase diagrams are shown in Figures 5, 7, 8, 10, 11, 12, 14, 16, 18, and 19. These data represent the first critical look at the R.E.-rich end of the equilibrium diagrams involving an entire period of the periodic table.

Figure 23, which represents the solubility of the various solutes in the two crystal forms of Pr, is probably the most interesting of the figures, because of the unpredicted (16) large solubilities exhibited by Hg and Tl. If Table 2 listing the standard alloying criteria is examined, the most likely elements to be soluble on the basis of size are Pb, Tl, Bi, Hf, and on the lower end of the ± 15% size rule (12), Hg. The electronegativity differences[1], except for Hf, are all greater than the ± 0.4 electronegativity units difference suggested by Darken and Gurry (13) for extensive solubility to occur. The valencies, except for Tl, are different from Pr. From this collected

---

[1]Although both Cs and Ba have electronegativity difference less than ± 0.4 electronegativity units these solutes were not considered in this discussion because Mott's analysis (8) predicts them to form immiscible liquids.

data it would appear the element most likely to be soluble would be Hf.

The results presented in Table 3 as calculated from Equation 3 shows the solubility of Hf in Pr at the reaction temperature is less than 0.026 at.% Hf. The solute with the maximum solubility in β-Pr is Hg, and as Figure 23 shows, the solubility decreases linearly through Tl, Pb, and Bi.

A factor that has not been considered much in connection with the extent of primary solid solution, and may very well play an important role in the alloying behavior of an element, is the Debye temperature, Θ_D.[1] Table 2 lists the Θ_D's as determined from specific heat data and Figure 31 shows the same values plotted as a function of their atomic numbers (85).

If a solid (86) is regarded as being made up of 3N harmonic oscillators, the total energy of the solid is proportional to the Θ_D. In Debye's model, for the specific heat of a solid the Θ_D represents the high frequency limit for a particular material. A higher Θ_D means that a solid has more energy than one with a smaller Θ_D, and this implies a more rigid lattice or at least one that requires more energy to separate the atoms.

---

[1] K. A. Gschneidner, Iowa State University, Ames, Iowa. Private communication. 1969.

With this in mind, it seems quite probable that for extensive solubility to occur the Θ_D's should be similar. Large differences in Θ_D, i.e. the solute being 25% $\pm$ 5% larger than the solvent, implies a large difference in elastic properties, and associated with this would be a corresponding energy increase. On the other hand solutes with a Θ_D less than the solvent should have an easier time adjusting to the host lattice because an element's compressibility increases as Θ_D becomes smaller (78), and therefore the solute should be more adaptable. This indicates that the difference in Θ_D's when $\Theta_D^{solute} < \Theta_D^{Pr}$ could quite easily be larger than the suggested upper limit.

Figure 31 shows that Cs, Ba, Hg, Tl, Pb, and Bi all have Θ_D's less than 125 K. Cs and Ba will be excluded from the remainder of the discussion because of their large size difference, and Mott's (8) analysis predicted them to be immiscible. Au, which has a solubility in β-Pr of 1.56 at.%, has a Θ_D of 165 K or within about 20% of the 137 K listed for Pr. For Hf, Ta, W, Re, Os, Ir, and Pt the Θ_D's are larger by at least 100 K, or 73%, and all of these elements have limited solubility. Except for Hf, there is no reason to be concerned with Θ_D because the size factor, electronegativity, and valence of each element indicate limited solubility. Although Au's solubility is still in the less than 5 at.% solute, or in the limited solubility range,

its 1.56 at.% solubility is larger than the nine previous elements, and from Table 2, it appears the only factor this could be related to is its θ_D. For Hg it is very likely that electronegativity is the controlling factor, because the size factor, the valence, and the Debye factor all favor extensive solid solution. All the factors are favorable for extensive solid solution to occur in Tl, except for the electronegativity difference. For Pb and Bi all factors are favorable, except for the electronegativity difference and the relative valence factor.

These data certainly show the importance of the size factor in controlling limited versus extensive solid solution behavior, for without a favorable size factor the other terms need not be considered. However to determine the maximum extent of primary solid solution formation all of the factors must be considered, and it is a complicated interplay of all of the factors that actually determines the solubility limit. In this study there does not appear any simple way to isolate a particular factor as the determining one.

Thermodynamic Parameters and Their Uses

In the theory section, the Q factor was derived and shown to be equivalent to the change in partial molal enthalpy for one component transferring from phase 1 to phase 2. Various

investigators (11, 77, 82, 83, 84) have shown Q to have a periodic behavior, for solutes from the same period of the periodic table, dissolved in a given solvent. This is true for either the liquid to solid reaction, Q_L, or the α to β transformation, Q_S, and Figures 29 and 30 show this periodicity as a function of the atomic number of the solute. Q values were assumed temperature independent to enable Equation 31 to be integrated. For Os through Au, this is a good approximation, while for Hg through Bi, Q varies more with temperature. The plotted Q_L values were calculated at 21 C below the melting point of Pr, while the Q_S values were calculated at from 5 to 11 C below the transformation temperature.

All of the Q_L and Q_S values shown in the figures are positive, indicating a lowering of the particular transformation temperature. Cs, Ba, Hf, and Re would also have positive Q_L and Q_S values because they lower the transformation temperatures. The phase boundaries could not be determined for these four systems, so an exact Q_L or Q_S value was not calculated. It was not possible to determine whether Q values would be positive or negative for Ta or W because of the small solubility of these solutes in Pr.

A negative Q_L or Q_S value indicates a transformation temperature has been raised, such as a peritectic reaction. Negative Q_L values have been calculated for Nb and V in La

(18, 45) or Ce (18, 52) and V in Sm (57) or Gd (57). Positive Q_L values would occur for Cr in Gd (57), Dy (57), or Er (57); Cr (67), Mo (18), W (18), Nb (18), and Ta (71) in Y; V (57) in Dy; V (57) and Nb (87) in Er. V and Nb are in the same column of the periodic table as Ta and since Pr is expected to act as a solvent in the same manner as La, Ce, and Sm Q_L for Ta would be predicted to be negative. Not enough data is available for W to make a prediction.

Uy and Burr (83, 88) have shown the phase stabilized for some Zr and Th based alloys was related to the Pauling valency. Those solutes with a valency less than the solvent stabilized the low temperature phase, while for solutes with a valency greater than the solvent, the high temperature phase was stabilized. For the solutes used in this study, the above analysis does not apply for either transformation when Pb or Bi are the solutes.

If the Pauling valencies are replaced by the number of electrons outside the last filled shell minus the valence of Pr and this is plotted against Q_L or Q_S, then Figures 32 and 33 are obtained. A minimum occurs in the Q_L value at Tl, which has the same number of valence electrons as Pr. From Tl, the Q_L increases almost linearly for solute valences larger or smaller than Pr. For Q_S, the minimum occurs at Pb and then increases for solutes on either side of Pb. No experimentally determined value appears for Bi because the

phase boundaries were not determined.

According to Uy (88), a large mismatch, sizewise, between the solute and the solvent leads to a large |Q| value. For Q_L values, this is followed reasonable closely (see Table 2 for atomic volumes), while for Q_S it is followed except for Au, which has the highest Q_S but not the largest volume difference. Uy (88) also suggests that at small relative valence factors, the size factor is significant. For Hg, Tl, Pb, and Bi, Figures 32 and 33 show the valence difference to be one or less. The size factor is favorable except possibly for Hg. This implies that the controlling factor is either the electronegativity, or the Debye factor. In point of fact, as was mentioned earlier the extent of primary solid solution is controlled by a number of factors that are difficult to separate into their individual contributions.

There are several practical uses for Q values, as suggested by Dwight (82). Conflicting equilibrium diagram data could be resolved by the calculation of their respective Q values. The value falling closest to the extrapolated or interpolated curve would more likely be the correct diagram. Secondly, the sign of Q gives an indication of whether an element is a high or low temperature phase stabilizer. Thirdly, the magnitude of Q provides an indication of the extent of solubility, a low |Q| value being

indicative of more solubility. For Bi, a predicted Q_S would be approximately 1000 cal/mole and it would be a β-Pr stabilizer, which was proven experimentally.

Kleppa and Weil (36) have shown that

$$\ln X_2^{liq.} = \frac{\Delta S_{Fus} + \Delta \bar{S}^{XS}}{R} - \frac{\Delta \bar{H}}{RT} . \qquad (33)$$

This is identical with Equation 32, if the constant of integration is assumed to be the entropy term and there is no solubility in the solid phase. When lnX is plotted against 1/T, the slope gives $\Delta \bar{H}/R$ and the intercept gives the entropy term. If the liquid is in equilibrium with the solid and the enthalpy of fusion is known, then excess quantities can be calculated. For Hf, Ta, W, and Re, the partial molal enthalpy and entropy are given in the following table.

Table 5. Calculated partial molal enthalpies and excess partial molal entropies for Hf, Ta, W, and Re

	$-\Delta \bar{H}$ (cal/mole)	$S_{fus.}$ (85) (e.u.)	$\bar{S}^{XS}$ (e.u.)
Hf	18,200	1.76	+9.18
Ta (20)	15,970	1.76	-4.47
W (20)	33,160	2.31	-2.06
Re[a]	33,000	2.29	+0.82

[a]Savitskii and co-worker (89), using arc-melting techniques, report preparing $PrRe_2$, but Elliott (90) mixing stoichiometrical amounts of Pr and Re, reported only Pr and Re after liquid phase sintering.

Weeks (91) reports the treatment of Kleppa and Weil (36) should hold for systems involving less than 4 at.% solute and essentially pure metal in equilibrium with liquid.

This analysis must be tempered by the fact only four alloys were used to determine the liquidus for Re and only four for Hf, but the results are at least qualitatively correct.

Equation 27a was defined (7) as the J function, and it is equivalent to the r.h.s. of Equation 18, which is the difference in the logarithms of the activity coefficients. From Darken and Gurry (13), the logarithm of the activity coefficients can be written as

$$\Delta\bar{F}_1^{XS,1} = RT \ln \gamma_1^1$$

and

$$\Delta\bar{F}_1^{XS,2} = RT \ln \gamma_1^2 \quad .$$

These excess partial molal free energies are convenient when a comparison is to be made with excess partial molal entropies and relative partial molal enthalpies. Equation 18 can be rewritten as,

$$\Delta S_{Fus}^{Pr}(T-T_1) + RT \ln\left(\frac{1-X_2^2}{1-X_2^1}\right) = \Delta\bar{F}_1^{XS,1} - \Delta\bar{F}_1^{XS,2} = J. \qquad (34)$$

If the difference in excess partial molal free energies, or J, were known, then the phase boundaries could be calculated. Tiller and Hiskes (3, 4, 5), Lupis (81), and Chiotti and co-workers (6) are all attempting to do this, as previously indicated, with some success for simple systems. Difficulties are encountered in going from a system that gives good results to an unknown system. It is not at all obvious how the equations should be changed as the components are changed. There is no doubt of the value in the above attempts because a lot of thermodynamic information is contained in the equilibrium diagrams. Knowing the form of the thermodynamic functions used for calculating the phase boundaries would help eliminate a lot of tedious experimental work, and help resolve differences in experimental work.

As Equation 34 demonstrates, J is easily obtainable from the equilibrium diagram data and the known enthalpy of fusion or transformation. J was plotted as a function of temperature for the liquid to solid reaction, in Os through Bi, and is shown in Figures 34 through 41. The J function for the α to β transformation, in Os through Pb, is shown in Figures 42 through 44, plotted as a function of temperature. In studying the J function versus temperature graphs, it is apparent that they are almost linear, or at worst, slightly parabolic in shape. An initial slope was calculated for the

liquid to solid reaction and $\Delta J/\Delta T = -2.88 \pm 0.15$, which means all eight solutes had an initial slope that agreed within 5% of an average value. For the α to β transformation, $\Delta J/\Delta T$ is less well defined because some of the systems have such little solubility, but an overall slope of $\Delta J/\Delta T = 1.55 \pm 0.15$ was calculated, which means all seven systems agree within about 10%. Since J appeared to be such a simple function of T, a brief attempt was made to fit J to a power series, but for some unexplained reason, this never worked very well. A calculated J was obtained by using the average value of $\Delta J/\Delta T$ and integrating it over the temperature range of interest.

Knowing J and the entropy of fusion for Pr allows the $\ln(\frac{1-X_2^2}{1-X_2^1})$ term to be calculated, and if either X_2^2 of X_2^1 is known, then the other composition can be calculated. Using the experimentally calculated liquidus values for the solutes studied, it was possible to calculate the solidi compositions for various $\Delta J/\Delta T$ values, and these data are shown in Table 6. Fairly reasonable results were obtained, at least the calculated values agreed qualitatively with the experimental values. The best agreement close to the Pr-rich end of the diagram is given by $\Delta J/\Delta T$ of -2.8 or -2.9. As the alloy becomes enriched in the solute, a smaller $|\Delta J/\Delta T|$ provides better agreement between the calcu-

lated and the experimental values.

Table 7 shows the same type of data calculated for the α to β transformation. Very good results are obtained using an average value of $\Delta J/\Delta T = -1.40$. The calculated X_2^{α} 's indicate which solutes are soluble and to what extent they are soluble.

These results are very interesting because what has been done is to say that J, or the difference in excess partial molal free energies, is constant for the eight systems Os through Bi for both transformations. At this point it may prove worthwhile to take a closer look at $\Delta J/\Delta T$. This will be done using the liquid to solid reaction as the example.

From Equation 34: $J = \Delta S^{Pr}_{Fus.}(T-T_1) + RT \ln\left(\frac{1-X_2^S}{1-X_2^{liq.}}\right)$.

$$\frac{dJ}{dT} = \Delta S^{Pr}_{Fus.} + R \ln \frac{1-X_2^S}{1-X_2^{liq.}} + RT\left[\frac{1}{(1-X_2^{liq.})} \frac{dX_2^{liq.}}{dT} - \frac{1}{(1-X_2^S)} \frac{dX_2^S}{dT}\right] , \qquad (35)$$

ΔS^{Pr}_{fus} is known and the second term is negligible for small values of X_2^1 and X_2^2. Since $\Delta J/\Delta T \simeq -2.75$, and

$\Delta J/\Delta T = \Delta S^{Pr}_{Fus} + X$,

then it is found that

$$X = -1.38,$$

which indicates the third term is approximately the same as $\Delta S^{Pr}_{fus.}$ According to Chiotti (6) the third term is equivalent to

$$\frac{1}{1-X_2^{liq.}} \frac{dX_2^{liq.}}{dT} - \frac{1}{1-X_2^{S}} \frac{dX_2^{S}}{dT} = \frac{\Delta \bar{H}^{S \rightarrow liq.}}{RT^2} = \frac{\Delta H^{Pr}_{Fus.}}{RT^2} , \qquad (36)$$

which means Equation 35 becomes

$$\frac{dJ}{dT} = \Delta S^{Pr}_{Fus.} + \frac{\Delta H^{Pr}_{Fus}}{T} , \qquad (37)$$

and this clearly shows why $\Delta J/\Delta T \simeq 2\Delta^{Pr}_{Fus}$ for temperatures near the melting point of pure Pr. This is a strong indication that the approximation of ΔH^{Pr}_{Fus} being independent of temperature is a good assumption.

As the alloys become richer in solute, a better fit between calculated X_2^S and experimental values is obtained as $|\Delta J/\Delta T|$ becomes smaller. This occurs for two reasons: the first is the neglect of the second term in Equation 35, the second is the omission of the heat capacity terms.

This analysis appears to be fine, and the agreement obtained between theory and experiment indicates a certain amount of internal consistency. But the test of any analysis is whether it is applicable to other systems.

While there is not a large amount of equilibrium diagram data available for the R.E.-rich end of the diagrams involving

solutes from the sixth period, there is a systematic study of the R.E.-Pb systems (22, 23, 24, 25, 26, 27) being carried out. The studies were not as detailed as this study, but at least qualitative information about the boundaries is known. Using what appeared to be the best $\Delta J/\Delta T$ value for the Pr-Pb system, which was -2.82, and the known liquidus data, the solidus was calculated for La, Gd, Dy, and Lu-Pb systems, which are the only trivalent systems studied to date. Table 8, Column 5, shows the calculated values, and except for La and possibly Gd, the agreement was not very good. If Equation 35 is rewritten as

$$\Delta J/\Delta T = -2.82 + \varepsilon_{R.E.-Pb}, \text{ where } \varepsilon_{R.E.-Pb} \qquad (38)$$

represents some type of interaction term that depends on the particular solvent. The best fit $\Delta J/\Delta T$ was selected by trial and error and then $\varepsilon_{R.E.-Pb}$ was obtained from Equation 38. Table 8, Column 6 shows the $\Delta J/\Delta T$ values used and the $\varepsilon_{R.E.-Pb}$ parameter calculated from Equation 38. Figure 45 shows how $\varepsilon_{R.E.-Pb}$ varies for La (22), Gd (27), Dy (23), and Lu (26). It can be seen that $\varepsilon_{R.E.-Pb}$ appears highest for Lu, decreasing linearly to zero at Sm or Eu. The ε_{La-Pb} value was approximately zero, which is encouraging because the light lanthanides are considered to have about the same alloying behavior, with the heavy lanthanides responding in a different manner. From Equation 37, it would seem likely to pick

$\Delta J/\Delta T \simeq 2\Delta S^{R.E.}_{Fus}$; but this does not work very well, except for Gd, and Table 8, Column 7, shows the calculated data.

It appears from this analysis the lanthanides from La through possibly Sm would alloy, at the R.E. rich end of the diagram, the same as the Pr-period six systems. Given the liquidus from any solute in the sixth period alloyed with La through Sm, it would be possible to calculate the solidus within 60 or 70 C of the melting point of the solvent. Many times reasonably good liquidus data is available for a system while solidus data is lacking. This analysis would provide an estimate of a solute's solubility, or the solidus composition.

If there was an independent method of obtaining one of the compositions, then the boundaries could be predicted a priori. One possible way to do this would be to use the Q parameter. If Equation 32 is rewritten as follows:

$$X_2^1 = X_2^2 \, e^{\frac{Q}{RT}} , \tag{39}$$

and then rearranging Equation 34 gives

$$\ln\left(\frac{1-X_2^2}{1-X_2^1}\right) = \frac{J-\Delta S^{Pr}_{Fus}(T-T_1)}{RT} = Z \tag{40}$$

Substitute Equation 39 into 40, and the following is obtained:

$$\ln\left(\frac{1-X_2^2}{1-X_2^2 \, e^{\frac{Q}{RT}}}\right) = Z$$

$$X_2^2 = \frac{1-e^{Z}}{1-e^{\frac{Q}{RT}+Z}} \cdot \frac{e^{-Z}}{e^{-Z}}$$

$$X_2^2 = \frac{e^{-Z}-1}{e^{-Z}-e^{\frac{Q}{RT}}} \quad . \qquad (41)$$

Using Equation 41 requires a knowledge of J, $\Delta S^{R.E.}_{Fus.}$ or Transf.' and Q.

Table 9 lists the calculated X_2^S values, for Pr-period six alloys, using a constant $\Delta J/\Delta T$, the $\Delta S^{Pr}_{Fus.}$, and the Q_L values taken from Figure 29. Good agreement is obtained for compositions at temperatures 100 C below the melting point of pure Pr.

Calculated X_2^α boundaries for a constant $\Delta J/\Delta T$, $\Delta S^{Pr}_{Transf.}$, and Q_S values taken from Figure 30 are shown in Table 7 (B) Columns 1 and 2. The calculated compositions almost completely describe the X_2^α boundary for Os, Ir, Pt, Au, and Pb. For Hg and Tl, which are the only solutes that lower the α to β transformation temperature by more than 43 C the agreement between calculated and experimental X_2^α's is reasonable for only a limited range below the α to β transformation in pure Pr. In the Pr-Hg system this range is about 20 C while for the Pr-Tl system this range is about 70 C below the transformation temperature of Pr.

Of course, this method should give reasonable results. The Q values were calculated from the experimentally determined equilibrium diagrams. However even if Q values change, as the solvent is changed, because of Q's periodicity (11, 77, 82, 83, 84), several experimentally determined Q values should locate the curve, and other systems could be estimated from the Q vs. atomic number curve.

This analysis was tried on the other R.E.-Pb systems (22, 23, 26, 27), that have liquidus and solidus data available. The average value of $\Delta J/\Delta T = -2.82$ and $Q_L = 2955$ from the Pr-Pb system was used to calculate X_2^S values, and as Table 8, Column 8, indicates, fairly good results were obtained. This may have been somewhat fortuitous because Equation 37 indicates that $\Delta J/\Delta T \simeq 2\Delta S_{Fus.}^{R.E.}$, which is approximately what was calculated for the liquid to solid transformations in the Pr-period six alloys. When $\Delta J/\Delta T = 2\Delta S_{Fus.}^{R.E.}$ and the Q-value of 2955 is used to calculate X_2^S, poorer results occur, as Column 9 in Table 8 indicates. Next, a Q value was calculated for each solvent from the equilibrium diagram data and when this was used along with $\Delta J/\Delta T = 2\Delta S_{Fus}^{R.E.}$, very good results were obtained between calculated and experimental X_2^S values. Table 8, Column 10, shows these data.

The calculated R.E.-Pb Q values are shown in Figure 45, and like the interaction parameter Lu, has the highest Q value.

The Q's decrease linearly from Lu through Dy and Gd to the value listed for Pr of 2955 at about Eu, and then Q appears to remain constant through La. This is in agreement with the discussion of the interaction parameter, and indicates that the light R.E.'s are very similar in their alloying behavior.

This discussion of the La (22), Gd (27), Dy (23), and Lu-Pb (26) systems must be tempered by the fact that the data in the dilute solution region, for the solidus is not that well known, but the behavior should at least be qualitatively correct.

The above analysis may appear to be just a number juggling exercise, but it can bring interesting results. Suppose, for example, it was desirable to know the effect of the elements from the sixth period on Nd. Q would be the same as for Pr, and the ΔS^{Nd}_{fus} is known; therefore X^S_2 compositions could be calculated from Equation 41.

Now if X^S_2 compositions were to be calculated for Tm, a little more work would be required because Q is unknown. Q has been shown to be periodic with respect to atomic number, and so if several solutes were determined experimentally, this would fix the Q curve and would allow values to be estimated for other solutes. From this information and the known $\Delta J/\Delta T = 2\Delta S^{R.E.}_{Fus.}$ value, the X^S_2 compositions could be determined. The experimentally determined systems would also

establish the transformation temperature and composition curves, the eutectic composition, and the maximum solubility curve--all of which varied periodically with atomic number. In effect, what is suggested is that with some experimental information for some judiciously chosen solutes from a period, and the knowledge of the periodicity of the above functions, the solidus could be calculated, the transformation temperatures determined, and the solubility limits and eutectic compositions estimated for the remainder of the solutes from the period.

Again, using Tm for an example, it is possible to estimate Q_L for the Tm-Pb system from Figure 45 (about 5500 cal/mole). Then, if Q_L versus atomic number could be shown to have the same shape for other R.E.-period six systems as it has for Pr-period six alloys the remaining Q_L values for the other solutes would be fixed by the value estimated for Pb. This would at least provide an estimate of the solubility of a period six solute alloyed with a heavy lanthanide. Experimental data would still be necessary to establish the periodicity of the transformation temperature and composition curves, the eutectic composition, and the maximum solubility curve.

CONCLUSIONS

This study of the Pr-period six alloys has supplied some of the equilibrium diagram information that has been lacking for the R.E.'s, in particular Pr.

Cs and Ba were found to be immiscible with liquid Pr. Figure 5 represents schematically the equilibrium diagram for Ba; Cs would be similar except for the 730 C horizontal.

Equations 1, 2, 3, and 4 describe the liquidus boundaries for the Ta, W, Hf, and Re systems respectively. The solubilities of Ta and W, Figure 7, are so small that their effects on Pr's melting point or allotropic transformation were assumed to negligible. Hf and Re lowered both transformation temperatures of Pr by only a few degrees.

Os, Ir, Pt, and Au, Figures 8, 10, 11, and 12 respectively, formed eutectics at the Pr-rich end of the diagrams. The α to β transformation temperature was lowered by alloying Os, Ir, Pt, or Au and can be represented by an inverted peritectic reaction.

Figures 14, 16, 18, and 19 represent the Pr-rich end of the equilibrium diagrams for Hg, Tl, Pb, and Bi. The liquid to solid reaction is a eutectic and the α to β transformation is a eutectoid reaction.

The equilibrium diagram data obtained are summarized in Figures 20, 21, and 22 and in Table 4. It is interesting to

note that all of the data plotted appears to vary in a periodic manner when graphed as a function of the atomic number of the solute.

Application of the common alloying rules indicated limited, or less than 5 at.%, solubility for all of the solutes, with Hf on the borderline (16). This study showed virtually no solubility for Hf in either α or β-Pr, even though size factor and electronegativity were favorable. Hg and Tl exhibited extensive solubility in β-Pr, 14.6 at.% Hg and 9.0 at.% Tl at their respective eutectic temperatures. The solubilities of all the solutes in α and β-Pr are shown in Figure 23, and the remainder of the solutes show limited solubility as predicted (16).

The size factor and Debye factor are favorable for extensive solubility to occur in Hg, Tl, Pb, and Bi. The electronegativity differences suggest limited solubility. Valence difference is one or less for Hg, Tl, and Pb, suggesting that valency is not the controlling factor. It seems very likely that θ_D may be the reason for Hf's limited solubility. For the other solutes, there does not appear to be such a clear-cut case for a single factor controlling the solubility. The data indicates how very important the size factor is and that the maximum solubility of one element in another is not normally a simple function controlled by one factor, but it is a complicated sum of several

factors, each making a contribution.

The experimental data obtained has been compared to some theories for dilute solution behavior that other investigators (7) thought might be applicable to the rare earths. The analysis of Jones (9) and Betterton and Frye (10) was shown not to apply to these systems. Calculation of the ΔH^{Pr}_{fus} and ΔH^{Pr}_{Transf} using ideal solution theory (13, 76) clearly showed the Pr-period six alloys were not ideal systems at the Pr-rich end of the diagrams (Figures 24, 25, 26, 27). Use of the power series expansion for the internal energy, Equation 28a and b, showed that it was not possible to describe these systems by regular solution theory.

From the equations (76) describing the equilibrium between two phases and from Jones (9) analysis, this study found that the difference in excess free energies or the ratio of the logarithm of the activity coefficients (13), called the J function (7), could be represented by a straight line (Figures 34 through 44). This applied to the liquid to solid and the α to β transformation for the eight systems Os through Bi for which this study provided extensive data about the phase boundaries, as shown in Figures 8, 10, 11, 12, 14, 16, 18, and 19. Calculation of the solidus using the average J value, the ΔS^{Pr}_{Fus}, and the known liquidus gave reasonable good results, as Table 6 indicates.

Another thermodynamic parameter which has been used to indicate phase stability is Q (11, 77, 82, 83, 84) which was shown to be periodic with respect to atomic number and positive for all the solutes studied. Combining Q with the J function allowed the calculation of the solidus for Pr-period six alloys. Good agreement was found between the calculated and experimental data, see Table 7b and 9.

This analysis was applied to some R.E.-Pb systems (22, 23, 26, 27) and reasonable results were obtained, as shown in Table 8. From these data it was possible to conclude that the light lanthanides, La through Sm, alloy with Pb in approximately the same manner, while the heavy lanthanides interact somewhat differently.

Furthermore, it was suggested that for the light R.E.'s the Q values determined in this study could be used to obtain estimates of the solubility for a solute from the fourth or fifth period as well as the sixth period. For other R.E.-Pb alloys, Q values could be estimated from Figure 45, and it is possible that if the shape of Q is the same for other systems, then the estimated value for R.E.-Pb would fix the Q versus atomic number curve. Combining this information with the knowledge of the periodic behavior of transformation temperatures, reaction compositions, and solubilities implies that estimates of these parameters can be made for undetermined systems.

Table 6. Calculated X_2^S compositions using constant $\Delta J/\Delta T$, ΔS_{Fus}^{Pr}, and the known $X_2^{liq.}$ compositions

Solute	Temp. K	Expt'l X_2^S	-ΔJ/ΔT 2.90	2.823	2.75	2.70	2.574
Os	1197	.0005	.0002	.0005	.0008	.0010	.0015
	1183	.00105	N.G.[a]	.0006	.0013	-	-
	1153	.0021	N.G.	N.G.	N.G.	.0005	.0034
	1103	.0038	N.G.	N.G.	N.G.	N.G.	.0010
Ir	1197	.0004	.00003	.0003	.0006	.0008	.0013
	1183	.0009	N.G.	.0008	.0015	.0020	.0032
	1153	.0016	N.G.	N.G.	.0003	.0014	.0044
	1103	.0027	N.G.	N.G.	N.G.	N.G.	.0051
Pt	1197	.0005	.0007	.0010	.0013	.0015	.0020
	1183	.0010	N.G.	.0011	.0018	.0023	.0035
	1153	.0021	N.G.	.0001	.0018	.0030	.0059
	1103	.0035	N.G.	N.G.	.0026	.0050	.0108
Au	1197	.0008	.0008	.0011	.0014	.0016	.0021
	1183	.00175	N.G.	.0014	.0021	.0026	.0038
	1153	.0039	N.G.	.0009	.0026	.0037	.0066
	1103	.0080	N.G.	N.G.	.0023	.0047	.0106
Hg	1197	.0018	.0012	.0015	.0018	.0020	.0025
	1183	.0055	-	.0046	.0054	.0058	.0071
	1163	.0100	N.G.	.0075	.0089	.0098	.0121
	1153	.0139	N.G.	-	-	-	.0143
	1123	.0230	N.G.	-	.0131	.0150	.0196
	1103	.0295	N.G.	-	-	-	.0220
	1073	.0410	N.G.	.0082	.0147	.0178	.0258
	923	.1256	N.G.	N.G.	N.G.	.0039	-
Tl	1197	.0025	.0043	.0045	.0048	.0050	.0055
	1183	.0085	.0098	.0105	.0112	.0117	.0130
	1153	.0226	.0187	.0204	.0221	.0232	.0261
	1103	.0496	.0297	.0332	.0365	.0388	.0445
Pb	1197	.0036	.0041	.0043	.0046	.0048	.0053
	1183	.0072	.0093	.0100	.0107	.0112	.0124
	1153	.0178	.0192	.0209	.0226	.0237	.0266
	1103	.0324	.0191	.0227	.0260	.0283	.0341
Bi	1197	.0018	.0023	.0026	.0029	.0031	.0036
	1183	.0046	.0032	.0048	.0056	.0060	.0073
	1167	.0082	-	.0071	.0083	.0092	.0113

[a]Equation is no longer valid.

Table 7. Calculated X_2^{α} boundaries

Solute	A: Calculated X_2^{α} compositions using constant $\Delta J/\Delta T$ and the experimental X_2^{β} values					B: Calculate X_2^{α} compositions using constant $\Delta J/\Delta T$ and Q_S values from Figure 30	
	Temp K	Expt'l X_2^{α}	$-\Delta J/\Delta T$ 1.55	1.45	1.40	$-\Delta J/\Delta T$ 1.55	1.40
Os	1067	.0020	.0027	.0030	.0031	.0015	.0012
Ir	1067	.0007	.0004	.0007	.0008	.0008	.0007
	1065	.0014	.0007	.0011	.0012	.0011	.0009
Pt	1067	.0005	.00002	.0003	.0004	.0005	.0004
	1063	.0006	.00002	.0004	.0007	.0009	.0007
Au	1067	.00012	N.G.[a]	-	.00017	.00015	.00012
	1063	.00021	"	.00005	.00026	.00026	.00021
	1053	.00045	"	N.G.	.00045	.00053	.00044
	1033	.00093	"	.0004	.0014	.0010	-
	1031	.00098	"	.0004	.0014	-	.0009
Hg	1067	.0006	N.G.	N.G.	N.G.	.0015	.0012
	1063	.0012	"	"	"	.0044	.0022
	1053	.0024	"	"	.00025	.0056	.0046
	1003	.0057	"	.0024	.0042	.0194	.0160
	953	.0067	"	.0049	.0080	.0318	-
	893	.0075	"	.0050	.0100	.0448	.0373
	793	.0092	"	N.G.	.0048	.0616	-
Tl	1067	.0019	.0017	.0020	.0021	.0025	.0020
	1063	.0035	.0029	.0034	.0036	.0044	.0036
	1053	.0081	.0059	.0068	.0073	.0092	.0076
	1003	.0217	.0231	.0268	.0281	.0319	.0264
	963	.0254	.0330	.0392	.0412	.0484	.0403
Pb	1067	.0070	.0090	.0093	.0094	.0047	.0039
	1063	.0117	.0132	.0136	.0138	.0084	.0069
	1053	.0207	.0214	.0222	.0227	.0175	.0144
	1051	.0223	.0228	.0238	.0242	.0193	-

[a]Equation is no longer valid.

Table 8. Calculated X_2^S compositions for Pb in La, Gd, Dy, and Lu

Solvent $T_{M.P.}$	Temp K	Composition Experimental X_2^{liq}	X_2^S	Calculate X_2^S values: $\Delta J/\Delta T = -2.82$ Known X_2^{liq}	$\Delta J/\Delta T = -2.82 + \varepsilon_{R.E.-Pb}$ & known X_2^{liq}	$\Delta J/\Delta T = 2\Delta S_{fus}^{R.E.}$, known X_2^{liq}	$\Delta J/\Delta T = -2.82$ $Q=2955$	$\Delta J/\Delta T = 2\Delta S_{fus}^{R.E.}$ $Q=2955$	$\Delta J/\Delta T = 2\Delta S_{fus}^{R.E.}$ Q=see individual R.E.
La	1173	.023	.006 or 7	.0076	.0084	.0110	.0060	.0047	.0049
1196	1148	.043	.012	.0107	.0120	.0177	.0122	.0096	.0099
ΔS_{Fus}^{La}=					$\Delta J/\Delta T = -2.75$				Q=2900
-1.24					$\varepsilon = +0.07$				
Gd	1548	.028	.010	.0118	.0084	.0096	.0098	.0114	.0101
1586	1523	.050	.017	.0239	.0170	.0195	.0159	.0185	.0163
ΔS_{Fus}^{Gd}=	1488	.075	.0250	.0343	.0250	.0272	.0240	.0278	.0246
-1.52					$\Delta J/\Delta T = -3.1$				Q=3200
					$\varepsilon = -.28$				
Dy	1648	.026	.007	.0144	.0074	.0123	.0080	.0094	.0051
1678					$\Delta J/\Delta T = -3.6$				Q=4300
ΔS_{Fus}^{Dy}=					$\varepsilon = -0.78$				
-1.53									
Lu	1898	.029	.004	.025	.0048	.0092	.0056	.0166	.0043
1934	1873	.046	.005	.0350	.0048	.0123	.0093	.0274	.0072
ΔS_{Fus}^{Lu}=	1773	.094	.006	.0646	N.G.	.0082	.0234	.0657	.0170
-2.12					$\Delta J/\Delta T = -4.7$				Q=6500
					$\varepsilon = -1.9$				

Table 9. Calculated X_2^S compositions using average $\Delta J/\Delta T$, ΔS_{Fus}^{Pr}, and a Q value obtained from Figure 29

Solute	Temp K	Expt'l X_2^S	-ΔJ/ΔT 2.70	2.574	2.82
Os	1197	.0005	.0007	.0006	.0008
	1183	.00105	.0017	.0016	.0019
	1153	.0021	.0038	.0034	.0041
	1103	.0038	.0068	.0062	.0074
Ir	1197	.0004	.0003	.0003	.0004
	1183	.0009	.0008	.0007	.0009
	1153	.0016	.0017	.0016	.0019
	1103	.0027	.0030	.0027	.0033
Pt	1197	.0005	.0004	.0003	.0004
	1183	.0010	.0009	.0008	.0010
	1153	.0021	.0020	.0018	.0022
	1103	.0035	.0036	.0032	.0039
Au	1197	.0008	.0006	.0006	.0007
	1183	.00175	.0016	.0015	.0018
	1153	.0039	.0036	.0032	.0039
	1103	.0080	.0063	.0057	.0069
Hg	1197	.0018	.0021	.0019	.0023
	1183	.0055	.0052	.0047	.0057
	1153	.0139	.0116	.0105	.0126
	1103	.0295	.0212	.0193	.0230
	1073	.0410	-	-	.0286
	923	.1256	-	-	.0486
Tl	1197	.0025	.0027	.0024	.0029
	1183	.0085	.0067	.0061	.0073
	1153	.0226	.0149	.0136	.0162
	1103	.0496	.0274	.0250	.0297
	1043	.0875	-	-	.0436
Pb	1197	.0036	.0020	.0018	.0022
	1183	.0072	.0051	.0046	.0056
	1153	.0178	.0114	.0103	.0124
	1103	.0324	.0208	.0189	.0226
Bi	1197	.0018	.0015	.0014	.0016
	1183	.0046	.0038	.0034	.0041
	1167	.0082	.0063	.0066	.0069

BIBLIOGRAPHY

1. Kubaschewski, O. and Chart, T. G. J. Inst. Metals (London), 1964-65, vol. 93, p. 329.

2. Wagner, C. Thermodynamics of Alloys, Addison-Wesley Publishing Co., Reading, Massachusetts, 1952.

3. Tiller, W. A. and Hiskes, R. Mater. Sci. Eng., 1967/68, vol. 2., p. 320.

4. Tiller, W. A. and Hiskes, R. Mater. Sci. Eng., 1969, vol. 4, p. 163.

5. Tiller, W. A. and Hiskes, R. Mater. Sci. Eng., 1969, vol. 4, p. 173.

6. Chiotti, P., Simmons, M. F. and Kately, J. A. U.S. Atomic Energy Commission Report IS-2084, 1969.

7. Gschneidner, K. A. and Waber, J. T. The Rare Earths, F. H. Spedding and A. H. Daane, eds., p. 386, John Wiely and Sons, New York, 1961.

8. Mott, B. W. U.S. Atomic Energy Commission Report AERE-R-5593, 1967.

9. Jones, H. Proc. Roy. Soc. (London), 1937, vol. 49, p. 243.

10. Betterton, J. O. and Frye, J. H. Acta Met., 1958, vol. 6, p. 205.

11. Olesen, W. and Wever, F. Arch. Eisenhütten, 1948, vol. 19, p. 97.

12. Hume-Rothery, W., Channel-Evans, K. M., and Mabbott,G. W. Phil. Trans. Roy. Soc., 1934, vol. 233A, p. 1.

13. Darken, L. S. and Gurry, R. W. Physical Chemistry of Metals, McGraw-Hill Book Co., New York, 1953.

14. Waber, J. T., Gschneidner, K. A., Larson, A., and Prince, M. Trans. Met. Soc. AIME, 1963, vol. 227, p. 717.

15. Rider, P. E., Gschneidner, K. A. and McMasters, O. D. Trans. Met. Soc. ATME, 1965, vol. 233, p. 1488.

16. Teatum, E. T., Gschneidner, K. A. and Waber, J. T. U.S. Atomic Energy Commission Report LA-4003, 1968.

17. Moeller, T. The Rare Earths, F. H. Spedding and A. H. Daane, eds., p. 9, John Wiley and Sons, New York, 1961.

18. Gschneidner, K. A. Rare-Earth Alloys, D. Van Nostrand Co., Princeton, N.J., 1961.

19. Spedding, F. H., Beaudry, B. J., Croat, J. J. and P. E. Palmer. Inter-American Conference on Materials Technology Proc. 1968, p. 151, 1968.

20. Dennison, D. H., Tschetter, M. J. and Gschneidner, K. A. J. Less-Common Metals, 1966, vol. 11, p. 423.

21. Miller, A. E., Daane, A. H., Habermann, C. E. and Beaudry, B. J. Sci. Instr., 1963, vol. 34, no. 6, p. 644.

22. McMasters, O. D., Soderquist, S. D. and Gschneidner, K. A. Trans. Quarterly ASM, 1968. vol. 61, no. 3, p. 435.

23. McMasters, O. D., O'Keefe, T. J. and Gschneidner, K. A. Trans. Met. Soc. AIME, 1968, vol. 242, p. 936.

24. McMasters, O. D. and Gschneidner, K. A. J. Less-Common Metals, 1967, vol. 13, p. 193.

25. McMasters, O. D. and Gschneidner, K. A. Trans. Met. Soc. AIME, 1967, vol 239, p. 781.

26. McMasters, O. D. and Gschneidner, K. A. J. Less-Common Metals, to be published.

27. Demel, J. T. and Gschneidner, K. A. J. Nucl. Mat'l, 1969, vol. 29, p. 111.

28. Sax, I. H. Dangerous Properties of Industrial Materials, Reinhold Publishing Corp., New York, 1957.

29. Ziebold, T. O. Analytical Chemistry, 1968, vol. 39, no. 8, p. 858.

30. Kehl, G. L. Principles of Metallographic Laboratory Practice. McGraw-Hill Book Co., New York, 1949.

31. Hume-Rothery, W., Christian, W. J. and Pearson, W. Metallurgical Equilibrium Diagrams, The Institute of Physics, London, 1952.

32. Lyman, T., ed. Metals Handbook Vol. 1, Properties and Selection of Metals, ASM, Metals Park, Ohio, 1961.

33. Berber, C. R. Nature, June 7, 1969, vol. 222, p. 929.

34. Rhines, F. N. Phase Diagrams in Metallurgy, McGraw-Hill Book Co., New York, 1956.

35. Peterson, D. T. and Hopkins, E. N. U.S. Atomic Energy Commission Report IS-1036, 1964.

36. Kleppa, O. J. and Weil, J. A. J. Amer. Chem. Soc., 1951, vol. 73, p. 4848.

37. Hahn, R. B. Treatise on Analytical Chemistry, Part II. Analytical Chemistry of the Elements N, P, Tl, Ti, Zr-Hf, I.M. Kolthoff and P. J. Elving, eds., vol. 5, p. 124, Interscience Publishers, New York, 1963.

38. Ryabchikov, D. I. and Lazarev, A. I. Zh. Anal. Khim, 1955, vol. 40, p. 228.

39. Geballe, T. H., Matthias, B. T., Compton, V. B., Corenzwit, E., Hull, G. W. and Longinotti. L. D. Phys. Rev., 1965, vol. 137A, no. 1A, p. A119.

40. Dwight, A. E., Conner, R. A. and Downey, J. W. Acta Cryst., 1965, vol. 18, p. 835.

41. Haschke, H., Novotny, H. and Benesovsky, F. Monatsch. Chem., 1966, vol. 97, p. 716.

42. Jeitschko, W. and Parthé, E. Acta Cryst., 1967, vol. 22, p. 551.

43. Gambino, R. J. J. Less-Common Metals, 1967, vol. 12, p. 344.

44. Veleckis, E., Van Deventer, E., Schaldaske, R., Tani, B. and Homa, M. U.S. Atomic Energy Commission Report ANL-6569, 1962.

45. Komjathy, S. A., Reed, R. H. and Rostoker, W. U.S. Atomic Energy Commission Report WADC-TR-59-483, 1960.

46. Bidayera, T. A. and Kuznetsova, R. I. Russ. Metal., 1967, vol. 1, p. 89.

47. Veleckis, E. and van Deventer, E. U.S. Atomic Energy Commission Report ANL-6543, 1962.

48. Savitskii, E. M. and Terekhova, V. F. Zhur. Neorg. Khim. 1958, vol. 3, p. 756.

49. Buschow, K. H. J. and Velge, W. J. Less-Common Metals, 1967, vol. 13, p. 11.

50. Ellinger, F. H., Land, C. C. Johnson, K. A. and Struebing, V. O. Trans. Met. Soc. AIME, 1966, vol. 236, p. 1577.

51. Vogel, R. and Klase, H. Z. Metallk., 1954, vol. 45, p. 633.

52. Savitskii, E. M., Baron, V. V. and Efimor, Y. V. Zhur. Neorg. Khim., 1967, vol. 7, p. 701.

53. Chukalin, V., Yarembash, E. and Vilenskii, A. Inorg. Mater., 1967, vol. 3, p. 1341.

54. Chiotti, P. and Mason, J. T. Trans. Met. Soc. AIME, 1965, vol. 233, p. 786.

55. Gebhart, J., Etter, D. and Tucker, P. Plutonium 1965, A. Kay and M. Waldron, eds., p. 392, Chapman and Hall, London, 1967.

56. Obrowski, W. Z. Metallk., 1962, vol. 53, p. 736.

57. Copeland, M. and Kato, H. Physical and Material Problems of Control Rods, Internat. Atomic Energy Agency, Vienna, Austria, 1964.

58. Buschow, K. H. J. and van der Goot, A. S. J. Less-Common Metals, 1968, vol. 14, p. 323.

59. Gebhardt, E., von Erdberg, M. and Lüty, U. Nuclear Metallurgy, 1964, vol. 10, p. 303.

60. Chiotti, P. and Mason, J. T. Trans. Met. Soc. AIME, 1967, vol. 239, p. 547.

61. Veleckis, E. and Van Deventer, E. U.S. Atomic Energy Commission Report ANL-6925, 1965.

62. Novy, V., Vickery, R., Kleber, E. Trans. Met. Soc. AIME, 1961, vol. 221, p. 580.

63. Croeni, J. G., Rhoads, S. C., Armantrout, C. E. and Kato, H. U.S. Bureau of Mines, Report Invest. no. 5796, 1961.

64. Kirchmayer, H. R. and Lugscheider , W. Z. Metallk, 1967, vol. 58, p. 185.

65. Savitskii, E. M. and Kamidov, O. Kh. Inorg. Materials, 1967, vol. 3, p. 571.

66. Zargaryan, V. Sh. and Abrikosov, H. Kh. Inorg. Materials, 1967, vol. 3, p. 687.

67. Terekhova, V. F., Markova, J. A. and Savitskii, E. M. Zhur. Neorg. Khim., 1961, vol. 6, p. 1252.

68. Lundin, C. E. and Klodt, D. T. Trans. Met. Soc. AIME, 1962, vol. 224, p. 367.

69. Carlson, O. N., Schmidt, F. A. and Diesburg, D. E. Trans. Quarterly ASM, 1967, vol. 60, p. 119.

70. Myklebust, R. and Daane, A. H. Trans. Met. Soc. AIME, 1962, vol. 224, p. 354.

71. Lundin, C. E. and Klodt, D. T. J. Inst. Metals, 1962, vol. 90, p. 341.

72. Schmidt, F. A. and McMasters, O. D. J. Less-Common Metals, 1968, vol. 15, p. 1.

73. Beaudry, B. J. J. Less-Common Metals, 1968, vol. 14, p. 370.

74. Chiotti, P., Mason, J. T. and Gill, K. Trans. Met. Soc. AIME, 1963, vol. 227, p. 910.

75. Proebstte, R. A. Ph.D. thesis, R.P.I., Troy, N.Y., 1960.

76. Kirkwood, J. G. and Oppenheim, I. Chemical Thermodynamics, McGraw-Hill Book Co., New York, 1961.

77. Waber, J. T. and Gschneidner, K. A. Plutonium 1960, E. Grison, W. Loard, and R. Fowler, eds., p. 109, Cleaver-Hume Press, London, 1961.

78. Mott, N. F. and Jones, H. The Theory of the Properties of Metals and Alloys, Dover Publications, New York, 1958.

79. Slater, J. C. Introduction to Chemical Physics, McGraw-Hill Book Co., New York, 1963.

80. Simmons, M. F. M.S. thesis, Library, Iowa State University, Ames, Iowa, 1964.

81. Lupis, C. H. P. Acta Met., 1968, vol. 16, p. 1365.

82. Dwight, A. E. Trans. AIME, J. Metals, 1956, vol. 206, p. 162.

83. Uy, J. and Burr, A. Trans. Met. Soc. AIME, 1966, vol. 236, p. 1009.

84. Worner, H. W. J. Australian Inst. Met., 1960, vol. 5, no. 2, p. 154.

85. Gschneidner, K. A. Solid State Physics, F. Seitz and D. Turnbull, eds., vol. 16, p. 276, Academic Press, New York, 1956.

86. Brillouin, L. Wave Propagation in Periodic Structures, Dover Publications, New York, 1953.

87. Love, B. U.S. Atomic Energy Commission Report WADD-TR-61-123, 1961.

88. Uy, J. C. Ph.D. thesis, Microfilm copy, Univ. Microfilms, Ann Arbor, Michigan, Rensselaer Polytechnic Institute, 1963.

89. Savitskii, E. M. and Khamnidov, O. Kh. Inorg. Materials, 1965, vol. 1, p. 1693.

90. Elliott, R. P. Rare Earth Research III, L. Eyring, ed. p. 215, Gordon and Breach, New York, 1965.

91. Weeks, J. R. Trans. Quarterly ASM, 1965, vol. 58, no. 3, p. 302.

APPENDIX

Pr_2Au - $PbCl_2$ type structure

a = 7.13 b = 5.01 c = 9.28

$Sin^2\theta_M$	I_M	HKL	$Sin^2\theta_C$	I_C
.0405	VW	102	.0393	140
.0433	VW	111	.0423	60
.0471	VW	200	.0468	71
.0539	VVW	201	.0537	12
.0642	S	112	.0630	480
.0715	M	210	.0704	182
.0751	MS	103	.0738	180
		202	.0744	185
.0779	VS	211	.0773	1000
.0875	S	013	.0858	695
.0958	S	020	.0947	575
		113	.0975	199
.0984	VVW	212	.0980	50
.1079	VW	203	.1089	73
.1123	M	004	.1104	93
		301	.1121	132
.1329	S	213	.1325	192
		302	.1328	178
.1353	MS	311	.1358	159
.1410	VVW	220	.1415	32
.1477	VW	221	.1484	6
.1584	W	204	.1584	72
.1697	M	123	.1685	108
		222	.1691	112
.1851	VW	105	.1842	49
		400	.1870	47
		223	.2036	55
.2058	M	024	.2051	73
		321	.2068	102
.2267	M	322	.2275	155
.2385	M	412	.2383	22
		314	.2393	182
.2523	M	224	.2519	68
		132	.2524	60
.2596	VW	230	.2598	25
		106	.2601	63
.2657	M	231	.2667	154

(Continued)

$Sin^2\theta_M$	I_M	HKL	$Sin^2\theta_C$	I_C
.2750	M	033	.2752	117
.2959	M	206	.2952	56
		404	.2975	30
.3011	M	315	.3014	88
.3631	M	017	.3618	60
.3893	M	226	.3899	72

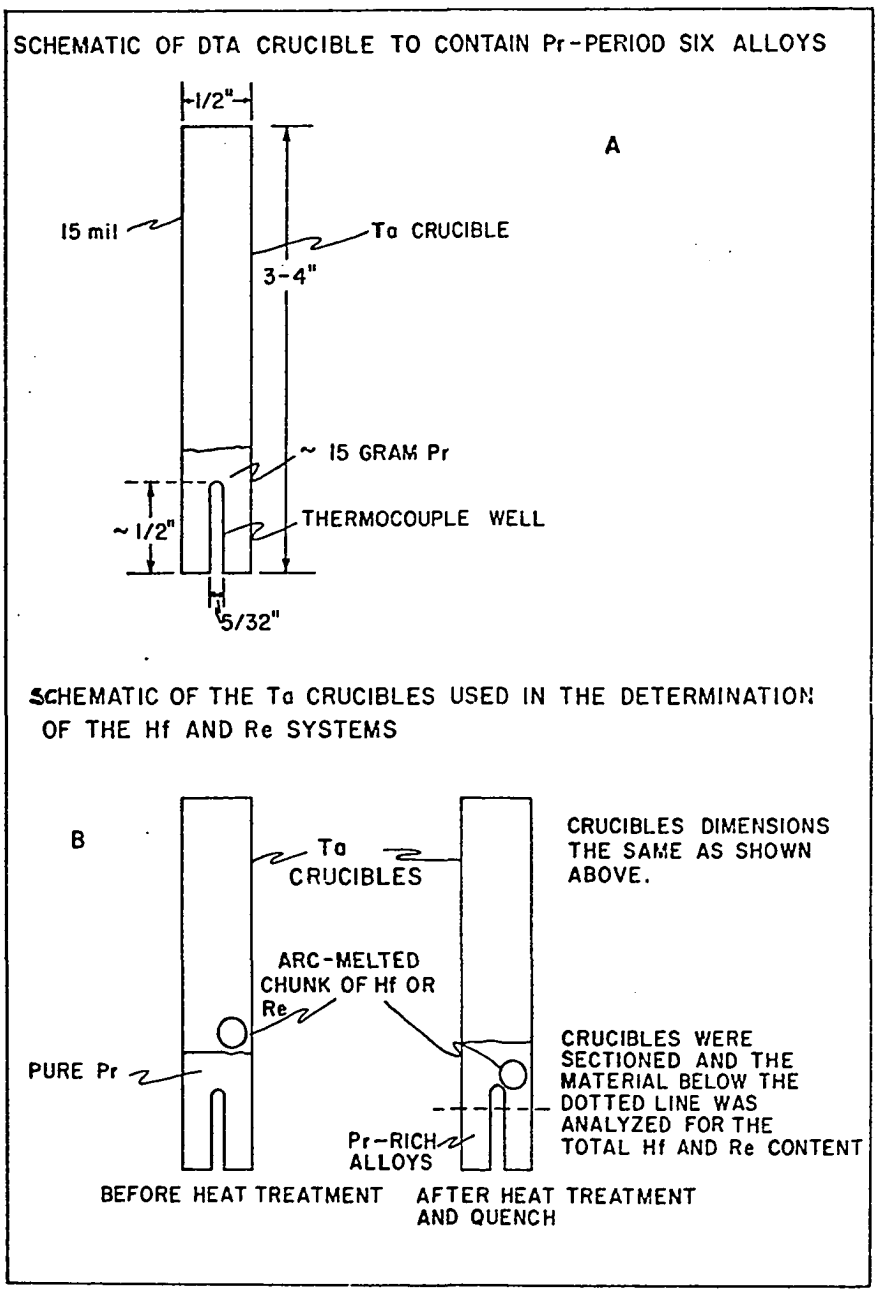

Figure 1
Schematic of D.T.A. Crucibles.

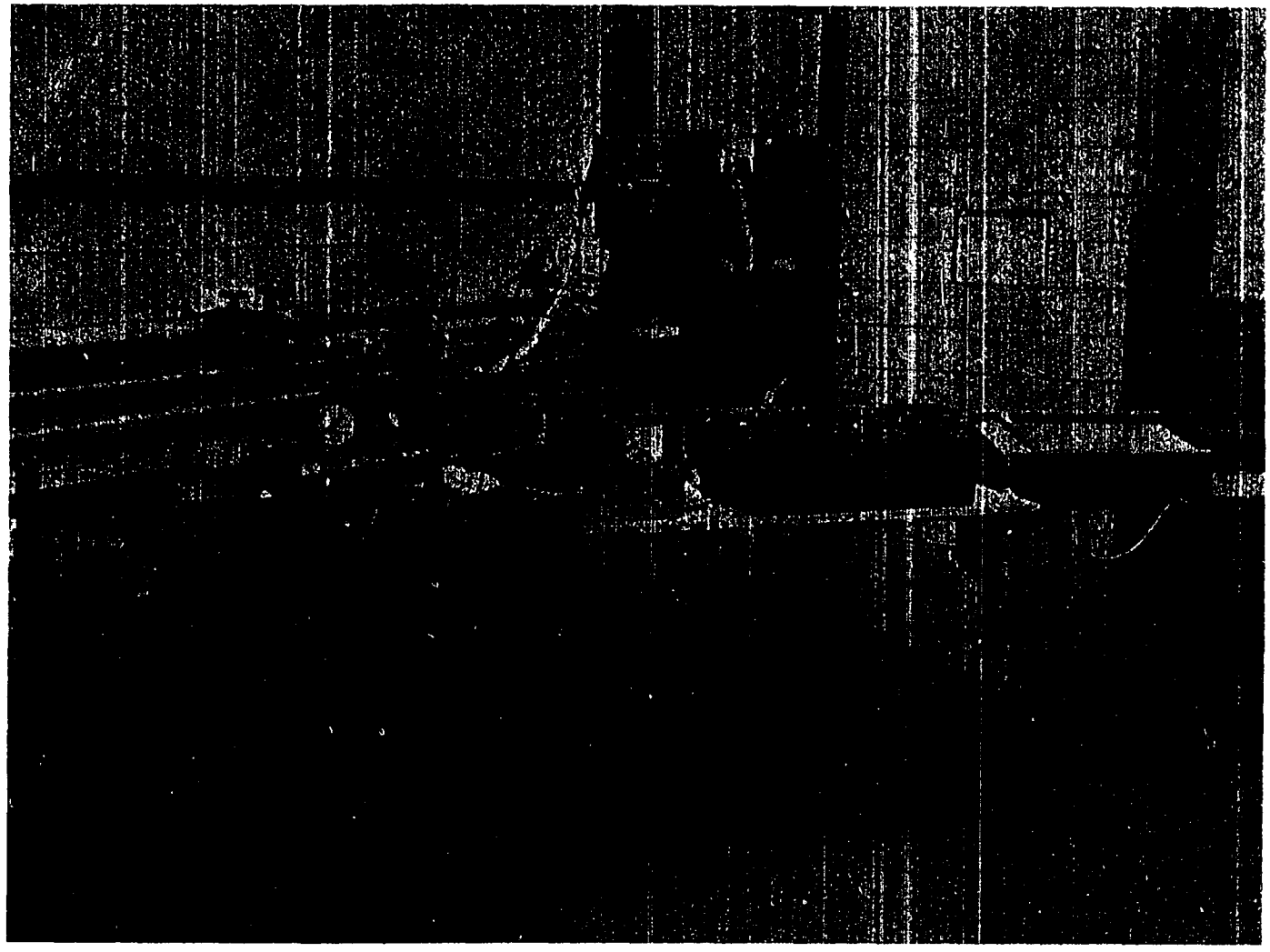

Figure 2

Photograph of the D.T.A. system, showing the vacuum chamber, furnace, temperature measuring equipment and the recorder.

Figure 3
Schematic of the D.T.A. system.

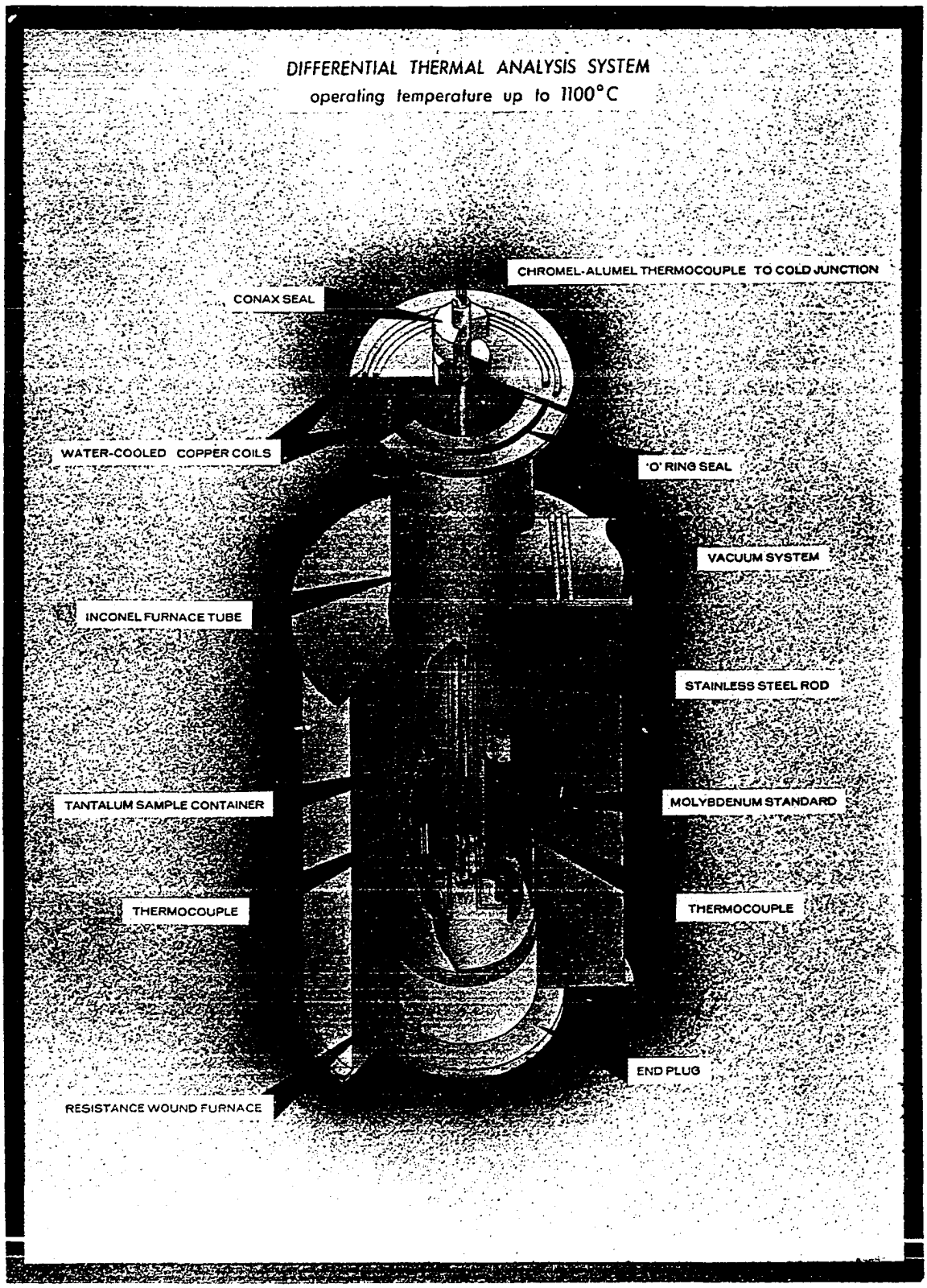
DIFFERENTIAL THERMAL ANALYSIS SYSTEM
operating temperature up to 1100°C
CHROMEL-ALUMEL THERMOCOUPLE TO COLD JUNCTION
CONAX SEAL
WATER-COOLED COPPER COILS
'O' RING SEAL
VACUUM SYSTEM
INCONEL FURNACE TUBE
STAINLESS STEEL ROD
TANTALUM SAMPLE CONTAINER
MOLYBDENUM STANDARD
THERMOCOUPLE
THERMOCOUPLE
END PLUG
RESISTANCE WOUND FURNACE

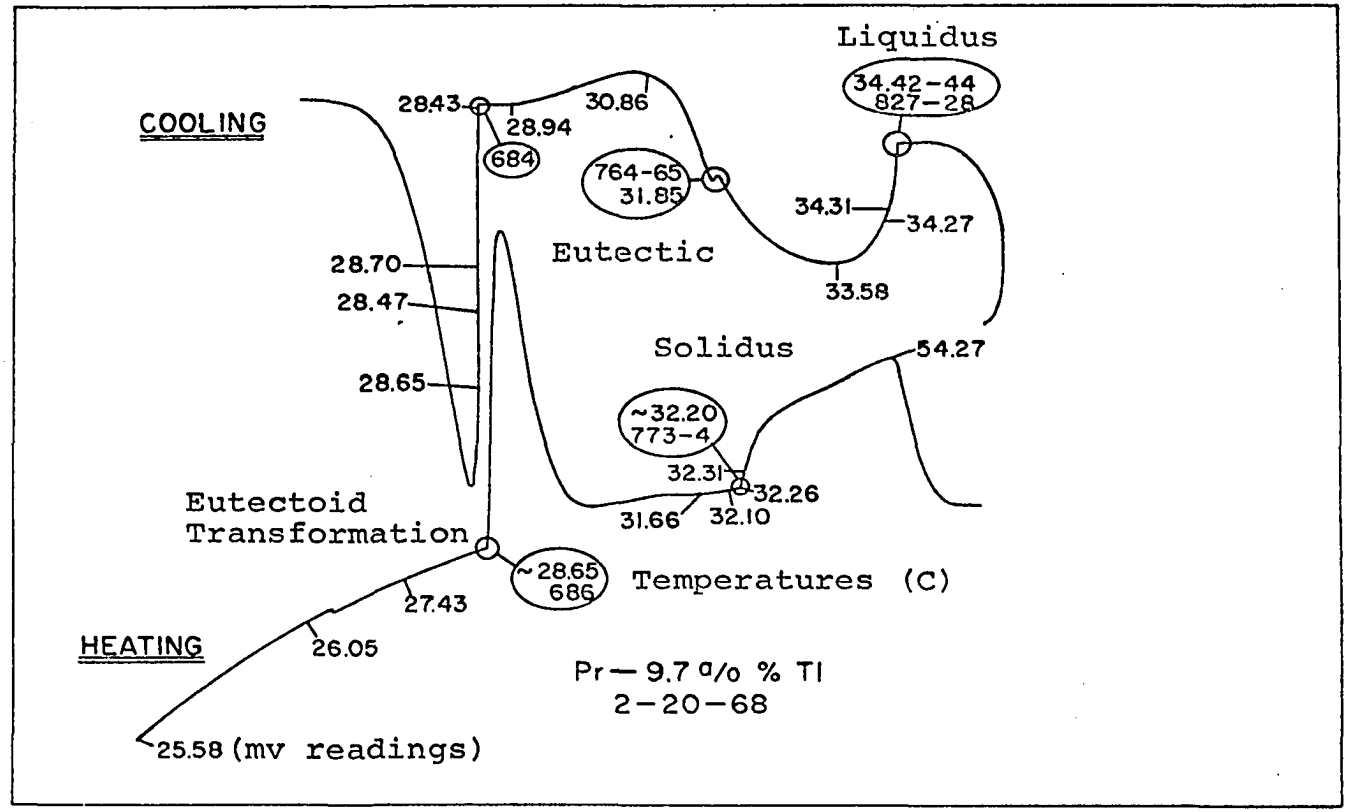

Figure 4
Differential thermal analysis trace showing the heating and cooling curves for a 9.7 at.% Tl alloy. The temperatures were monitored by a potentiometer.

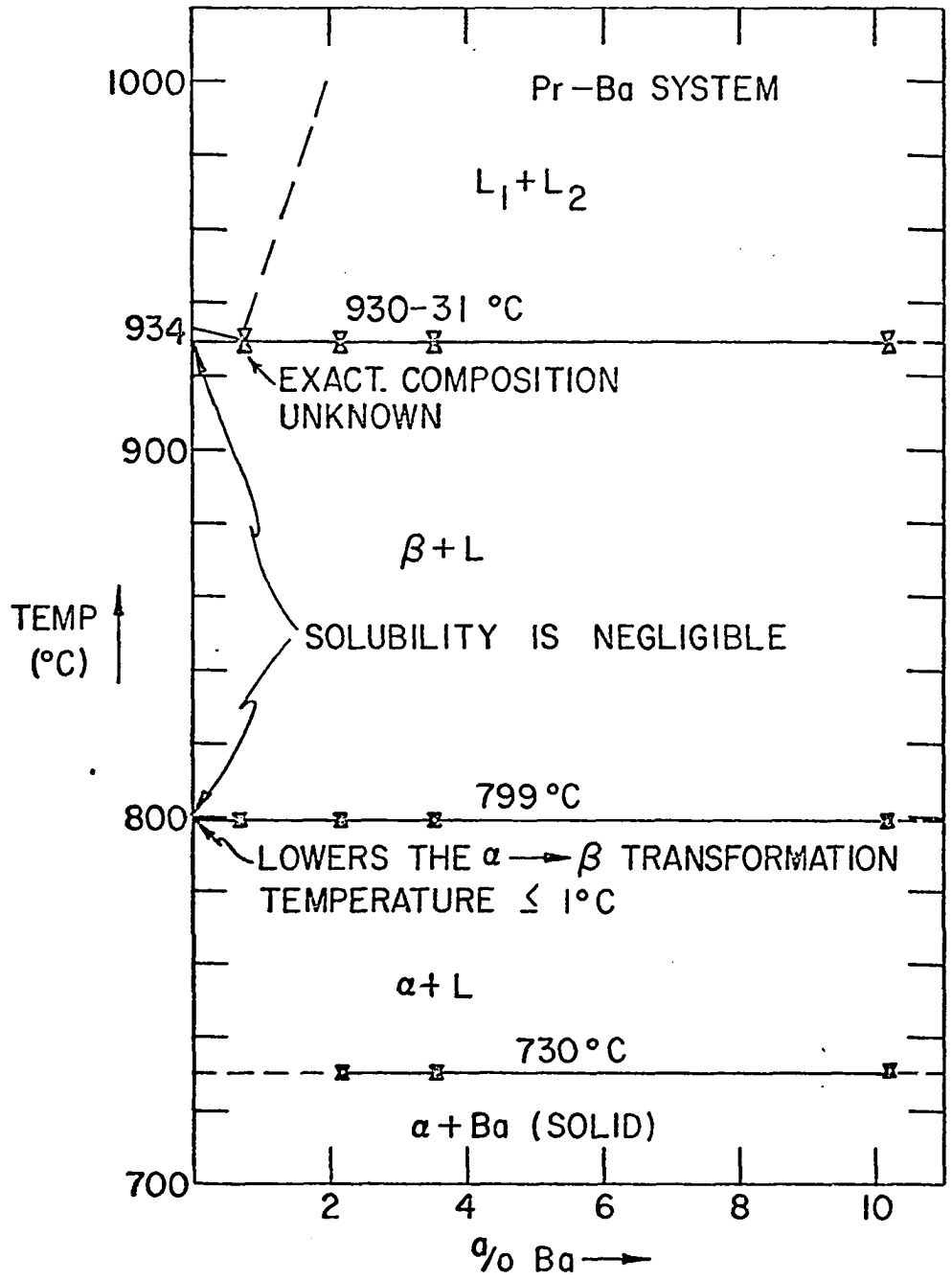

Figure 5
Pr-Ba system.

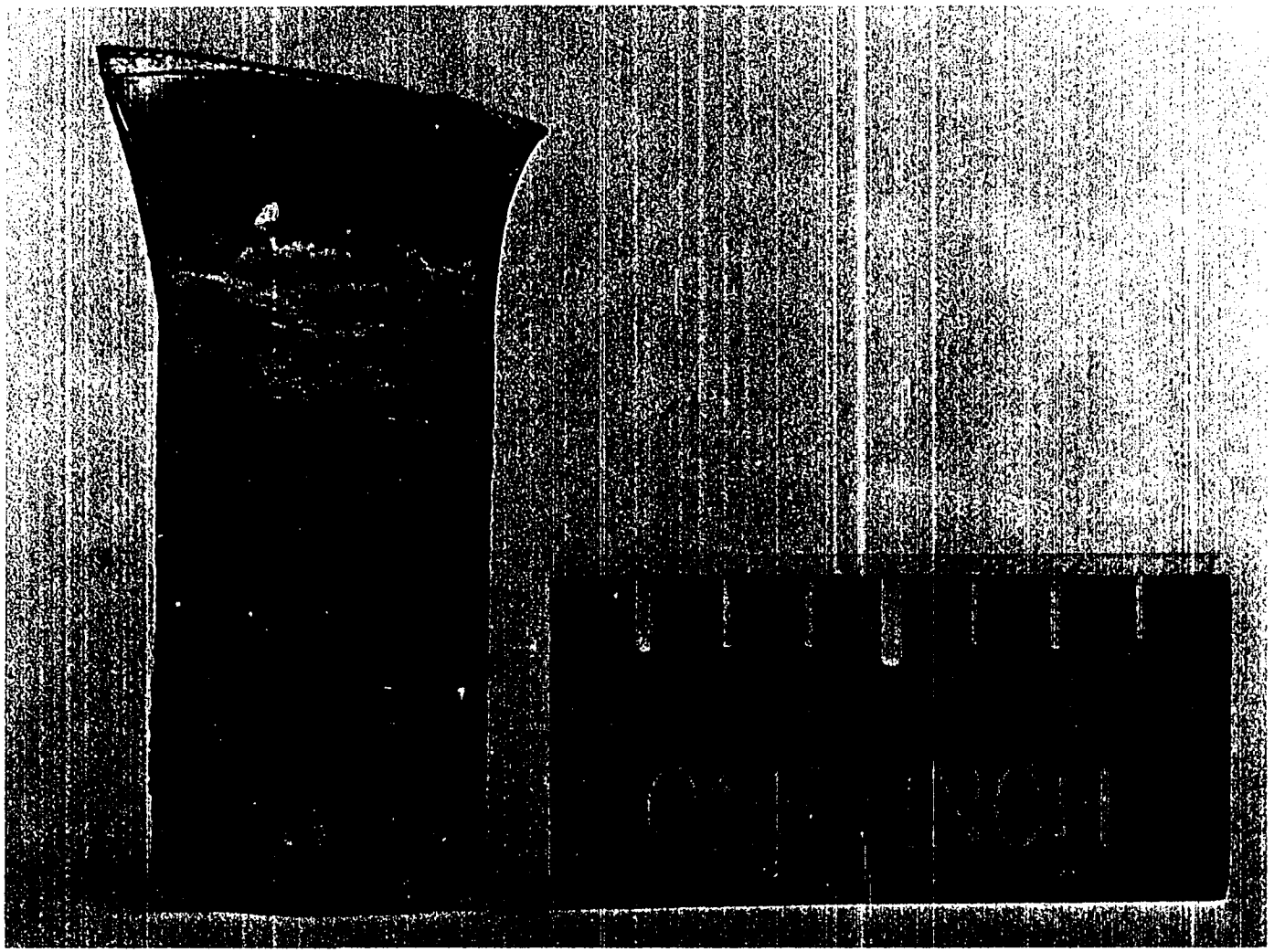

Figure 6

Pr-Ba system. A section through the D. T. A. crucible showing the immiscibility of the two components.

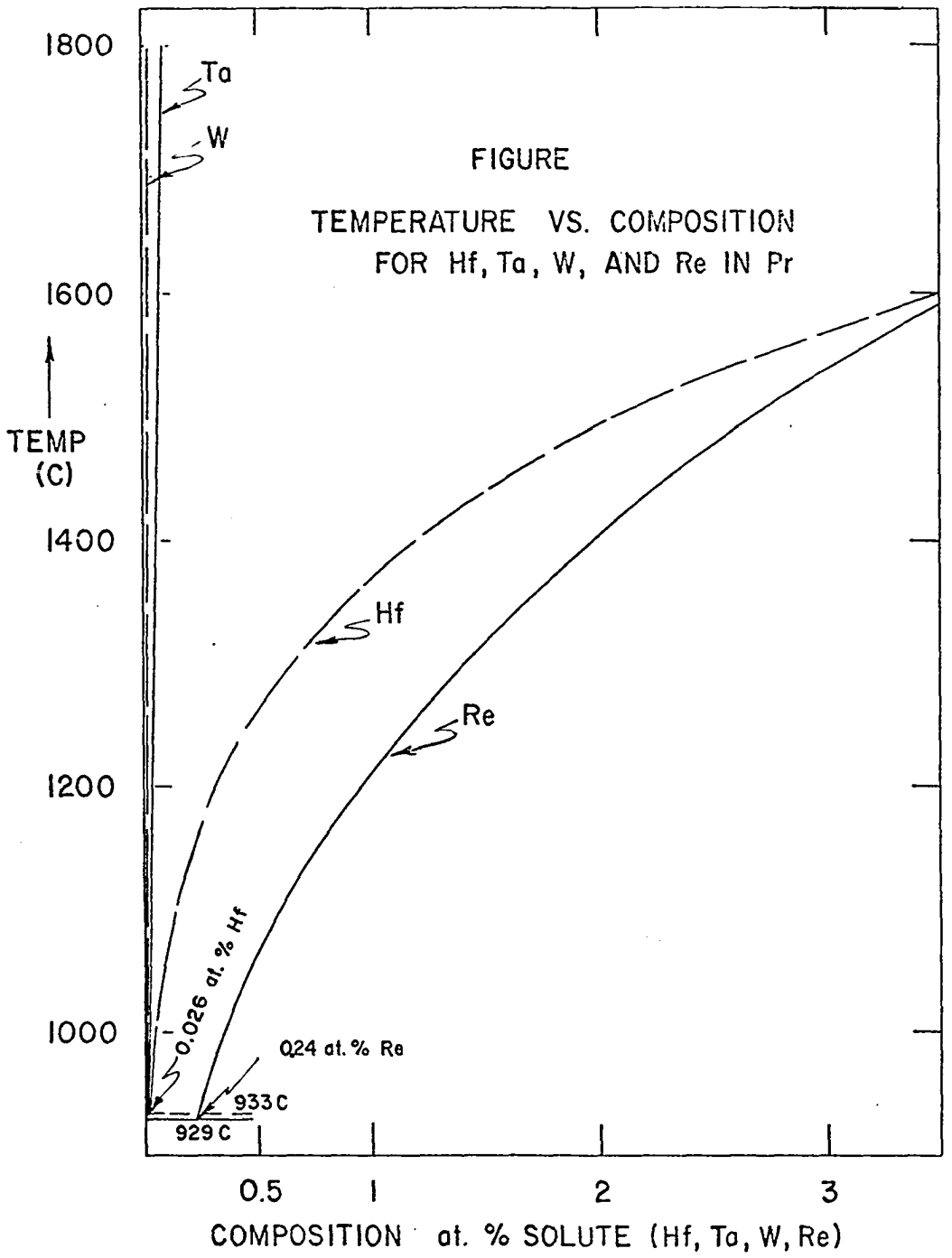

Figure 7
Liquidus for the Pr-Hf,-Re,-Ta, and -W system.

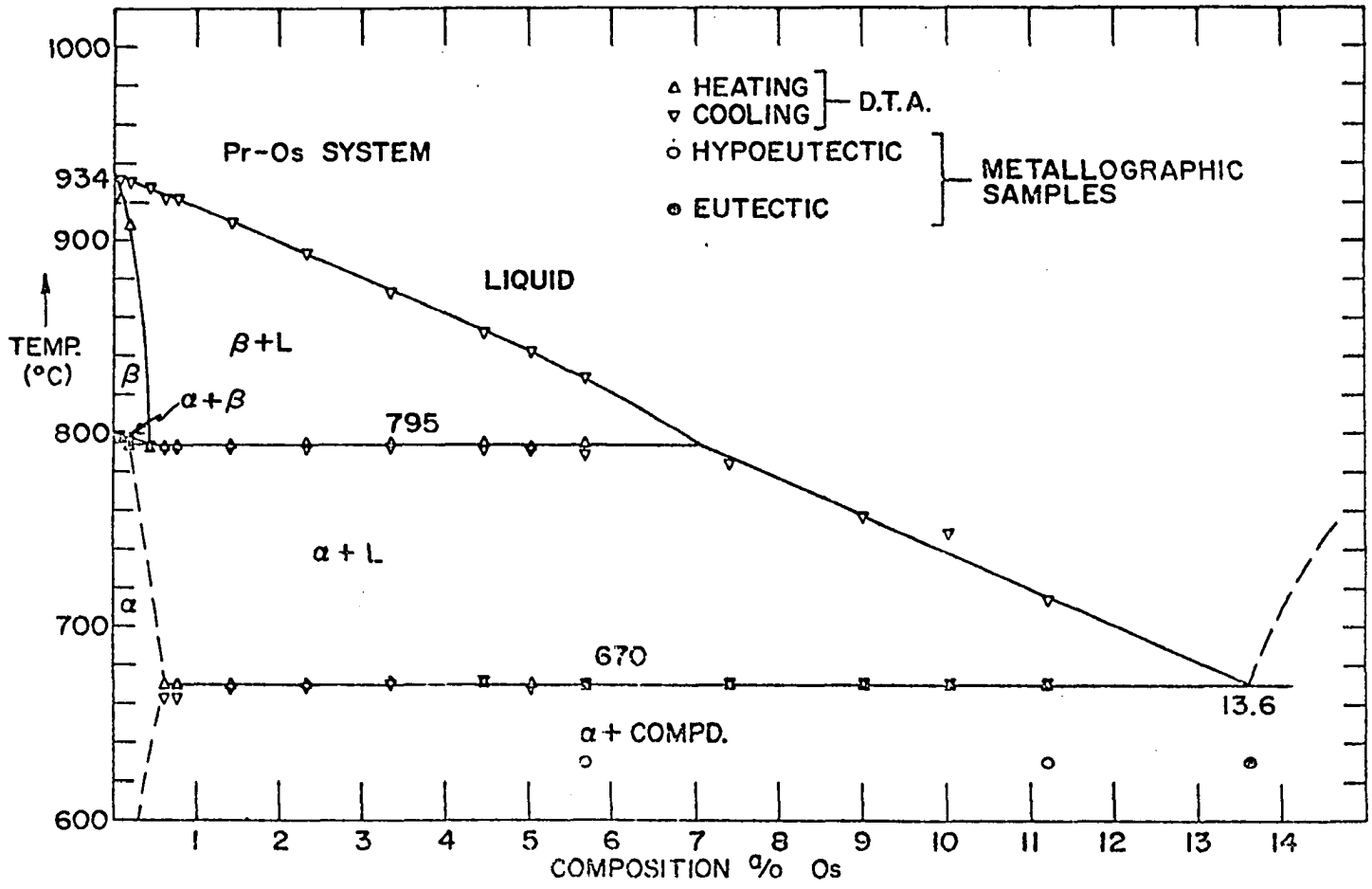

Figure 8
Pr-Os sytem.

Figure 9
Representative eutectic structures.

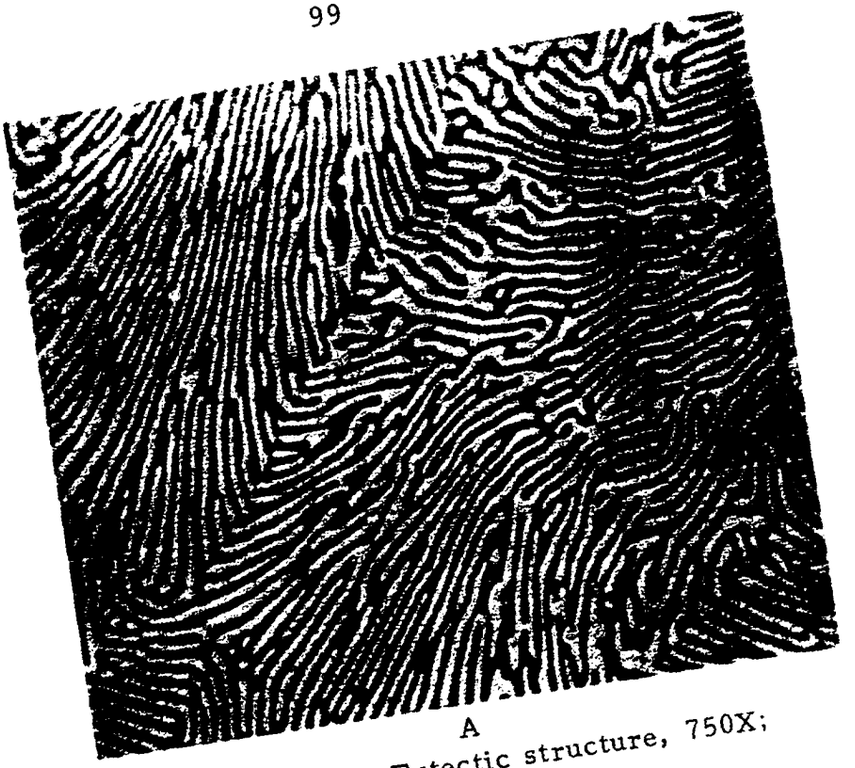

A

Pr-Os system, Eutectic structure, 750X;
Electropolished.

B

Pr-Pb System Eutectic Structure, 200X;
Mech. Pol.; Air Etched

Figure

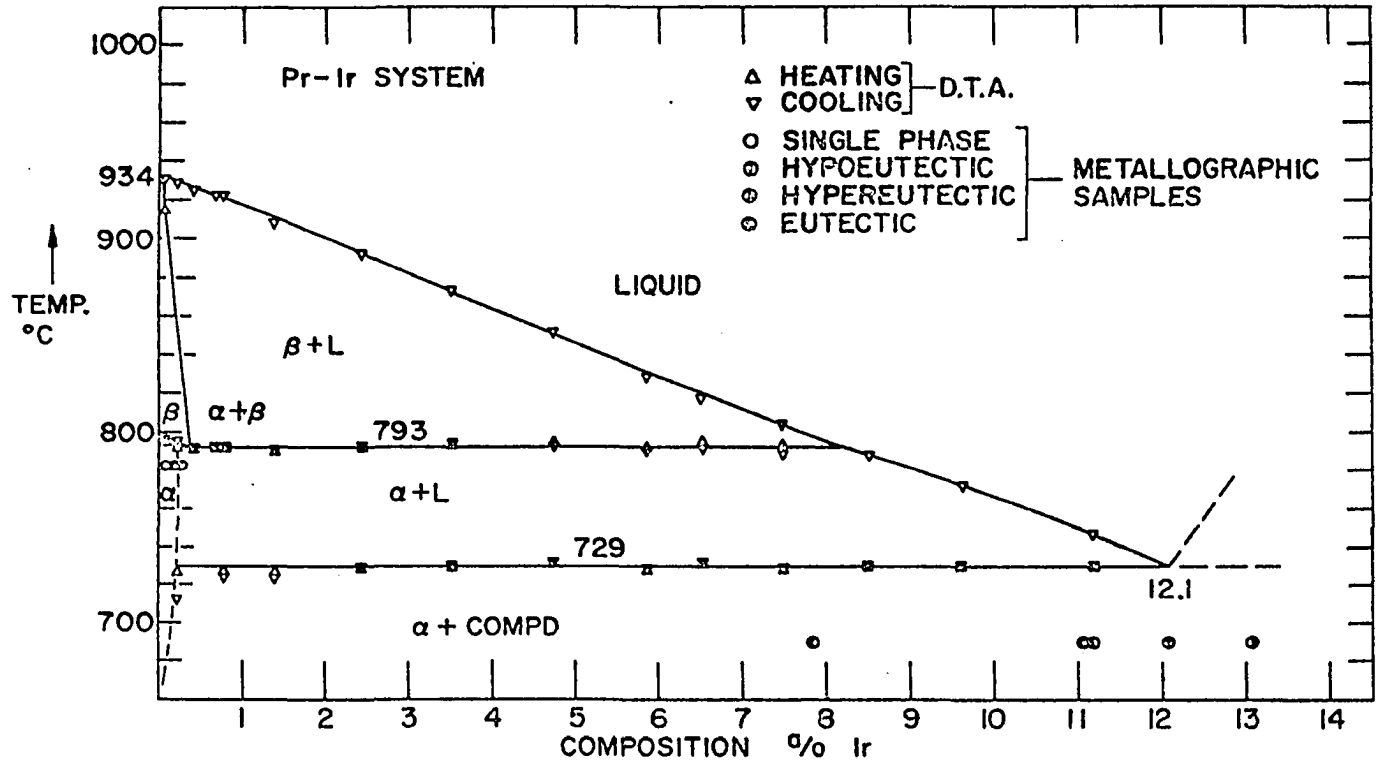

Figure 10
Pr-Ir system.

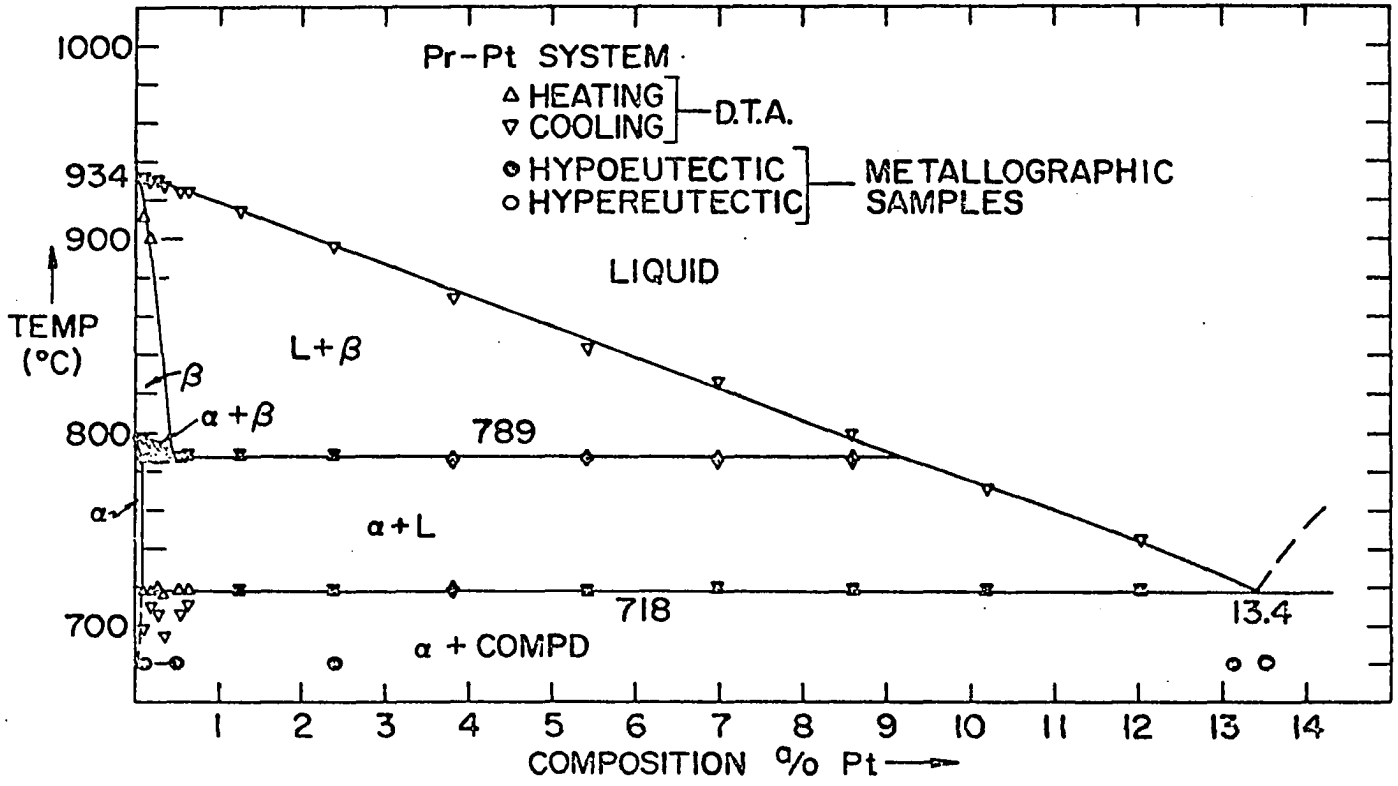

Figure 11
Pr-Pt system.

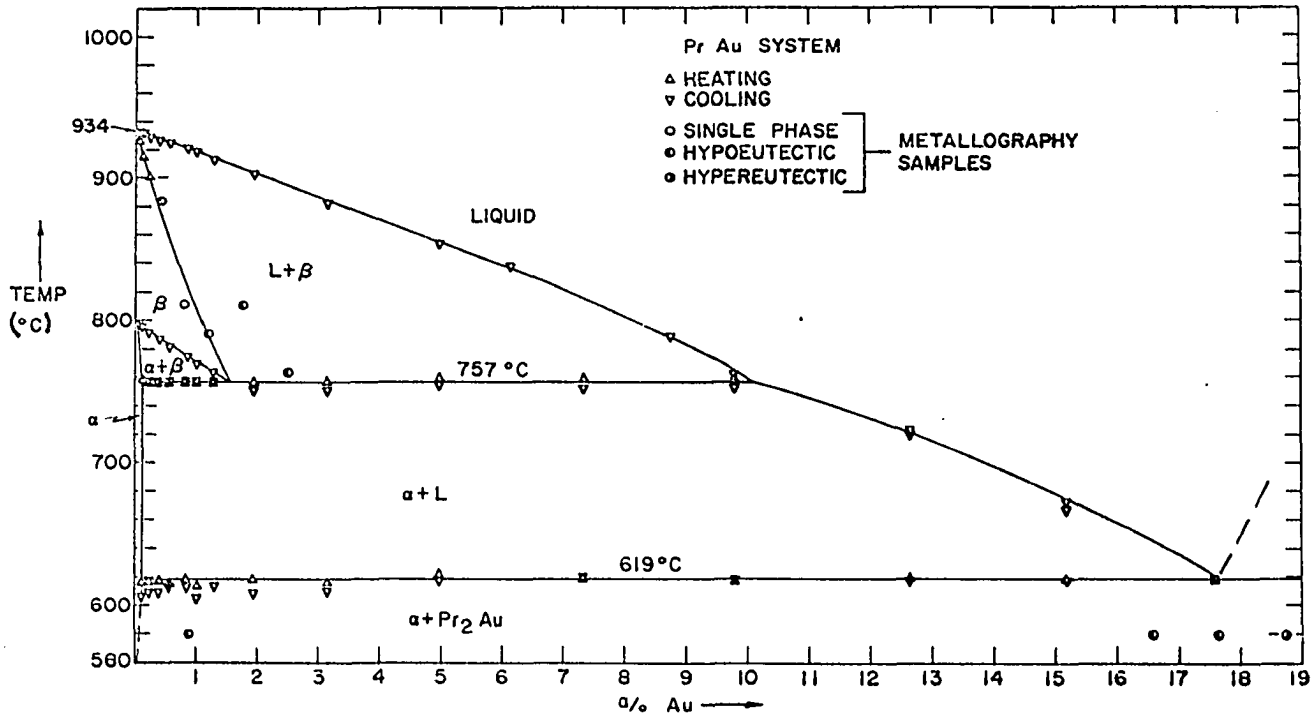

Figure 12
Pr-Au system.

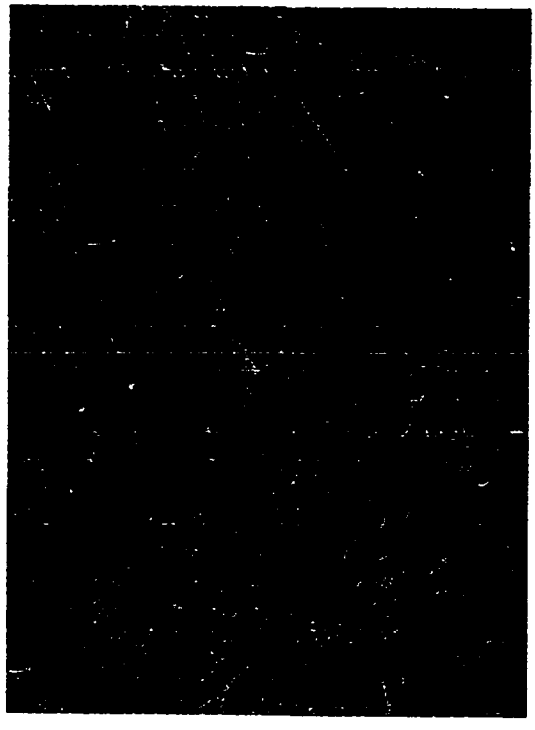

A

Pr-Bi system, Eutectic structure, 200X; Mechanically polished Etchant: Roman's solution

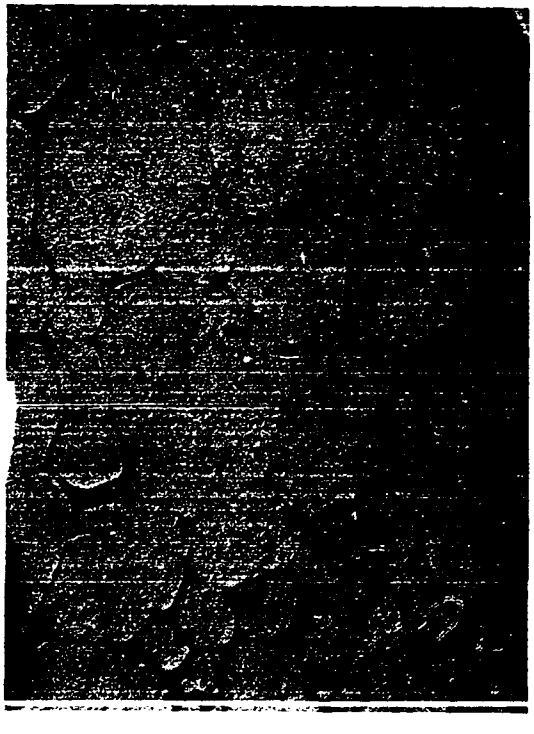

B

1.2 At.% Au, Water quenched from the β + liquid region. 50X; Mechanically polished; Roman's solution.

Figure 13
Photomicrographs.

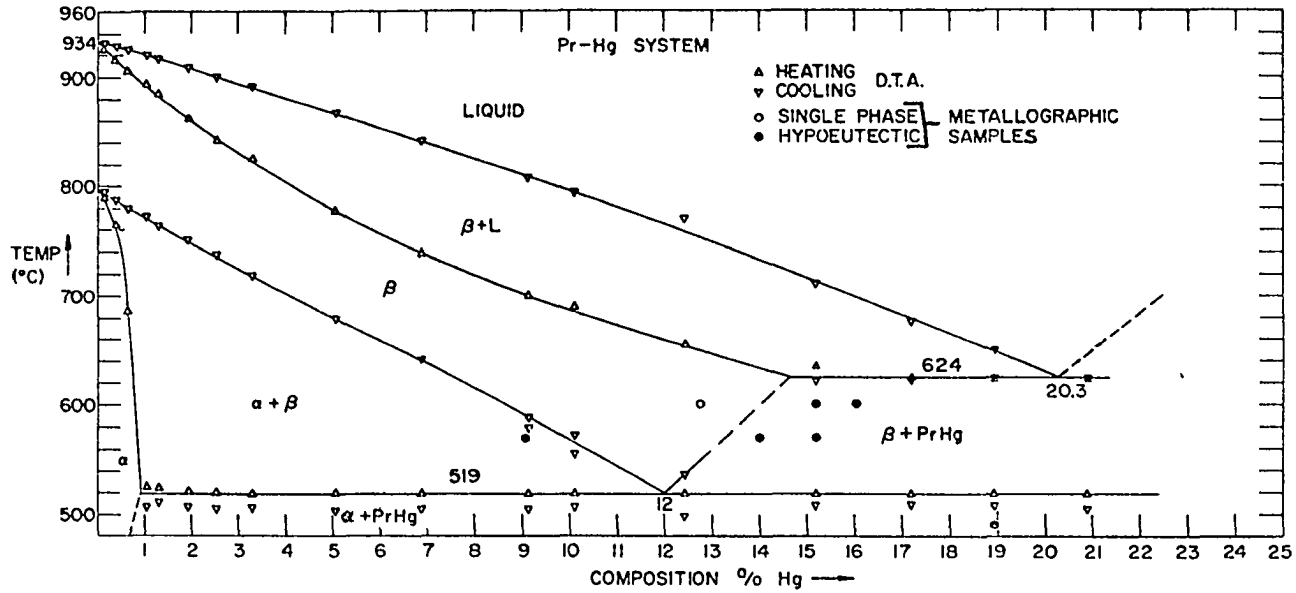

Figure 14
Pr-Hg system.

Figure 15
Photomicrographs of some quenched Pr-Hg alloys.

Figure

Samples heat treated at 570°C and then oil quenched to room temperature. 250X; Mechanically polished; Air etched

A

Pure Pr. This was a control sample

B and C were quenched from two phase regions.

B

9.06 At.% Hg

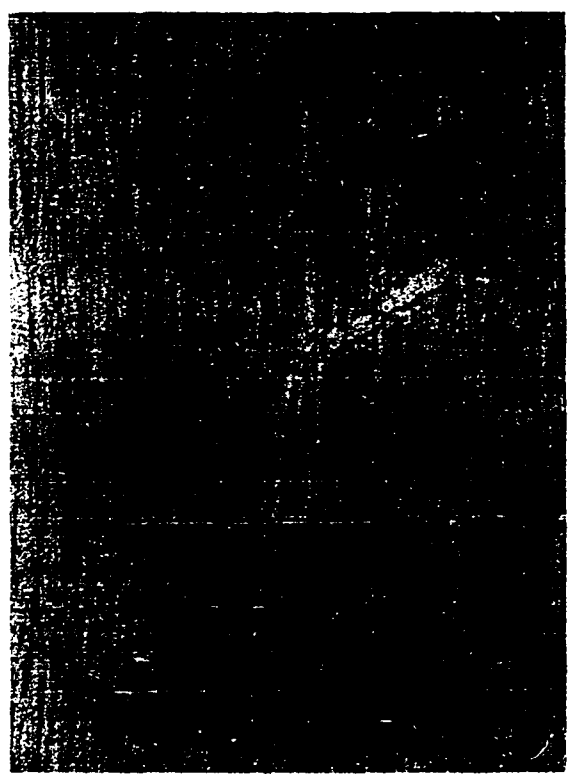

C

14.00 At.% Hg

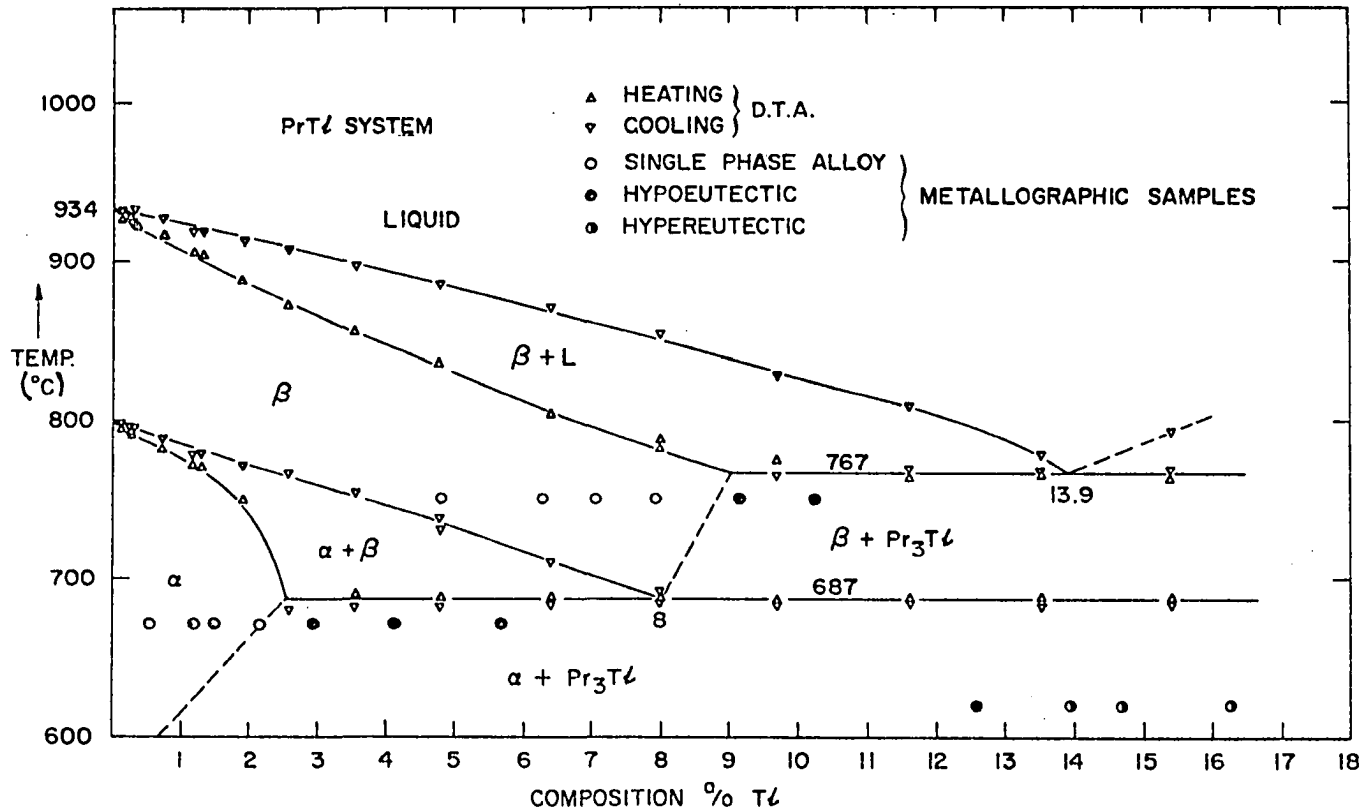

Figure 16
Pr-Tl system.

Figure 17
Eutectic alloys for the Pr-Tl system. In photo A the primary phase is the light colored material while in photo B the dark phase located in the center of the light colored phase is the primary phase.

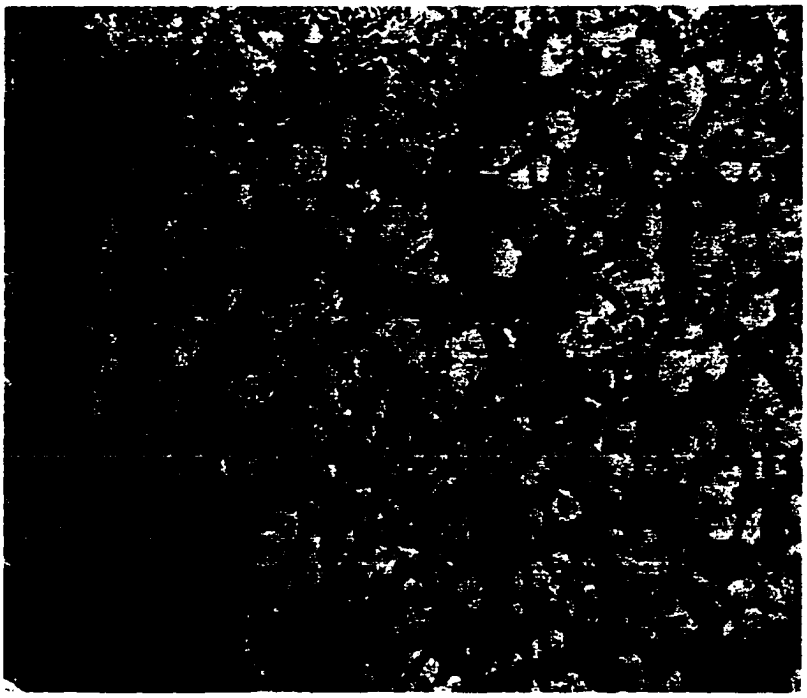

A

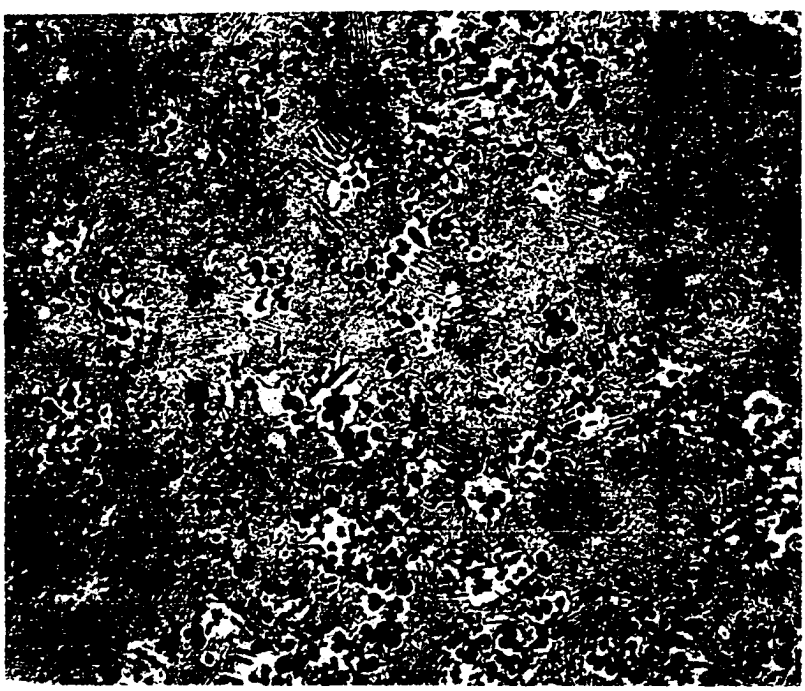

B

Figure

Pr-Ti system, Eutectic alloys, A is hypoeutectic and B is hypereutectic 100X; Mechanically polished; Air etched.

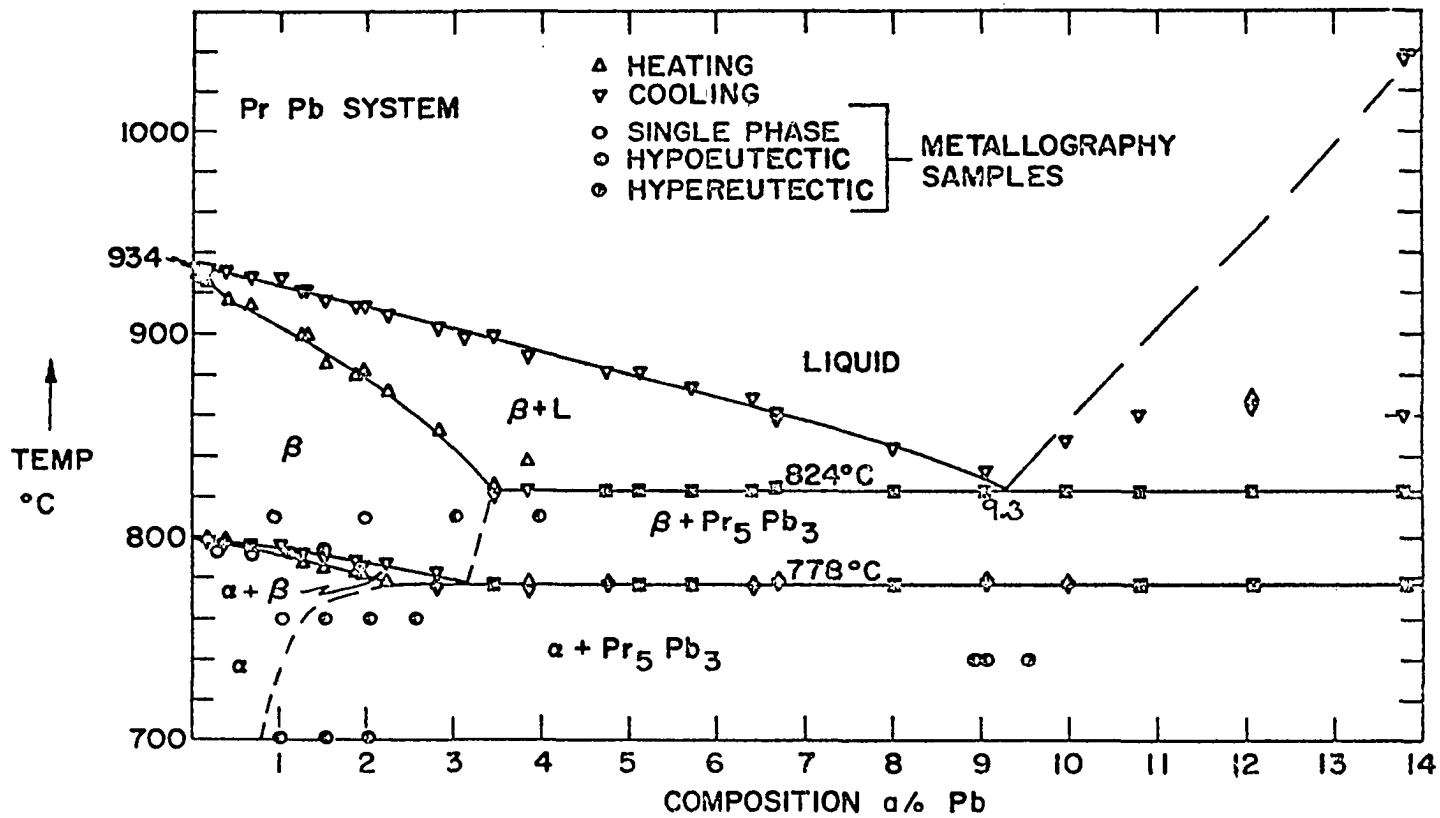

Figure 18
Pr-Pb system.

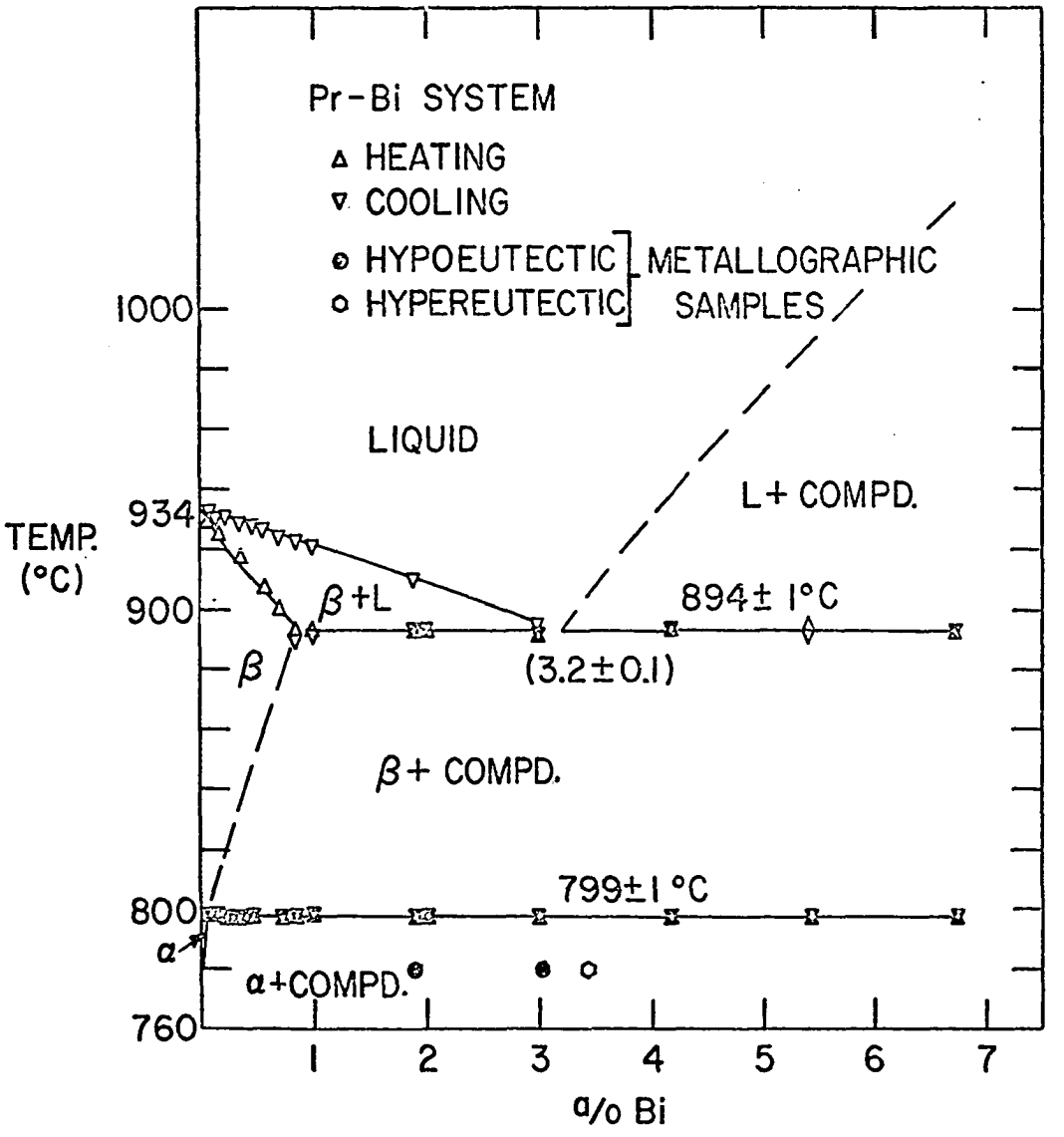

Figure 19
Pr-Bi system.

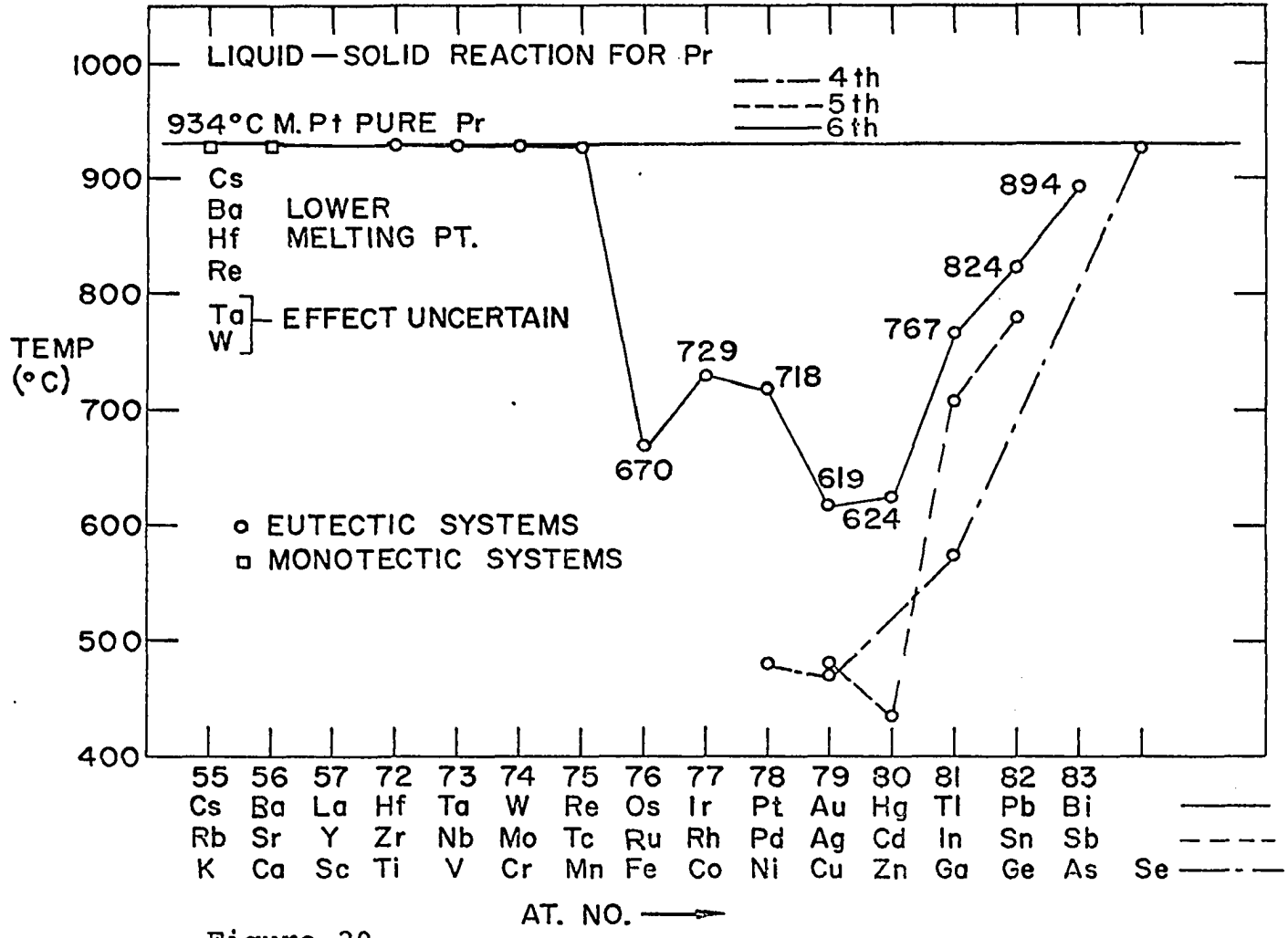

Figure 20
Effect of solutes on the melting point of Pr.

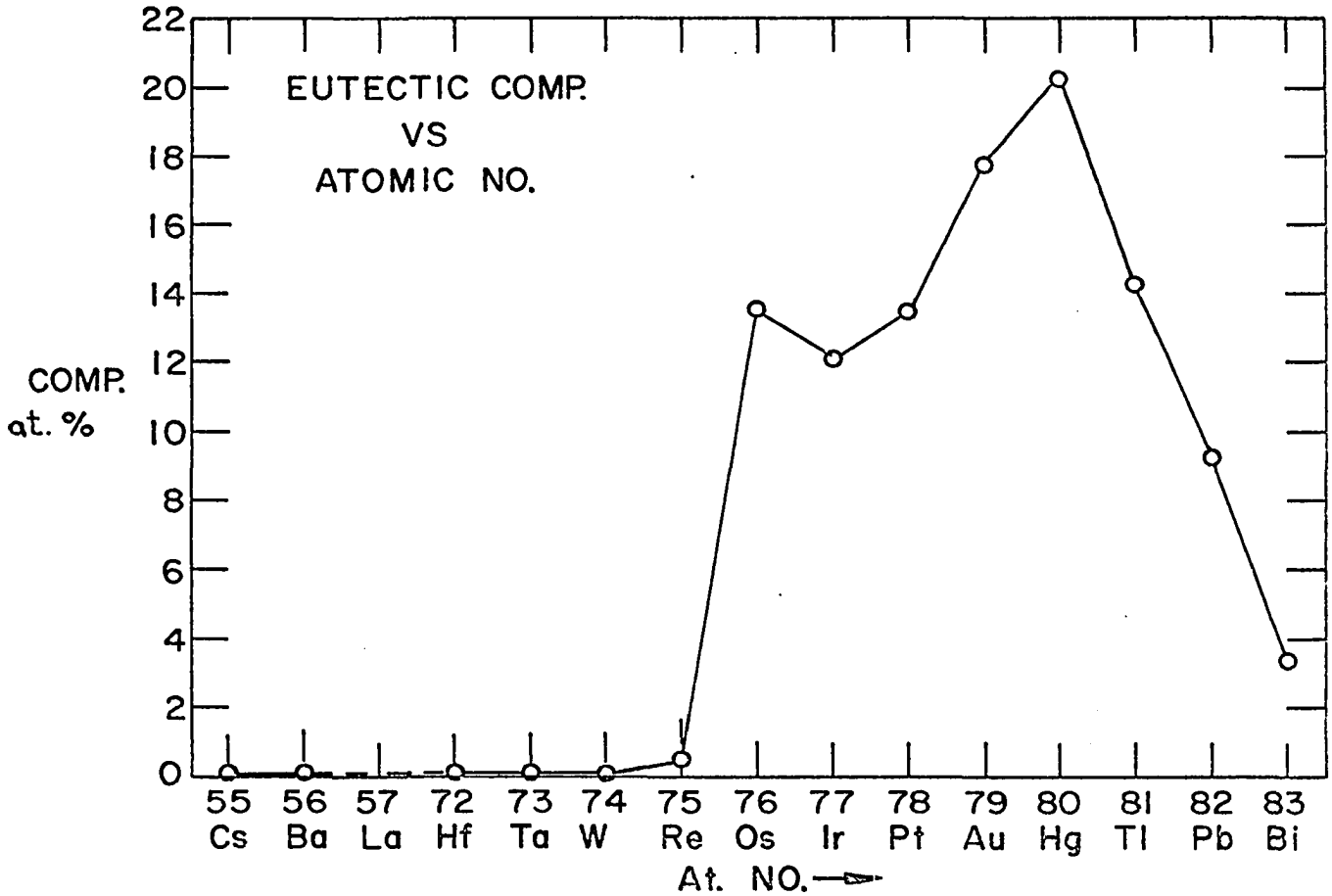

Figure 21
Eutectic composition vs. atomic number.

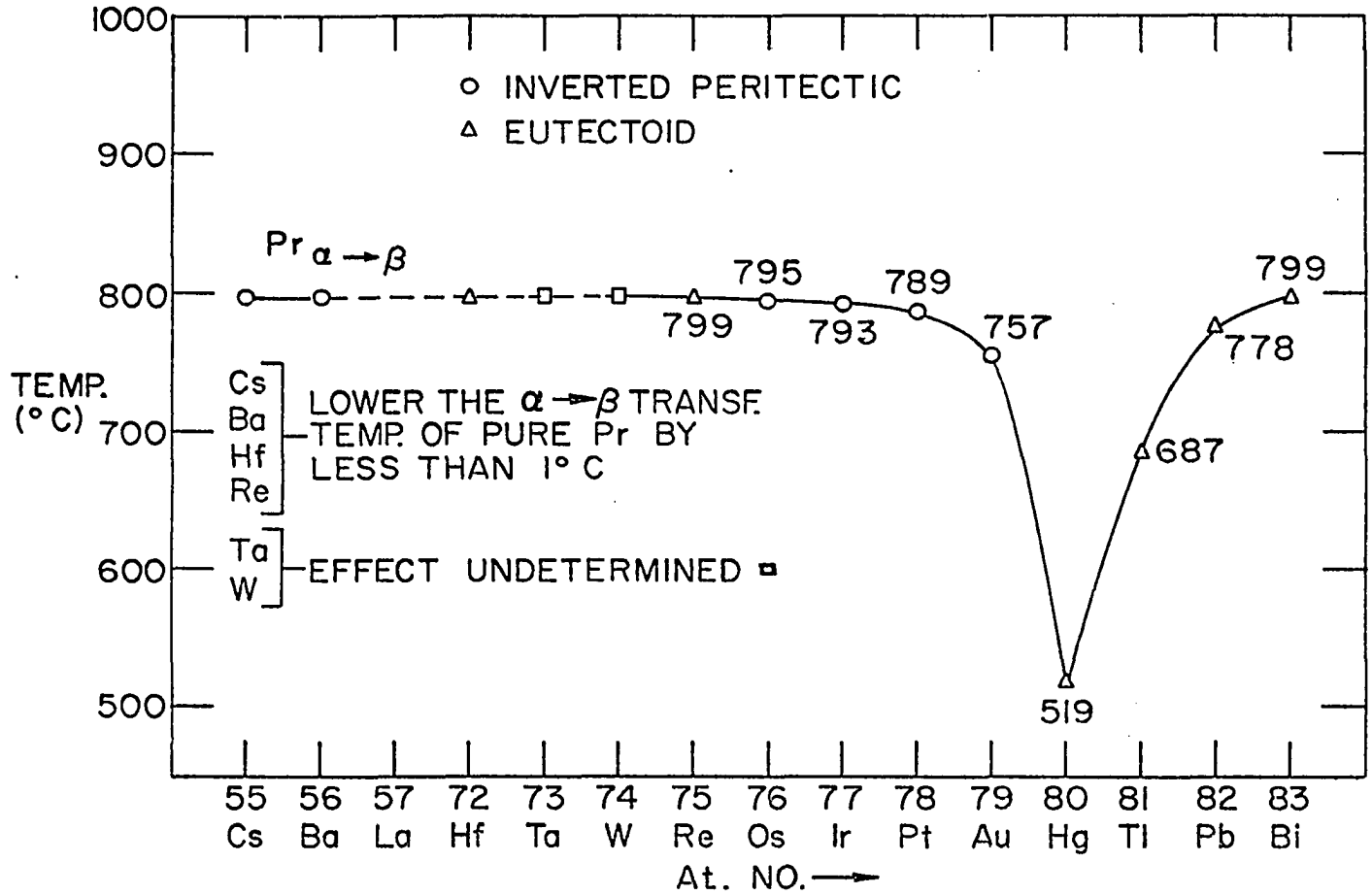

Figure 22
Effect of period six solutes on the α to β transformation in Pr.

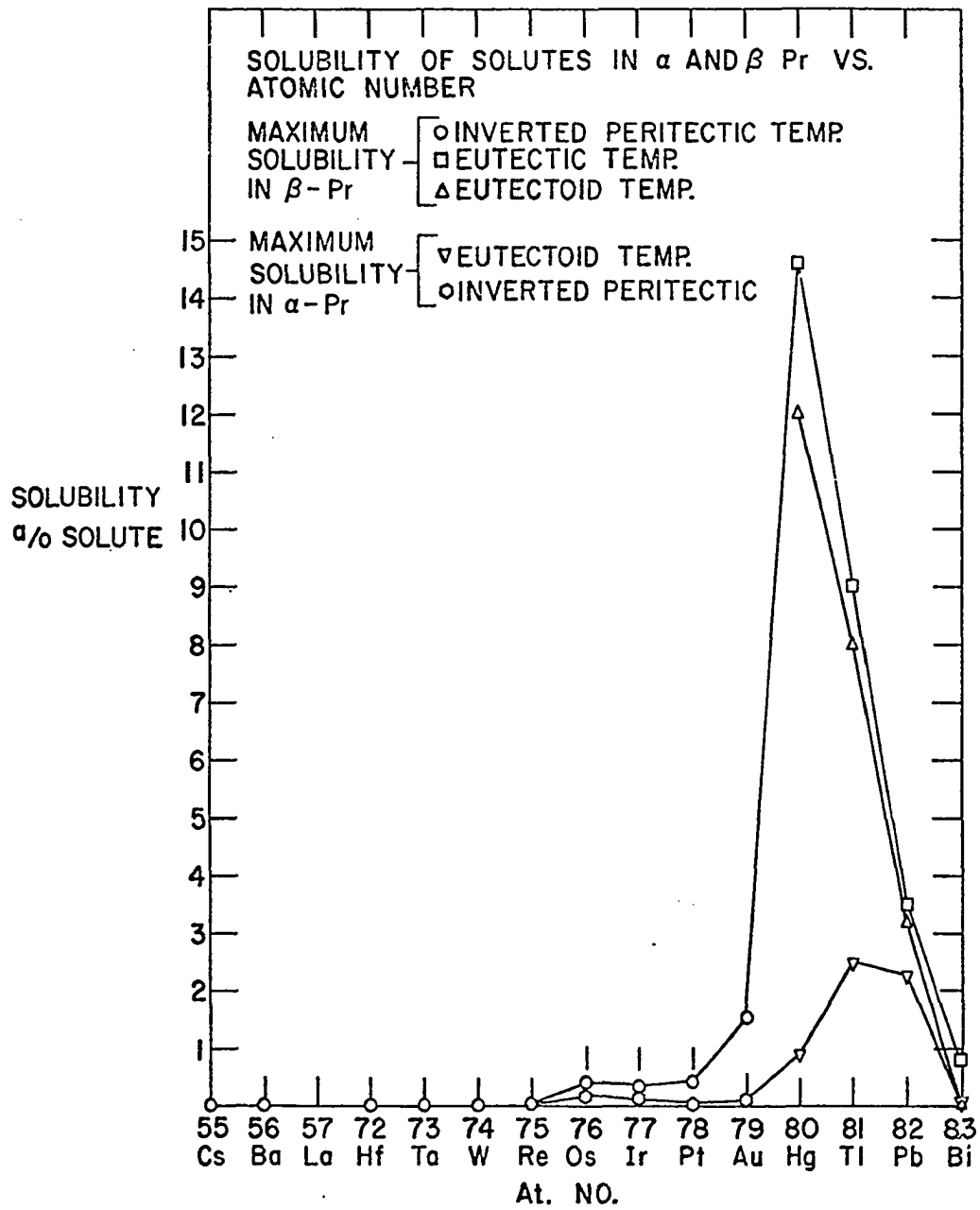

Figure 23
Solubility of period six solutes in Pr.

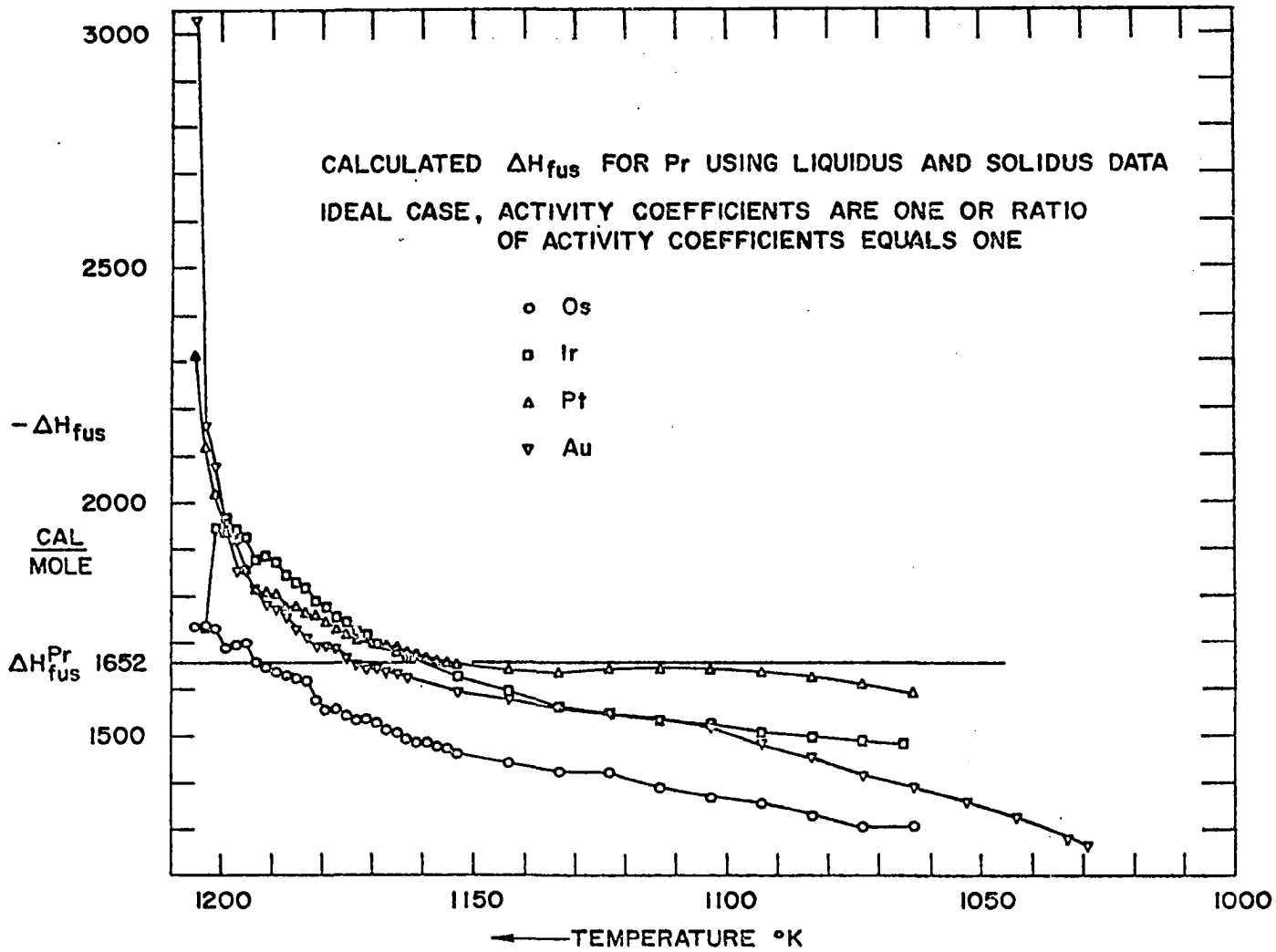

Figure 24
Calculated ΔH^{Pr}_{Fus}.

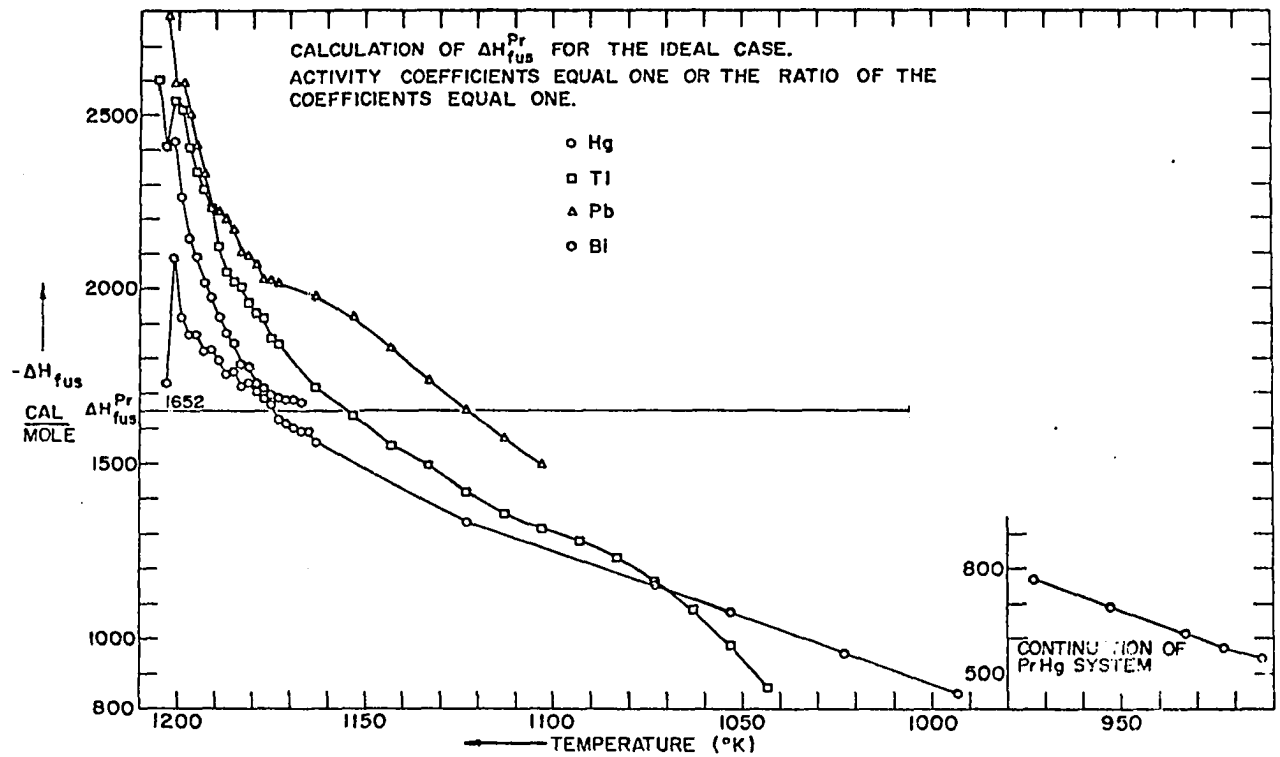

Figure 25
Calculated ΔH^{Pr}_{Fus}.

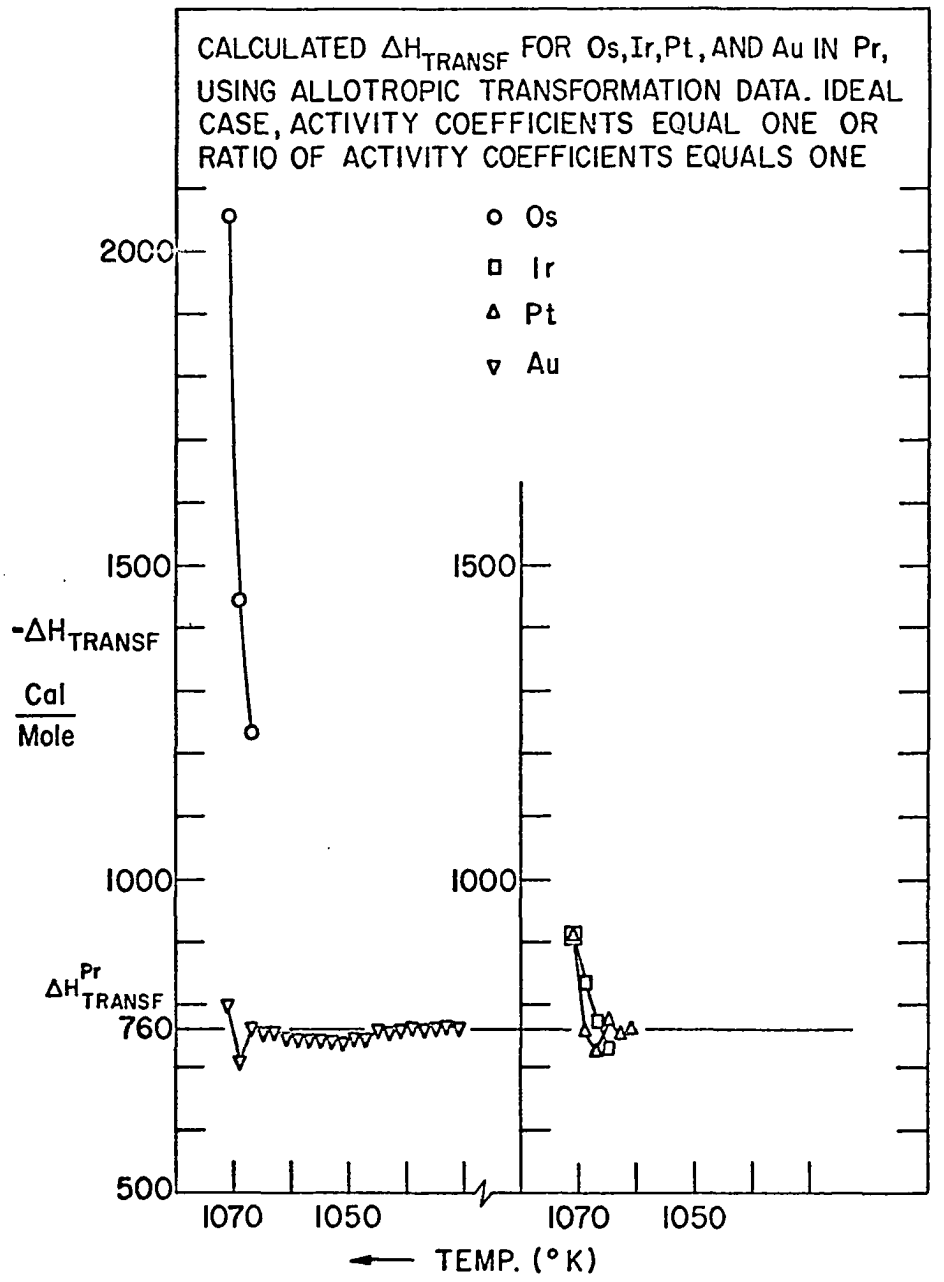

Figure 26
Calculated $\Delta H^{Pr}_{Transf.}$

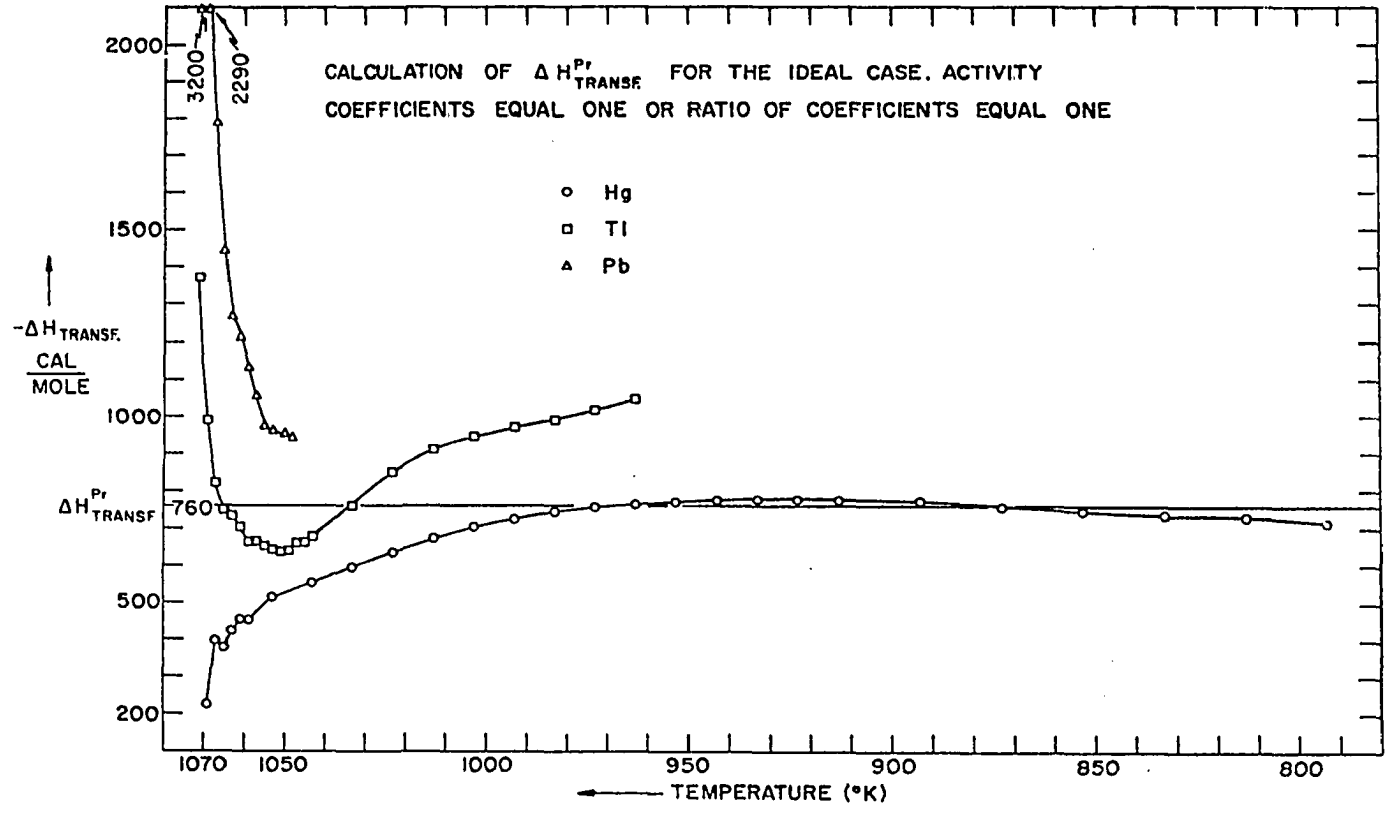

Figure 27
Calculated $\Delta H^{Pr}_{Transf.}$

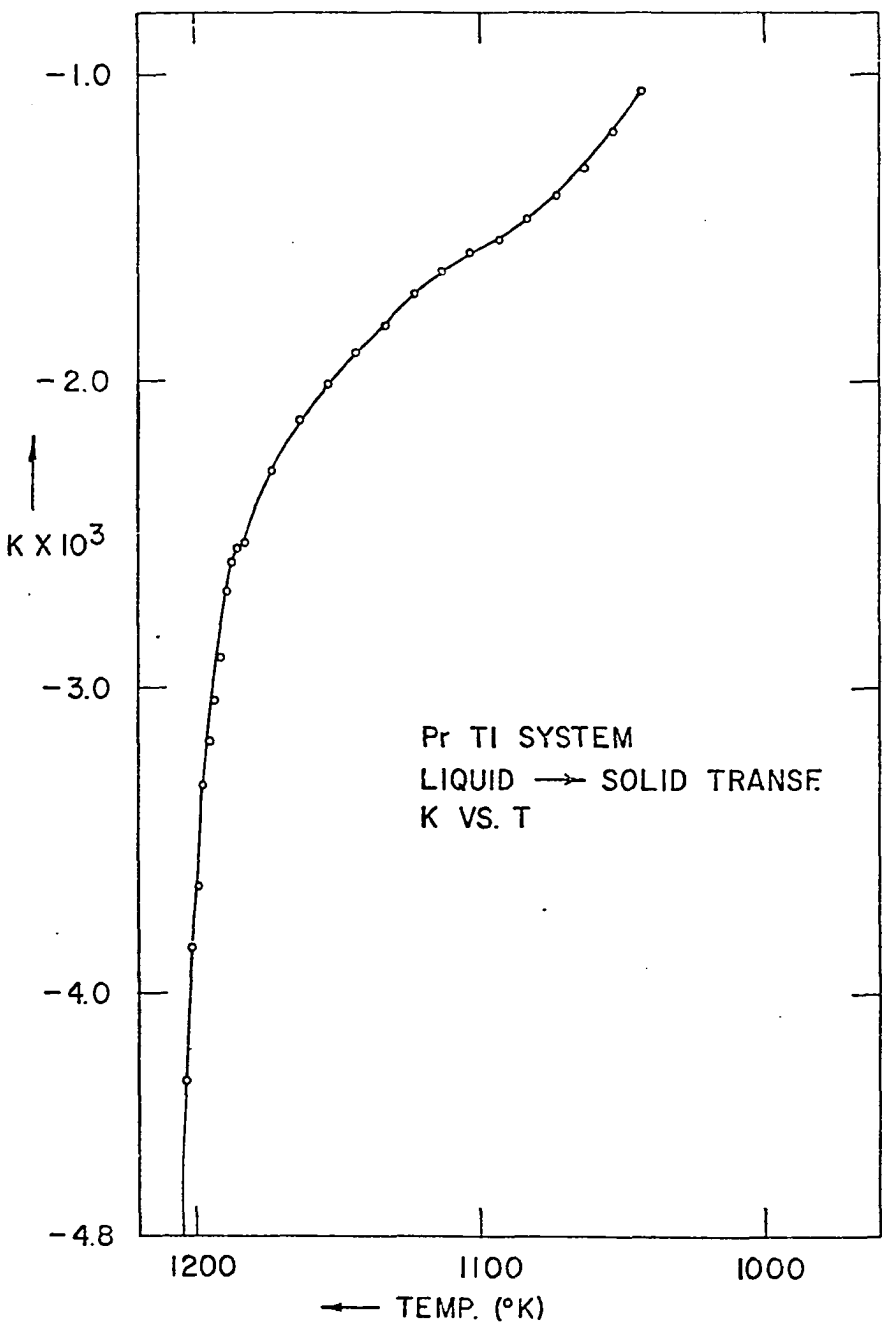

Figure 28
Representative K-function.

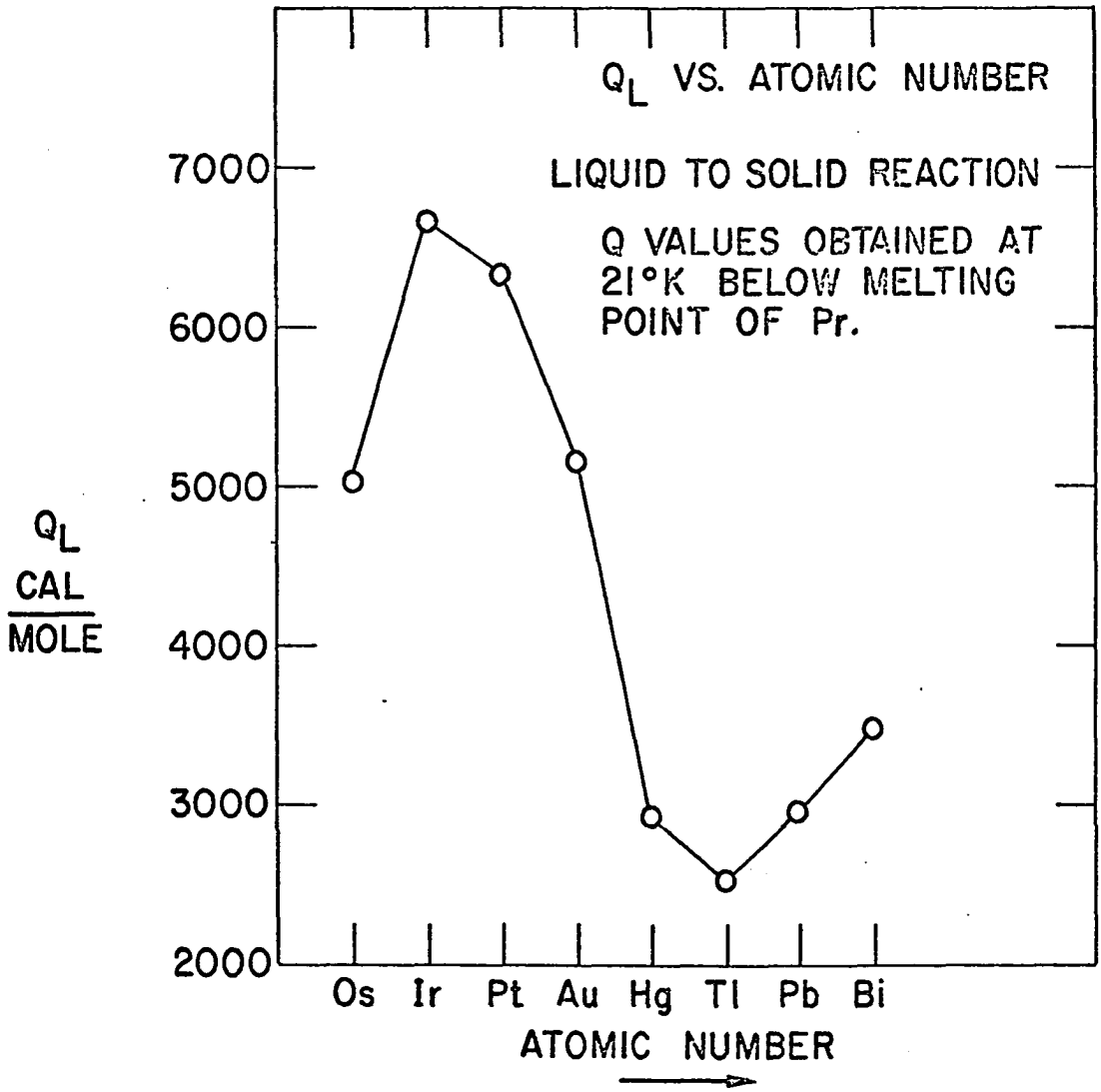

Figure 29
Q_L values.

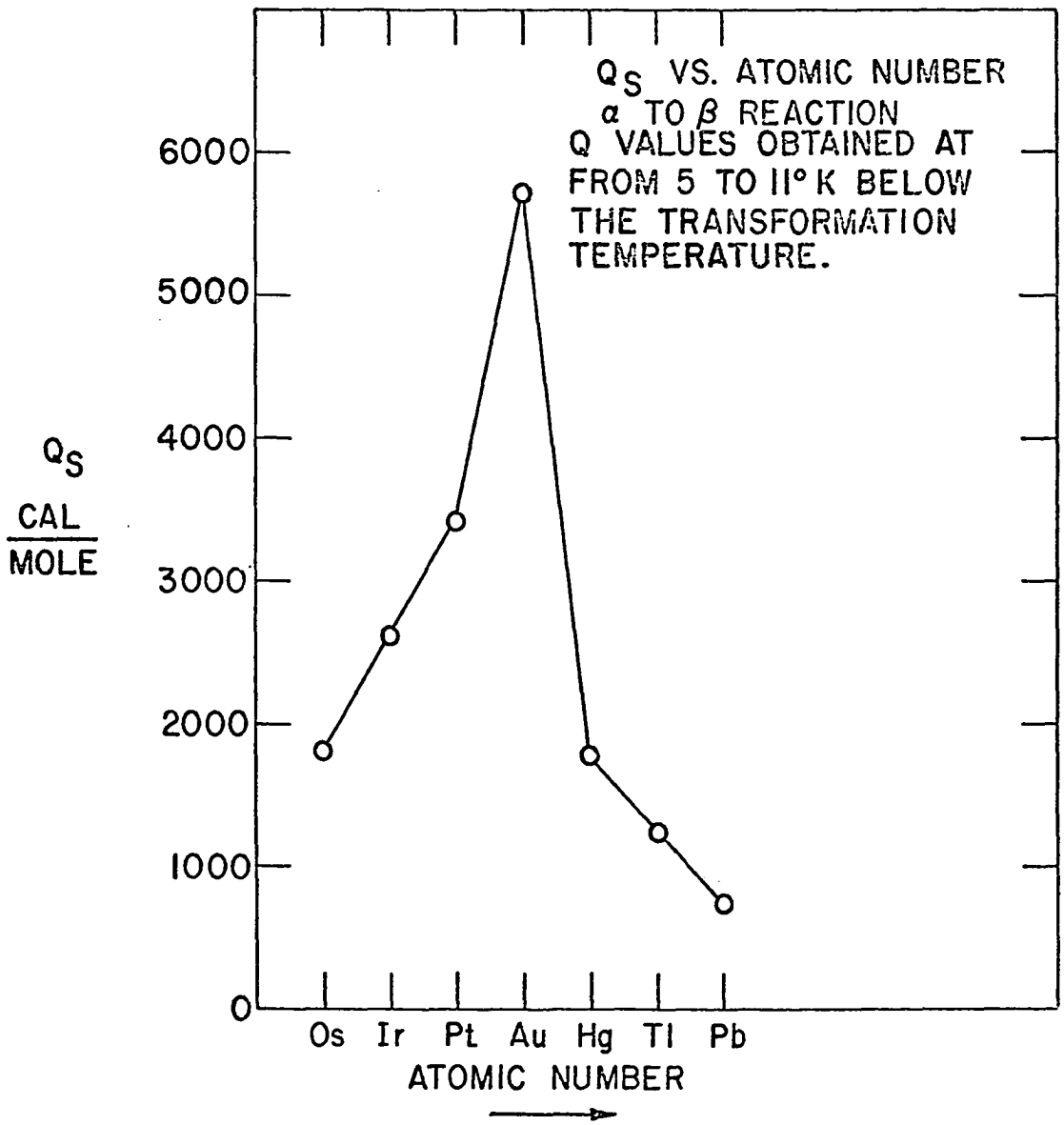

Figure 30
Q_S values.

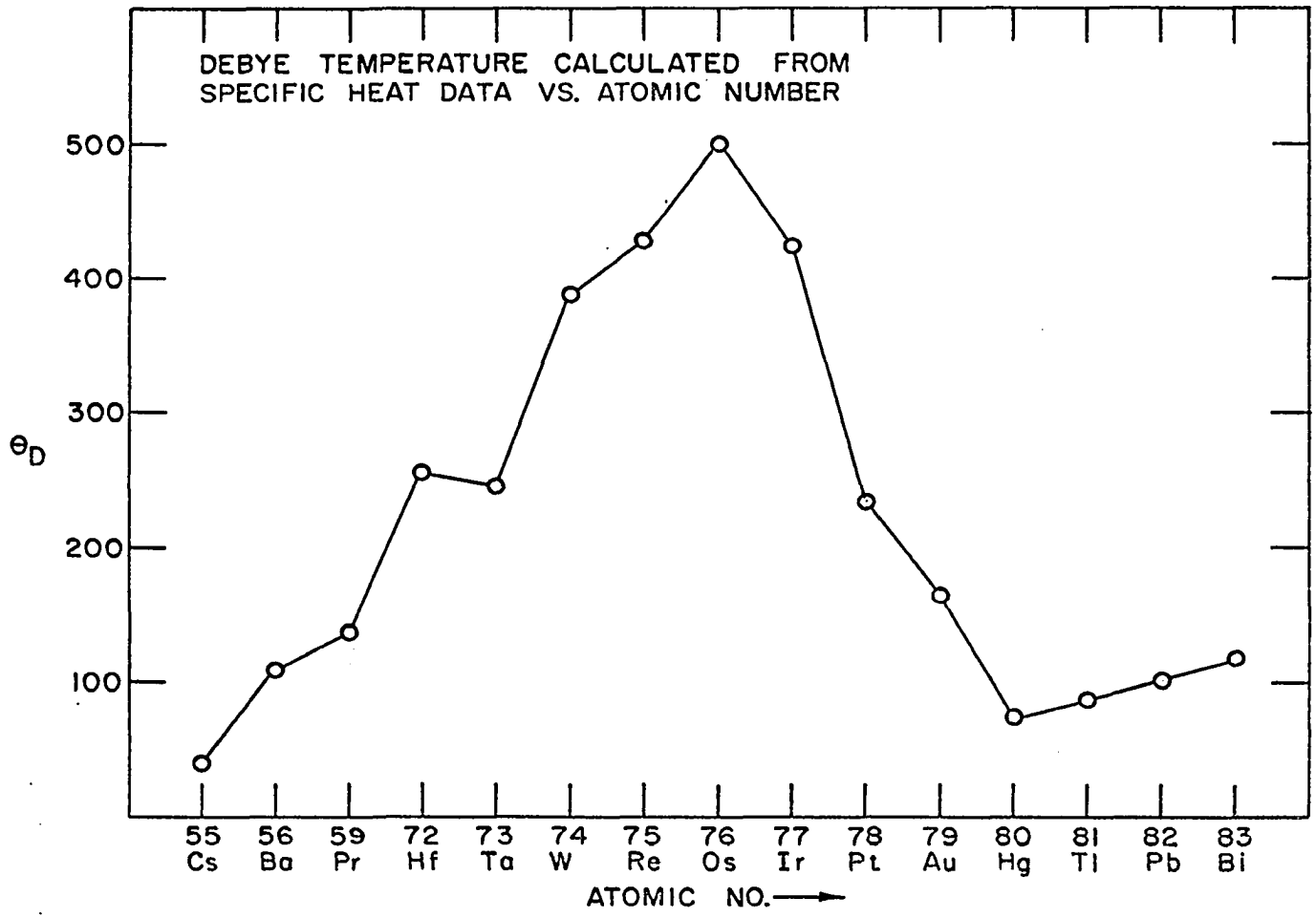

Figure 31
Debye temperatures for period six elements.

Figure 32
The difference in the number of valence electrons between the period six solutes and Pr as a function of Q_L.

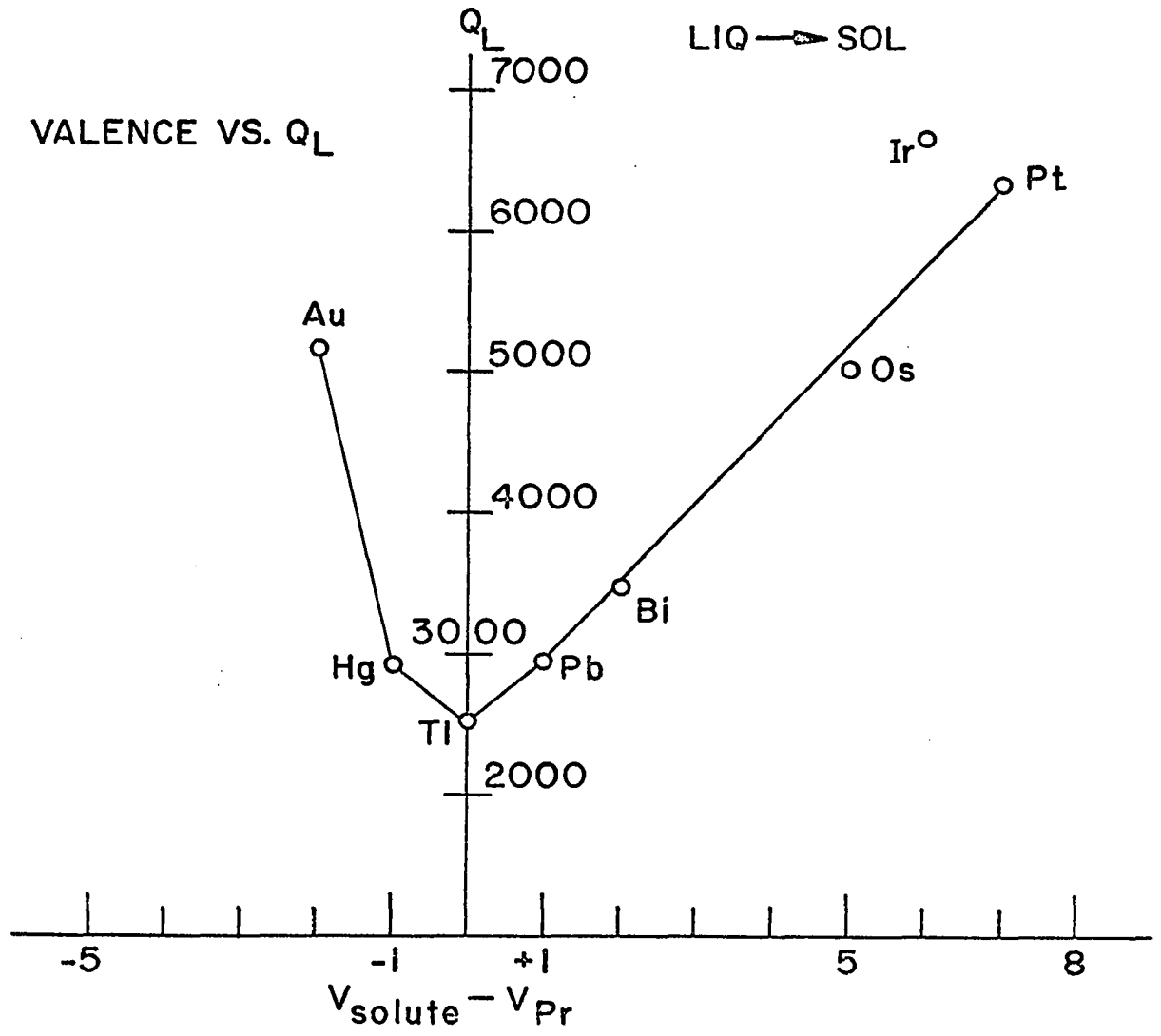

NO. OUTER ELECTRONS AS V_{solute}

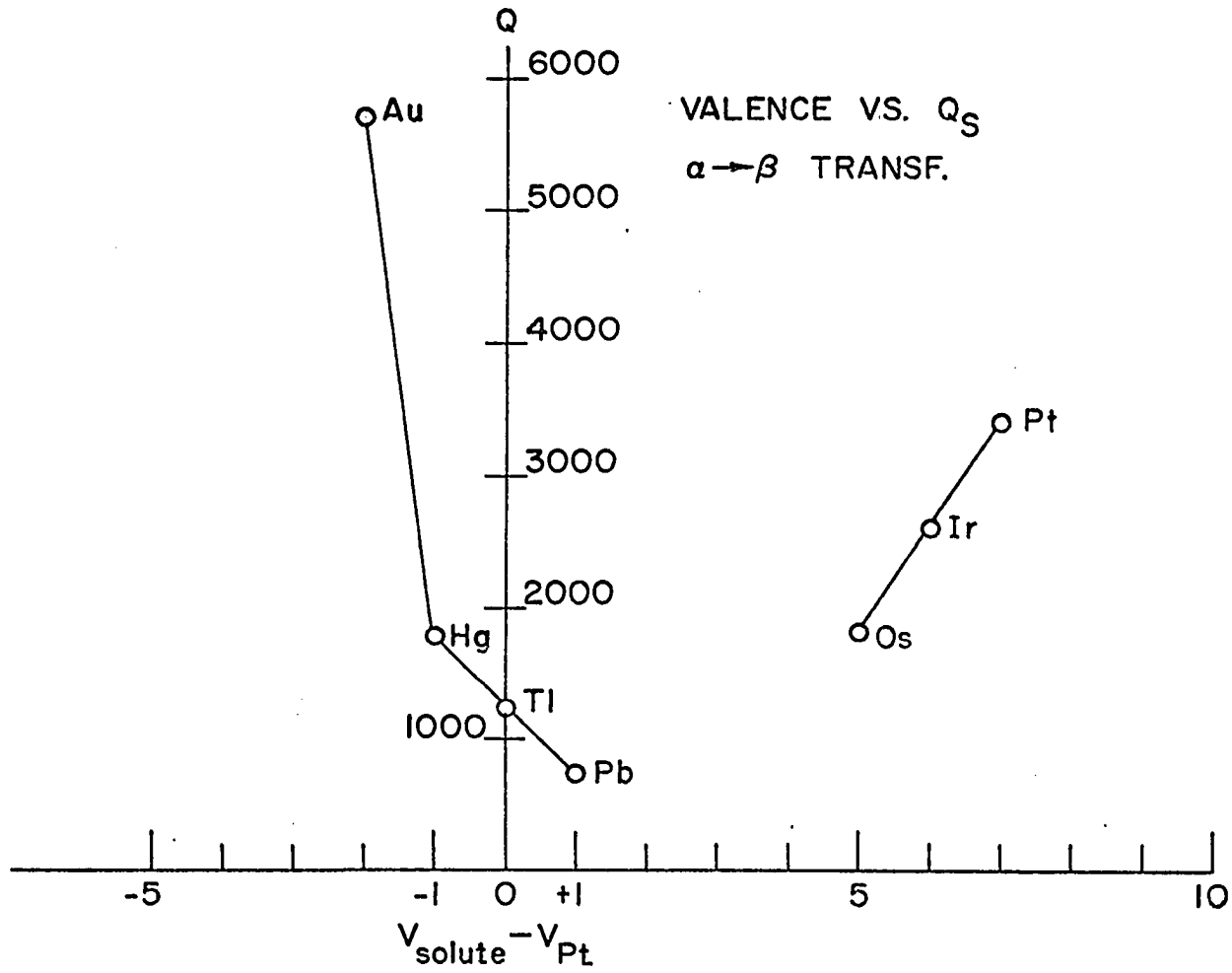

Figure 33
The difference in the number of valence electrons between the period six solutes and Pr as a function of Q_S.

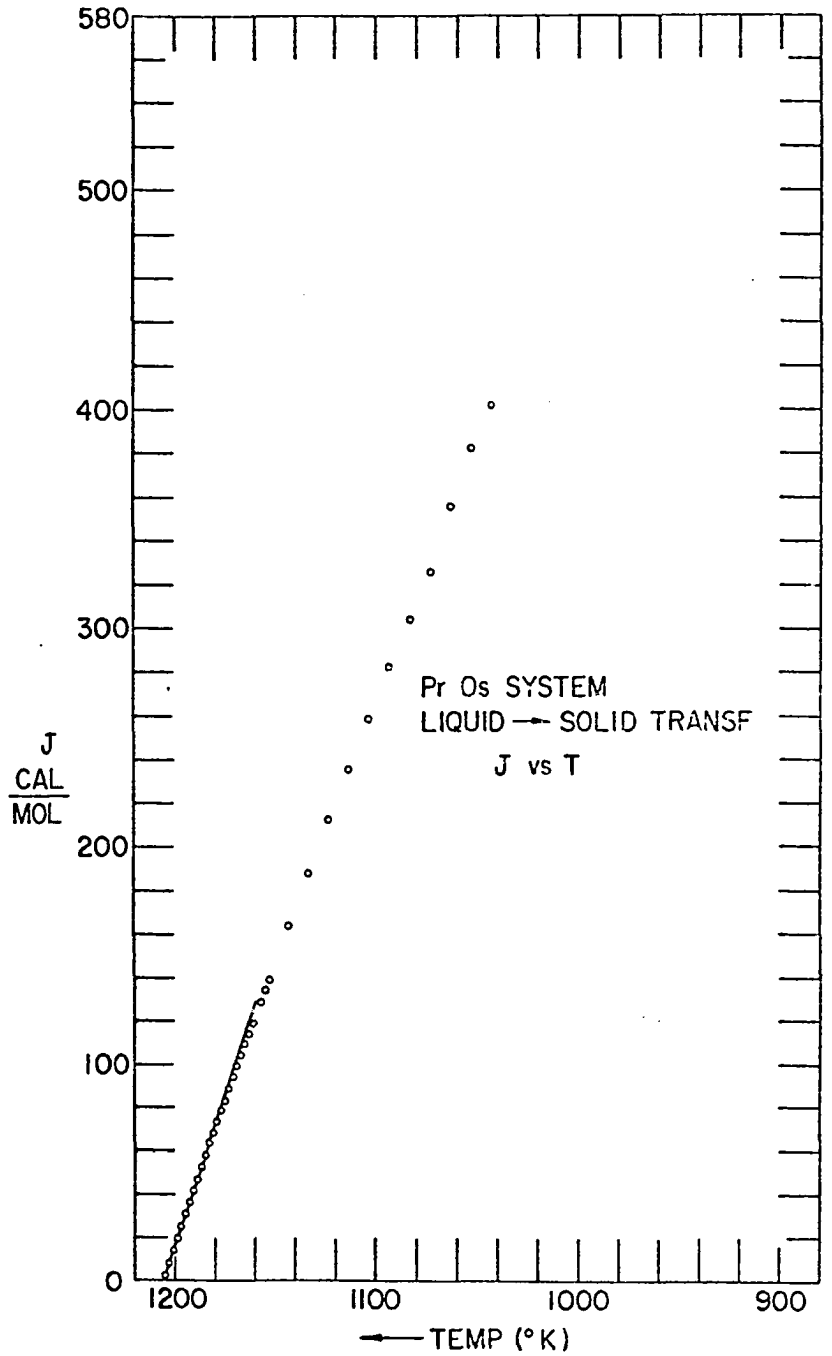

Figure 34
J-function.

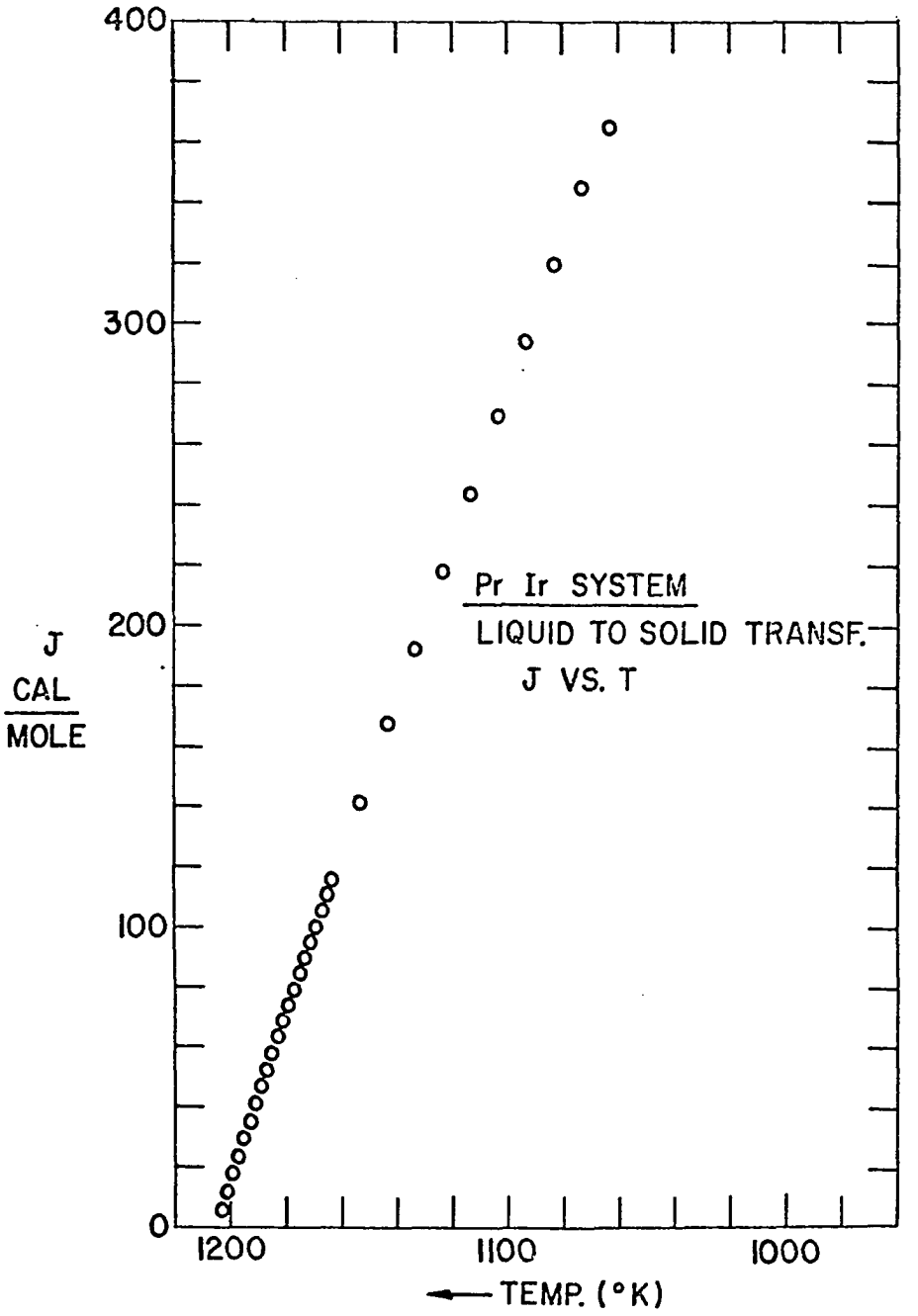

Figure 35
J-function.

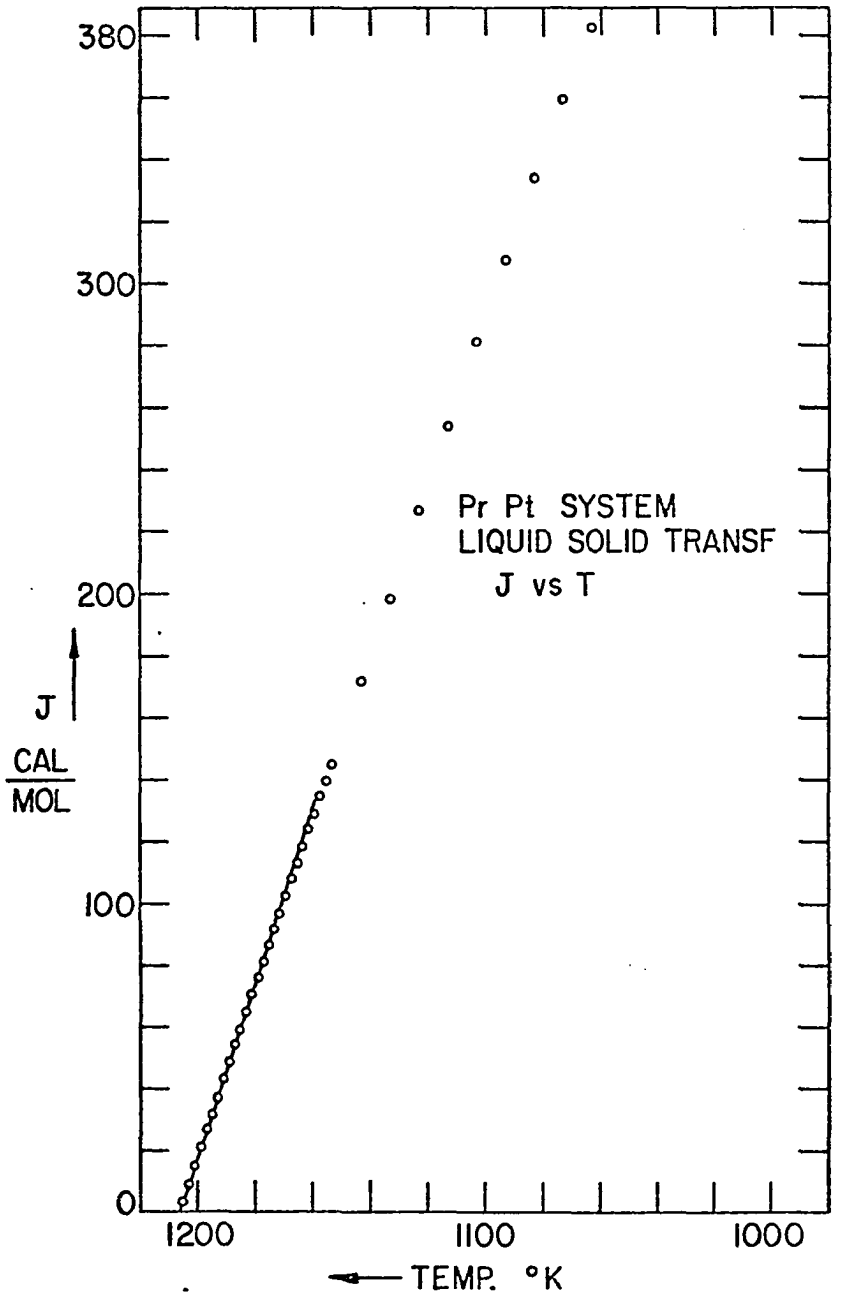

Figure 36
J-function.

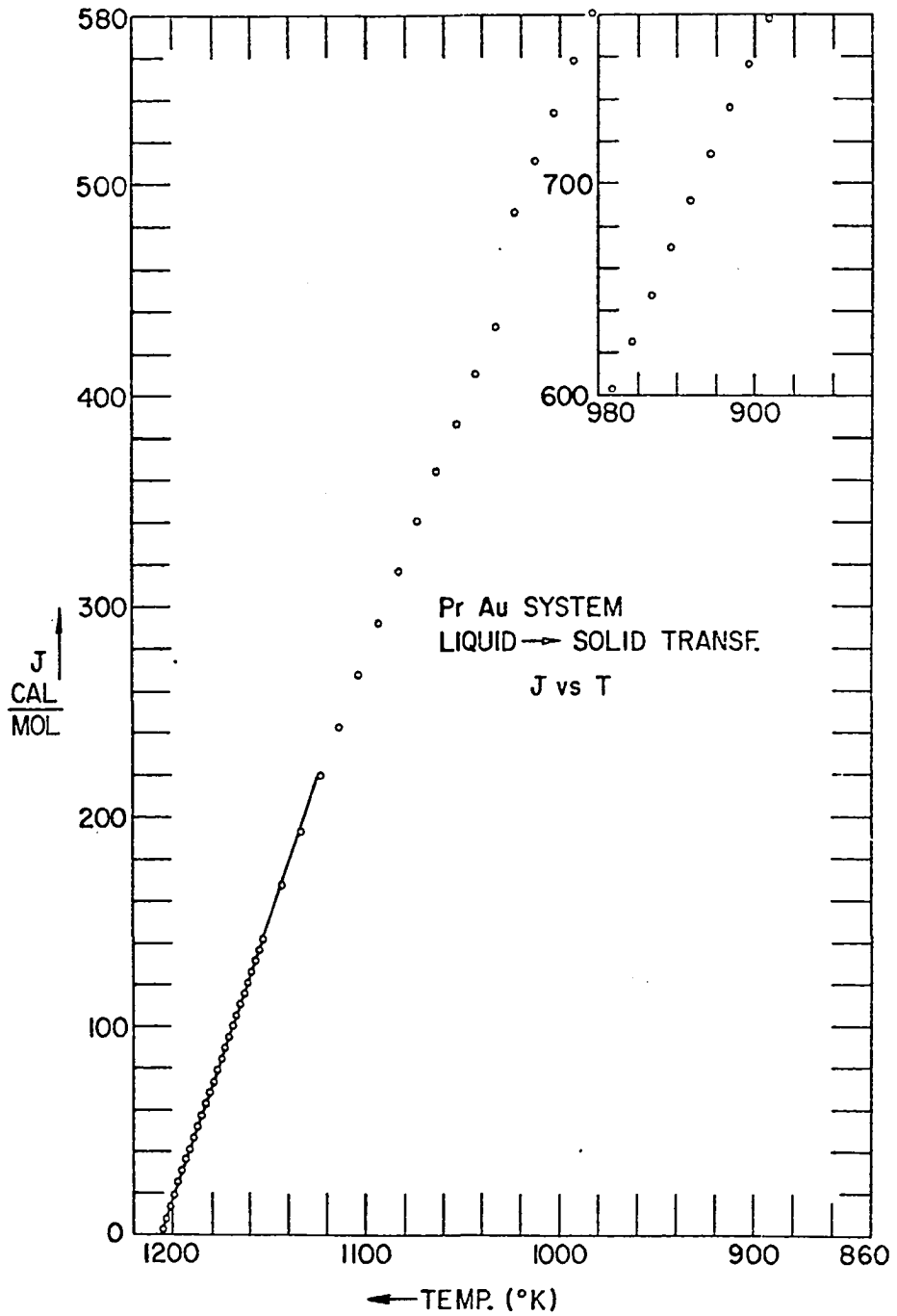

Figure 37
J-function.

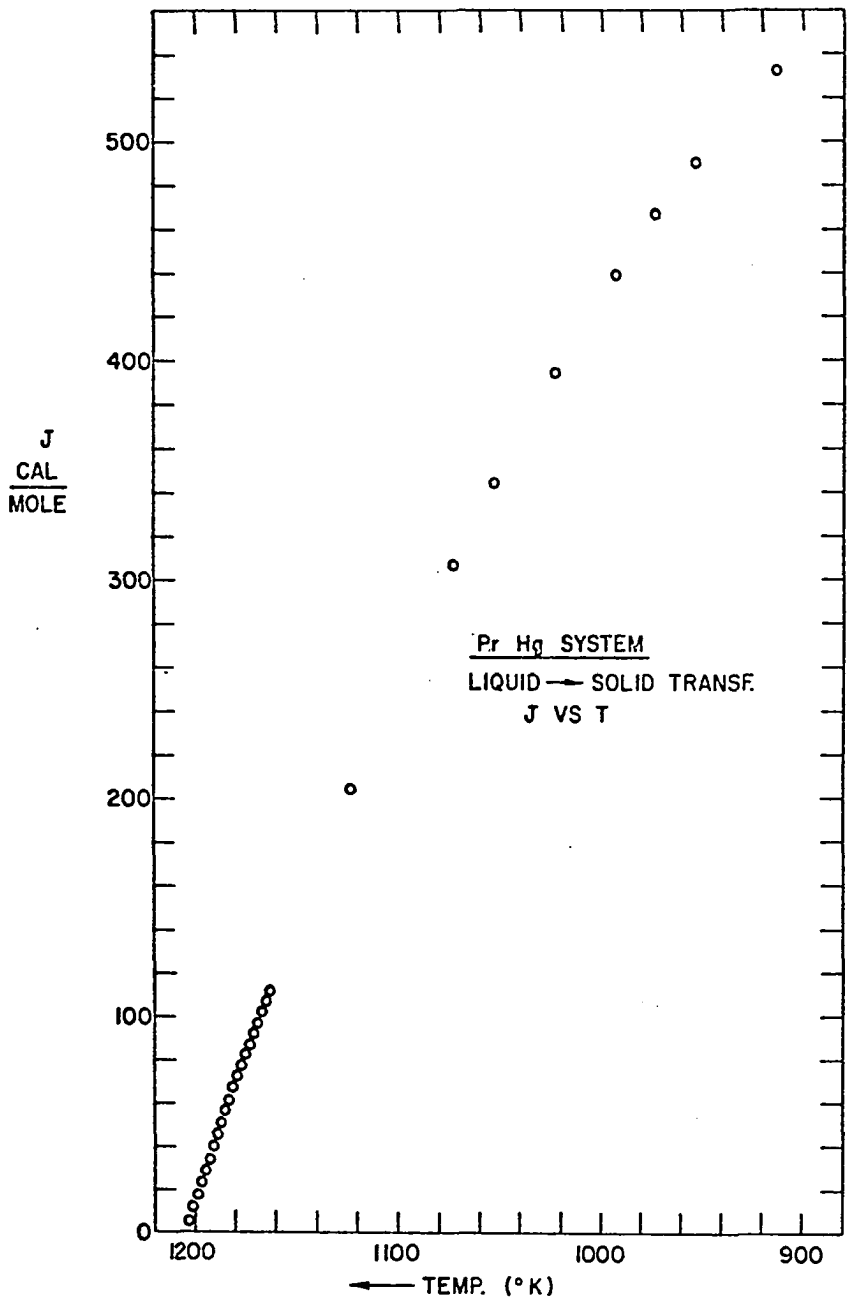

Figure 38
J-function.

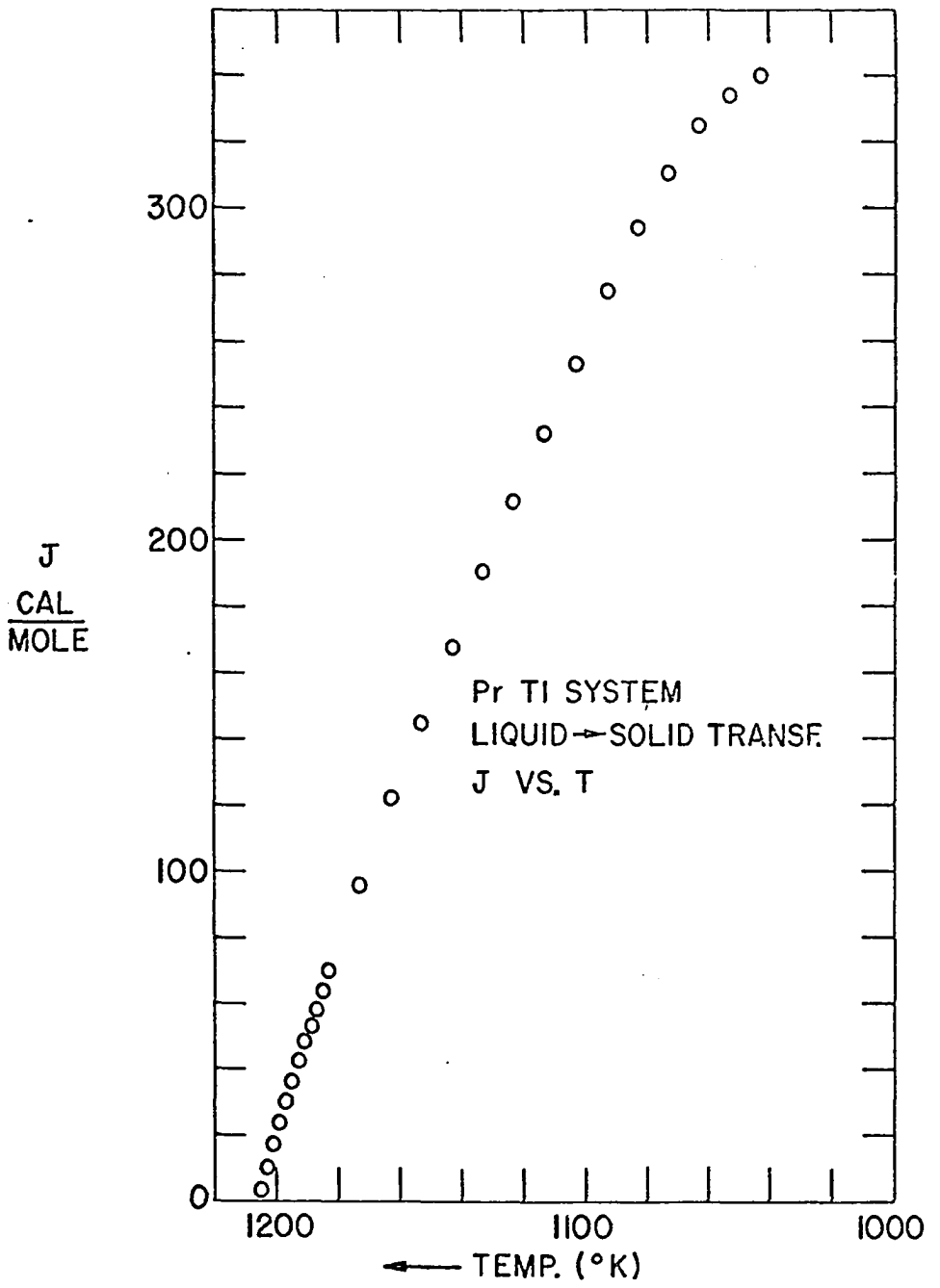

Figure 39
J-function.

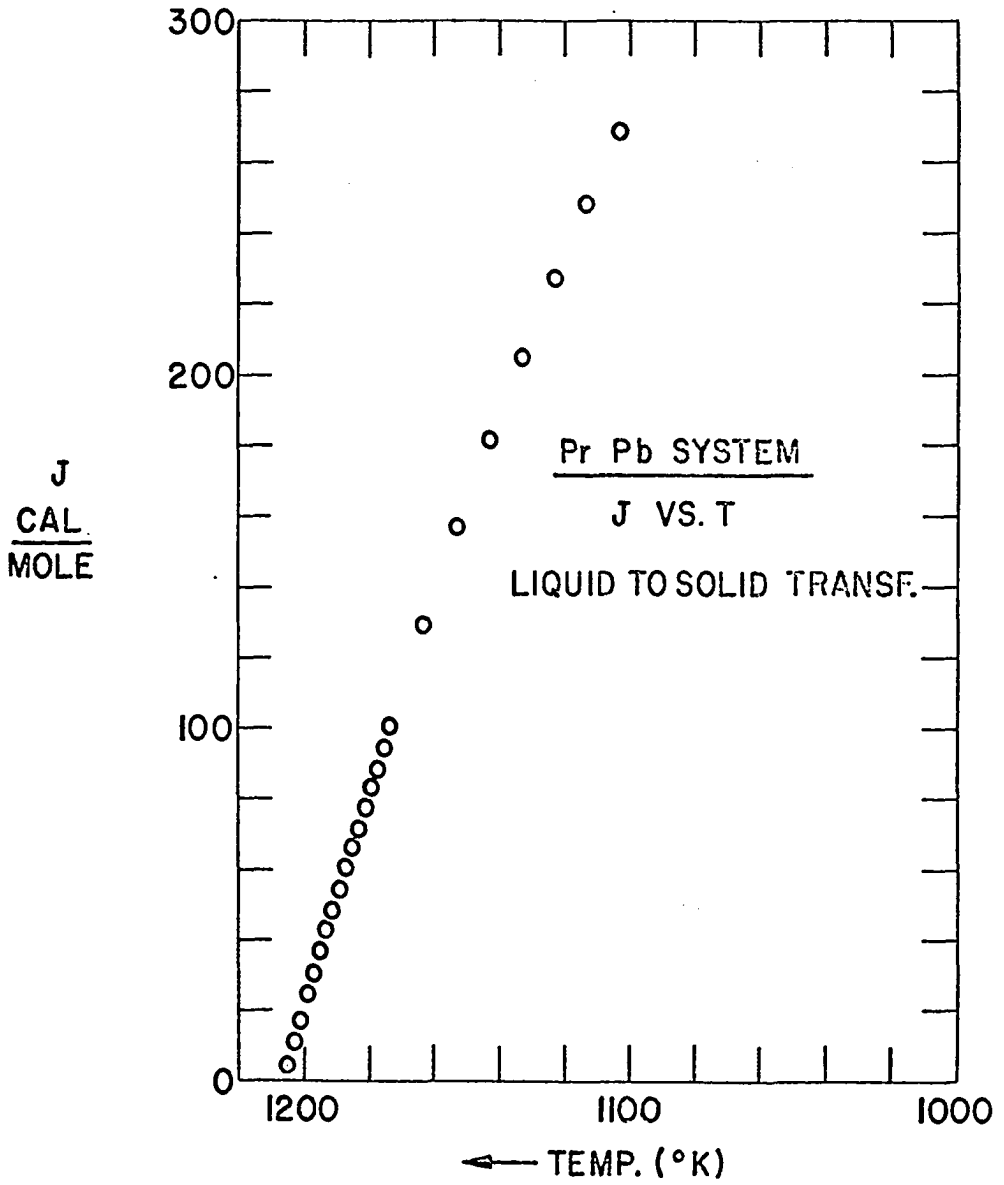

Figure 40
J-function.

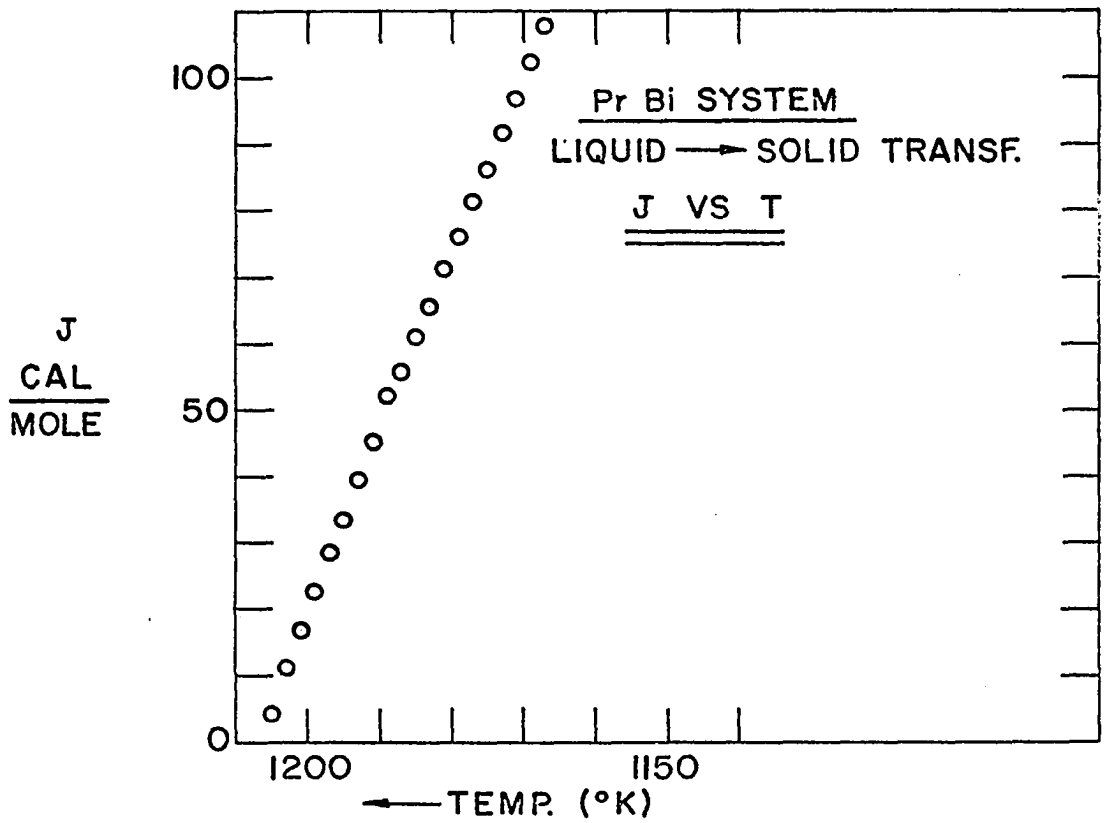

Figure 41
J-function.

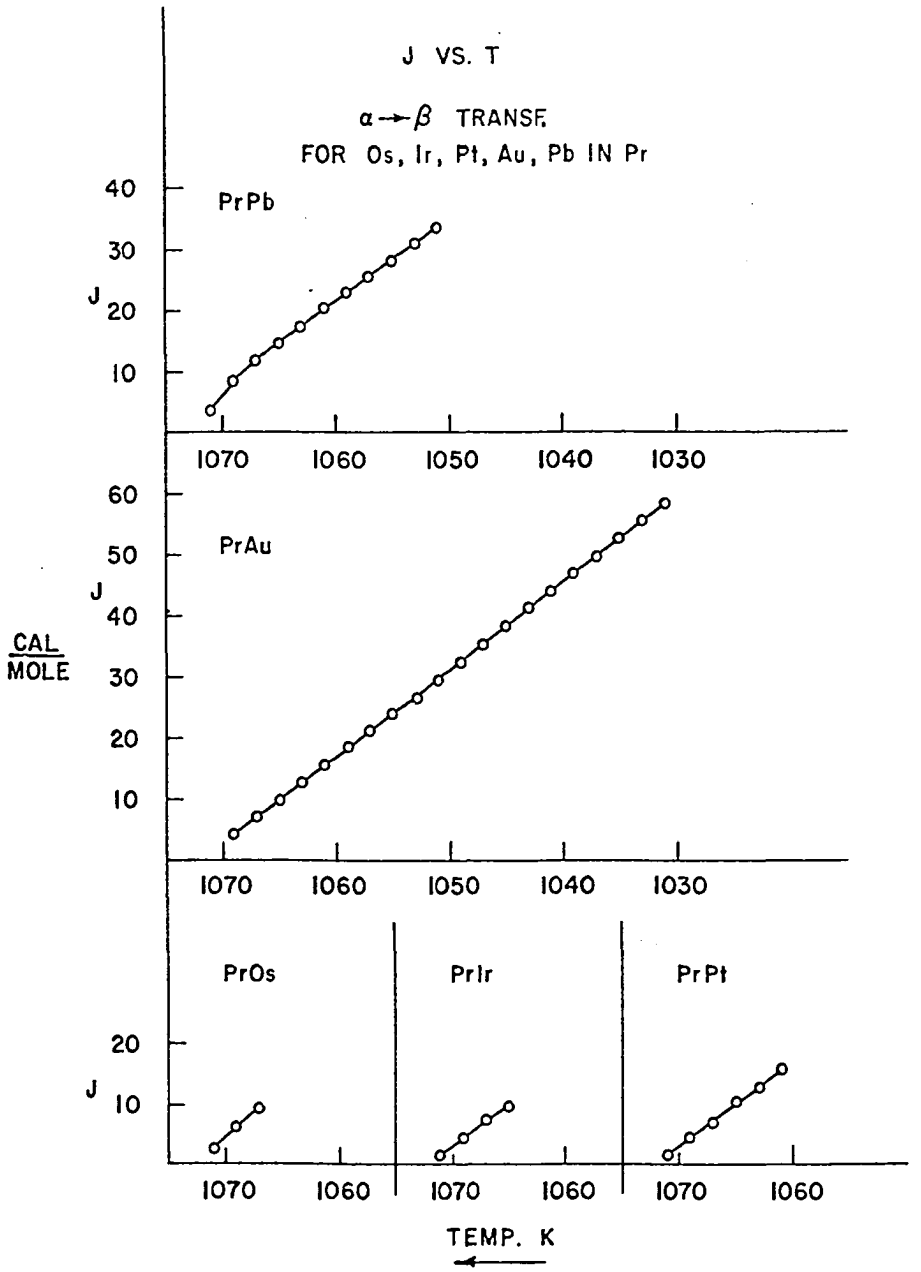

Figure 42
J-function.

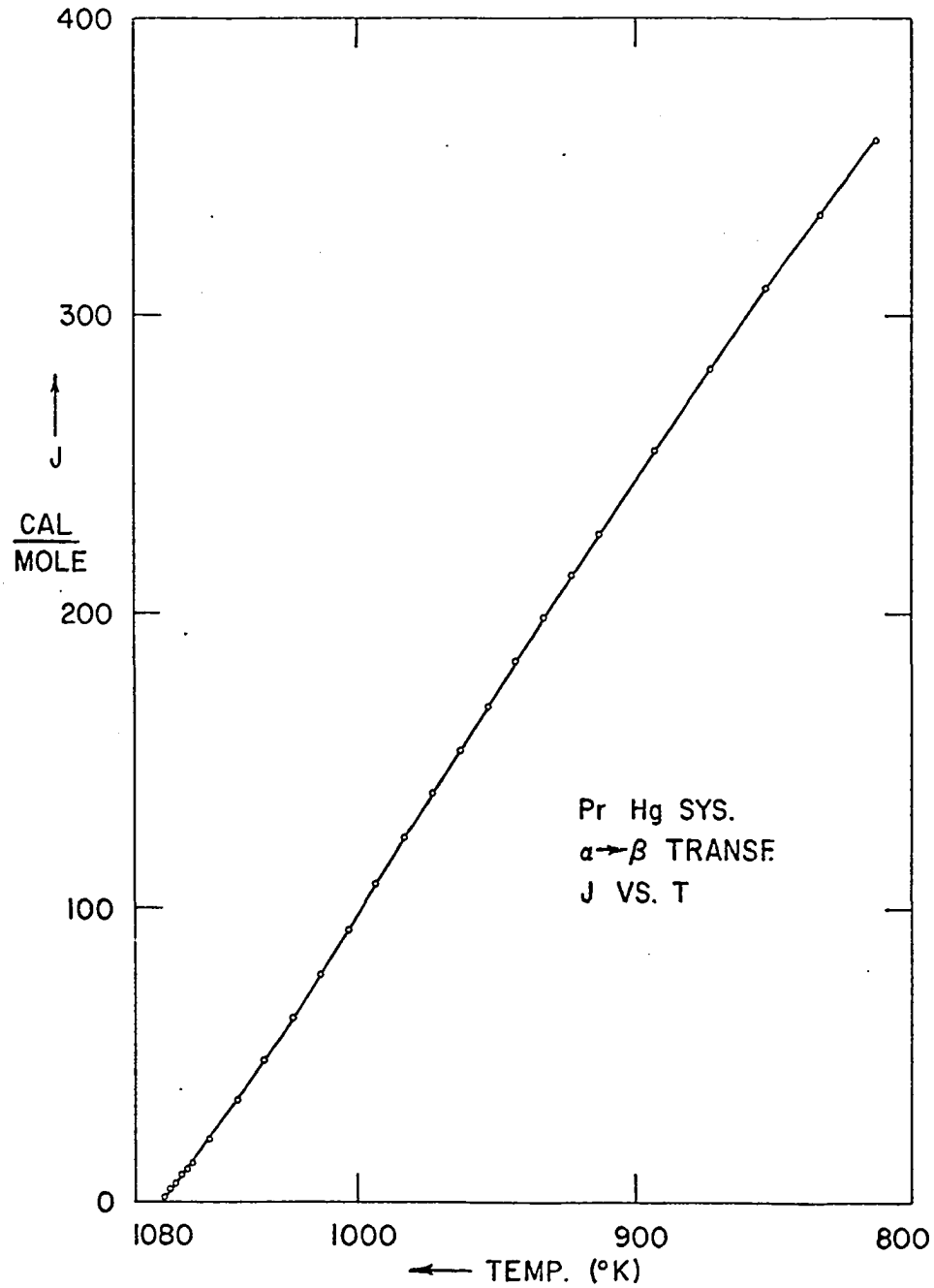

Figure 43
J-function.

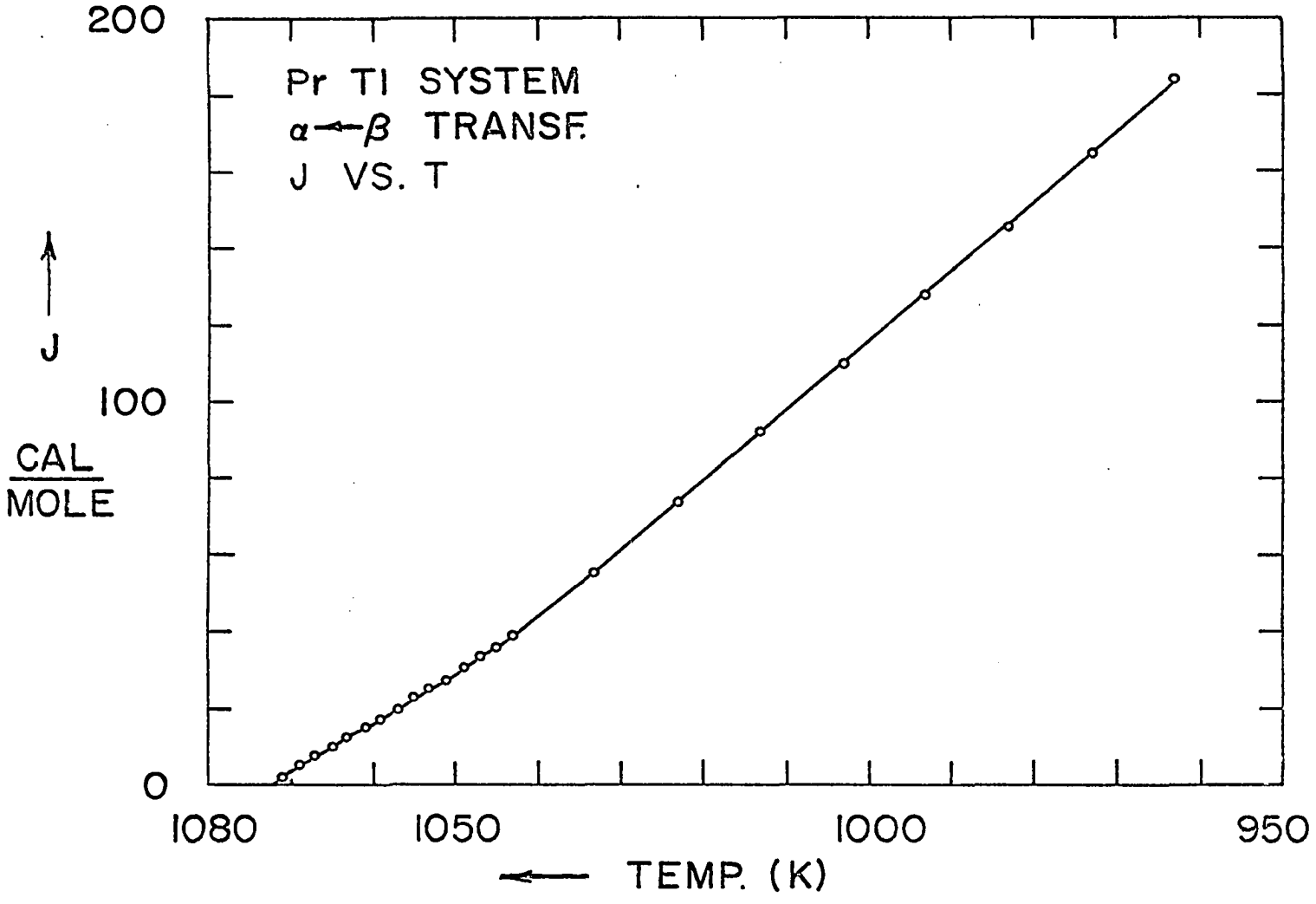

Figure 44
J-function.

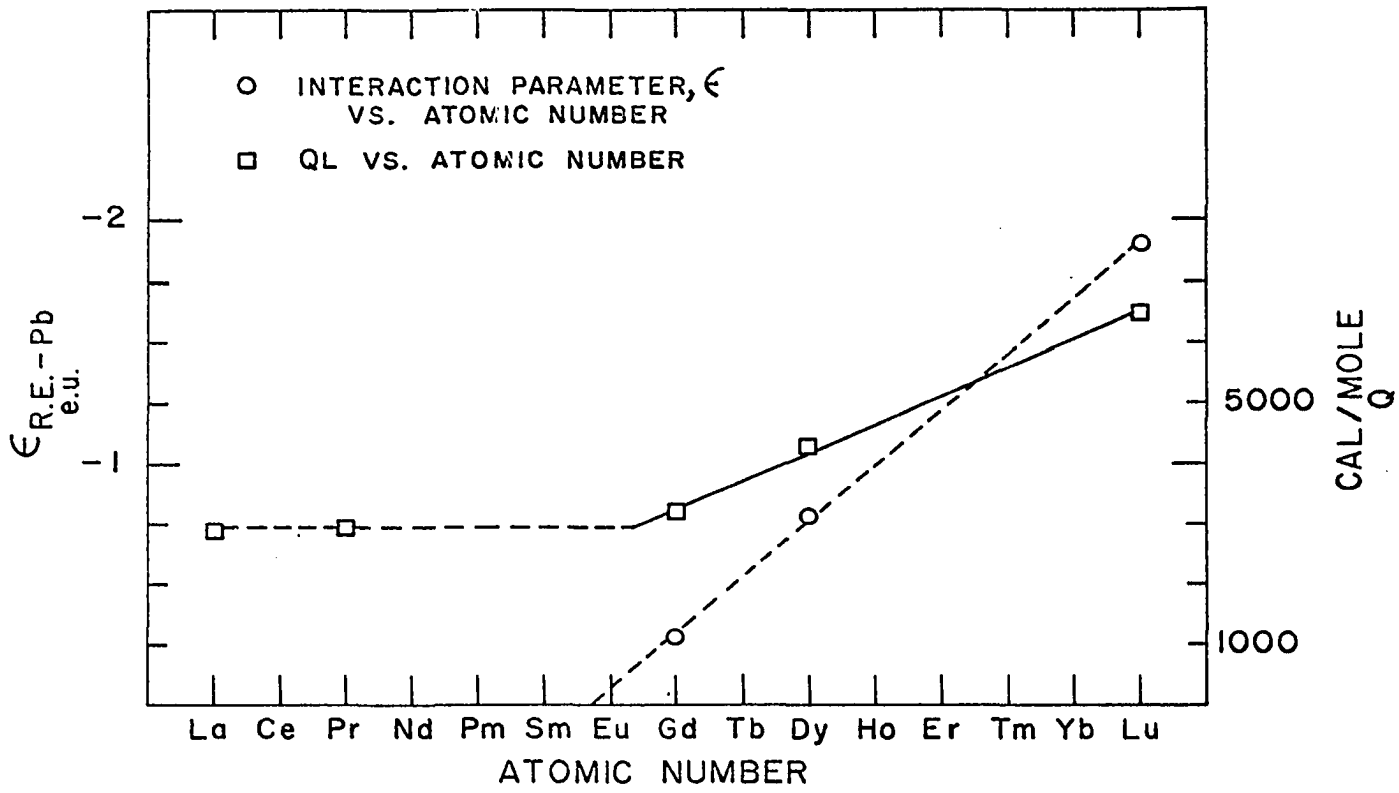

Figure 45
The interaction parameter and Q_L versus the atomic number of the lanthanides.